

# Thermal Analysis of an Oil and R-22 Cooled Compressor Motor

by

Patrick Cheong-Yu Leung

B.S., Mechanical Engineering  
Purdue Univeristy, West Lafayette

Submitted to the Department of Mechanical  
Engineering in partial fulfillment of the  
requirements for the degree of

Master of Science in Mechanical Engineering

at the

MASSACHUSETTS INSTITUTE OF TECHNOLOGY

September, 1994

© Massachusetts Institute of Technology, 1994. All Rights Reserved.

Author .....

Department of Mechanical Engineering

September, 1994

Certified by .....

Professor Peter Griffith

Department of Mechanical Engineering

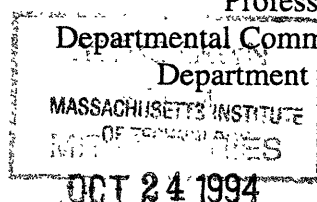
Thesis Supervisor

Accepted by .....

Professor Ain A. Sonin, Chairman

Departmental Committee on Graduate Students

Department of Mechanical Engineering



LIBRARIES

# **Thermal Analysis of an Oil and R-22 Cooled Compressor Motor**

by

Patrick Cheong-Yu Leung

Submitted to the Department of Mechanical Engineering on  
September, 1994, in partial fulfillment of the requirements for the  
degree of Master Science in Mechanical Engineering

## **Abstract**

In this study, an oil and R-22 cooled electric motor of a SC37 hermetic compressor manufactured by the Carrier Corporation is analyzed. The analysis includes the identification and evaluation of the cooling management of the current design.

Two analytical models based on first principles were developed. The fluid mechanics model, based on a fluid resistance network, is used to model the flow behavior in the motor compartment. The model indicated that 20% of the cold suction vapor was discharged into the upper plenum where heat was transferred from the motor compartment to the vapor before compression. The model also indicated that the mass flow of the vapor circulating around the motor was 81.0 lbm/hr at 90 psia and 140 F. Both the fraction and the mass flow rate are dictated by the geometry of the motor compartment and the motor speed. The motor heat transfer model is used to predict the steady state temperature distribution in the motor compartment at different suction conditions and motor losses. The model is also used to estimate the amount of heat transferred from the motor to the suction vapor as well as to the ambient air through the shell. It is capable of predicting the effects of physical dimension changes inside the compressor.

Two experiments were also preformed in this study. The first experiment is the measurement of the outside convective heat transfer coefficient of the SC37 compressor shell in a 38TKB condenser. The coefficient was determined by measuring the rate of condensate formed on the inside an empty shell's wall while it was supplied with saturated steam. Empirical correlations were also developed based on the measured data.

The other experiment, the dynamometer test, measured the temperature distribution inside an instrumented SC37 compressor at different operating conditions and studied the cooling mechanism of the motor. It was found that the motor was evidently cooled by the cold suction vapor in the upper plenum. Motor heat was conducted to the top winding end turns and then convected to the R-22 vapor in the upper plenum. Additional motor cooling were done by the circulating R-22 vapor stream and heat convection through the compressor shell to the ambient air. The results also showed that the circulating oil had little effect in the overall motor cooling. The comparison of the results with the simulations of the motor heat transfer model validated the model in terms of correct predictions of the overall temperature distribution and the adjustment with the changes in the mass flow rate and the temperature of the suction vapor.

Thesis Supervisor: Peter Griffith

Title: Professor of Mechanical Engineering

## Acknowledgments

I would like to thank Professor Peter Griffith for giving me the opportunity to work with him on this project. I am very thankful for his encouragement, guidance, patience, kindness and smile.

I would also like to thank the Carrier Corporation for providing financial support of this project and the people at the Carrier Corporation and UTRC for their generous time and technical support.

I thank all the members in the Carrier-MIT Program. Their sound advice and insight helped me in many ways to complete the project and to learn about team-work. Many thanks to the guys of the Heat Transfer Lab for the companionships and supports and to Tiny, Bob, and Norm of the M.E. machine shop for their help and patience. Thank also goes to Leslie Regan of the M. E. Graduate Office for her sincere caring.

I thank my family: Dad (Kei-Chuen Leung), Mom (How-Yin Fown), and my two beloved brothers, Thomas and Robert. And my special thank to Jackie Tang. Without their support and encouragement, none of this would have been possible. This thesis is dedicated to them.

Finally, I praise the Lord for His Love.

Patrick Leung  
September, 1994

# Table of Contents

<b>Chapter 1</b>	<b>Introduction .....</b>	<b>5</b>
1.1	Problem Statement.....	5
1.2	Background.....	5
1.3	Preview .....	7
<b>Chapter 2</b>	<b>Analytical Model 1: The Fluid Mechanics Model.....</b>	<b>9</b>
2.1	Introduction.....	9
2.2	Vapor flow paths inside the SC37 compressor .....	9
2.2.1	Flow path from the suction pipe to the scroll pump .....	9
2.2.2	Flow paths circulating through the motor .....	11
2.3	Elements of the model: Fluid resistance and the “pump” .....	12
2.3.1	Fluid resistance .....	12
2.3.2	The “pump” .....	13
2.4	Fluid resistance network .....	14
2.4.1	Flow path from the suction pipe to the scroll pump .....	14
2.4.2	Flow paths circulating through the motor .....	16
2.5	Circulation of the Lubricating Oil .....	18
2.6	Numerical calculations .....	20
<b>Chapter 3</b>	<b>Analytical Model 2: The Motor Heat Transfer Model .....</b>	<b>22</b>
3.1	Introduction.....	22
3.2	Thermal network.....	22
3.2.1	The “split” zone .....	25
3.2.2	Thermal influence of the lubricating oil .....	26
3.2.3	Control volumes .....	27
3.2.4	Resulting system of equations .....	32
3.3	Cooling mechanism for the motor .....	34
3.4	Implementation of the model using a Fortran computer program .....	35
<b>Chapter 4</b>	<b>Experiment 1: Measurement of the Outside Convective Heat Transfer Coefficient of the SC37 Compressor Shell in a 38 TKB Outdoor Condenser .....</b>	<b>36</b>
4.1	Introduction.....	36
4.2	Procedure .....	37
4.2.1	Setup .....	37
4.2.2	Assumptions .....	40
4.2.3	Measurement .....	40
4.2.4	Empirical correlations calculation .....	41
4.3	Results and Discussions.....	44
<b>Chapter 5</b>	<b>Experiment 2: The Dynamometer Test .....</b>	<b>49</b>
5.1	Introduction.....	49
5.2	Procedures.....	49
5.2.1	Setup .....	49
5.2.2	Measurement .....	52
5.3	Results and Discussions.....	55
5.3.1	Results from the experiment .....	55

5.3.2 Comparison with simulations of Motor Heat Transfer Model .....	58
<b>Chapter 6 Conclusions .....</b>	<b>62</b>
6.1 Summary of results .....	62
6.2 Recommendations for future work .....	63
<b>References .....</b>	<b>65</b>
<b>Appendix A</b> Calculation of the fluid resistance of the SC 37 compressor .....	<b>66</b>
<b>Appendix B</b> Calculations of the heat transfer coefficients of the SC37 Compressor ....	<b>68</b>
<b>Appendix C</b> Fortran computer program for the motor heat transfer model .....	<b>73</b>
<b>Appendix D</b> Data of Experiment 1 .....	<b>81</b>
<b>Appendix E</b> Data of Experiment 2: measured temperature distributions .....	<b>84</b>
<b>Appendix F</b> Data of Experiment 2: Comparison with the simulation results .....	<b>92</b>

# **Chapter 1**

## **Introduction**

### **1.1 Problem Statement**

In this thesis, an oil and R-22 cooled electric motor of a SC37 hermetic compressor manufactured by the Carrier Corporation is analyzed. The analysis includes the identification and evaluation of the cooling management of the current design. Analytical models based on first principles are developed as well. The models are used to predict the effect of changes in the present compressor configuration and operation.

### **1.2 Background**

The hermetic compressor is the one of the basic components of the vapor-compression refrigeration cycle, along with an expansion valve, a condenser, and an evaporator. For air-conditioning, the condenser is placed outdoors and the evaporator is placed indoors. The refrigerant (R-22 in this case) leaves the evaporator as a low-pressure, low-temperature saturated or superheated vapor and enters the compressor. It is compressed and leaves as high-pressure, high-temperature superheated vapor. The refrigerant then enters the condenser. It is de-superheated and condensed while heat is transferred out the condenser to outdoors' ambient air. The refrigerant leaves the condenser as high-pressure, medium temperature, saturated liquid and enters the expansion valve, in which it expands at constant enthalpy (assuming adiabatic expansion). It leaves the expansion valve as a low-pressure, low-temperature, and low quality vapor and enters the evaporator. It is evaporated to saturated state while heat is transferred from the indoor air.

The hermetic compressor studied in this project is manufactured by the Carrier Corporation. It consists of a scroll pump and an electric motor. A schematic is shown in Figure 1.1. Low-pressure, low-temperature R-22 vapor flows from the suction pipe into

the compressor. It flows past and through the deflector plate and enters the scroll pump for compression. Compressed hot vapor is discharged to the top dome of the compressor and flows out the compressor and into the condenser.

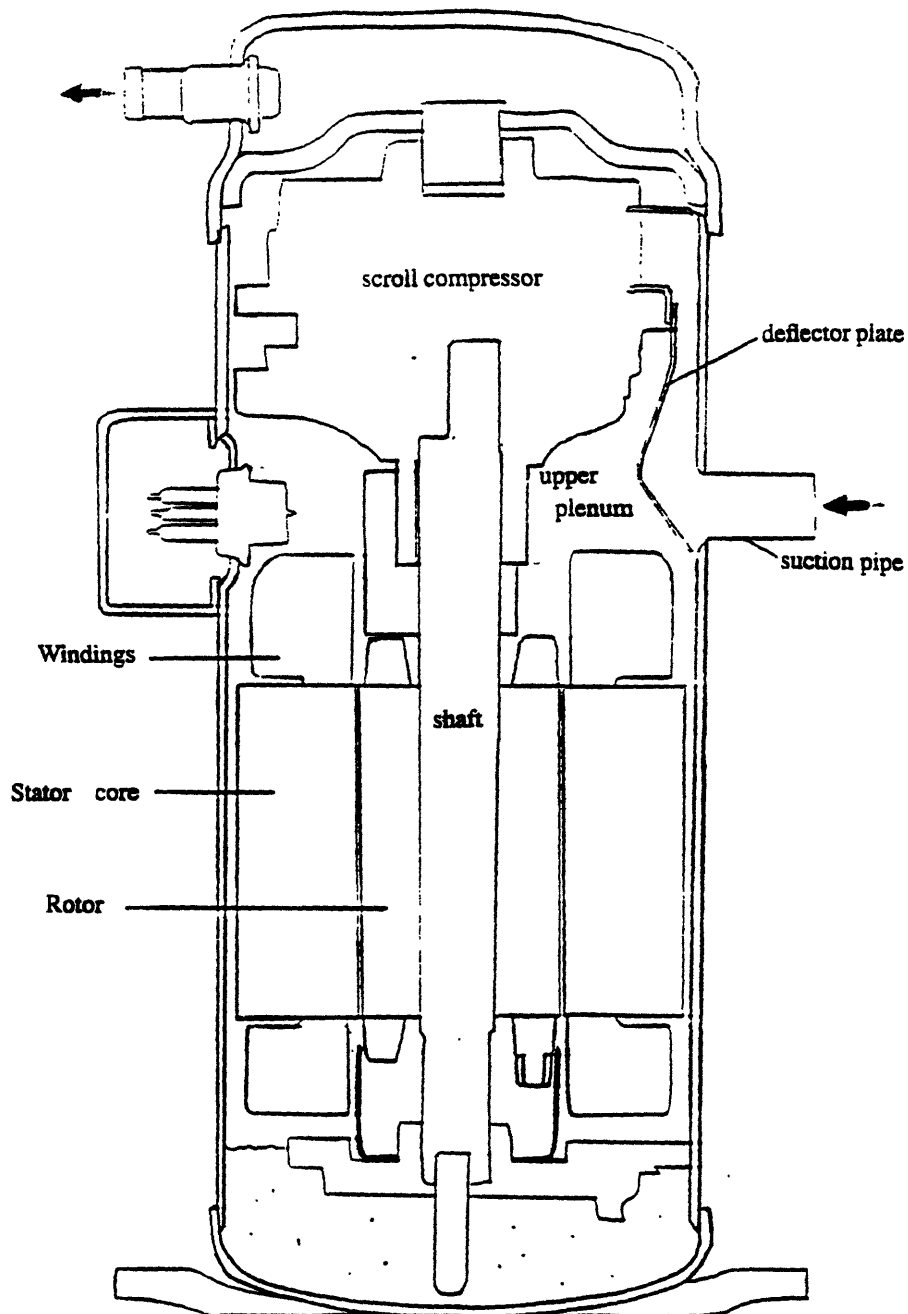


**Figure 1.1:** Schematic of the hermetic compressor analyzed

In the present design, a fraction of the cold R-22 vapor that flows from the suction pipe is discharged through the bottom hole of the deflector plate and flows into the compartment where the motor is mounted. This vapor is heated by the motor before entering the scroll pump for compression. This ultimately increases the average inlet vapor temperature before compression and thus leads to a reduction in the pump capacity and efficiency. In addition, the circulation of the vapor and the lubricating oil in the motor compartment affects the motor temperature distribution and efficiency. Thus, understanding the flow pattern of the vapor and the lubricating oil in the motor compartment and their roles in the motor cooling are important in the compressor analysis.

### **1.3 Preview**

In the following chapters, two analytical models and two sets of experiments are presented. Chapter 2 describes the fluid mechanics model and the analysis of the vapor flow behavior in the motor compartment. This model yields estimates of the amount of the cold vapor which is discharged through the bottom hole of the deflector plate and the amount of the vapor circulating through the motor. The fluid resistance network, which is an essential element of the model, is explained in detail as well.

Chapter 3 describes a motor heat transfer model. This model is based on a thermal network composed of a number of control volumes within the motor compartment and the knowledge of the R-22 vapor flow behavior from the fluid mechanics model. With the inputs of the motor losses<sup>1</sup> and the suction conditions, the model can be used to determine the steady state temperature distribution in the motor compartment.

Chapter 4 describes the first experiment, the measurement of the outside convective heat transfer coefficient of the SC37 compressor shell in a 38 TKB outdoor condenser.

---

1. The motor losses are estimated based on the motor model by Umans [1].



This measurement is needed because of the uniqueness of the air flow pattern inside the condenser's casing. Empirical correlations are provided as well. These results are incorporated into the motor heat transfer model.

Chapter 5 describes the second experiment, the dynamometer test. In this experiment, the temperature distribution inside the compressor was measured at different suction conditions and motor loads. This experiment was used to identify the cooling mechanism of the motor and revealed the roles of the R-22 vapor and the circulating oil in the motor cooling. The experimental results are compared to the simulations from the motor heat transfer model to show how good the model is.

Chapter 6 summarizes the findings in this study and provides recommendations for future work.

## Chapter 2

### Analytical Model 1: The Fluid Mechanics Model

#### 2.1 Introduction

This chapter describes the R-22 vapor flow behavior inside the SC37 compressor. First, the flow paths inside the compressor are identified. Then each flow path is transformed into the fluid mechanics model which is a fluid resistance network. The model is used to estimate the overall volume flow rate as well as the fraction diverted into each branch.

#### 2.2 Vapor flow paths inside the SC37 compressor

By examining the physical arrangement of each component inside the SC37 compressor, two systems of vapor flow paths were identified. One consists the flow path from the suction pipe to the scroll pump and the other consists the flow paths of the R-22 vapor circulating through the motor.

##### 2.2.1 Flow path from the suction pipe to the scroll pump

There are two parallel branches, which are labelled as “m” and “g”, from region “a” (the end of the suction pipe) to “b” (the entrance of the scroll pump), as shown on Figure 2.1. Of all the cold vapor which flows through the suction pipe, the most, with a volume flow rate of  $Q_m$ , flows past the deflector plate and through the 90° plastic elbow before entering into the scroll pump. A smaller amount of the vapor, with a volume flow rate of  $Q_g$ , is discharged through the hole at the bottom of the deflector plate and flows into the upper plenum above the motor. Under steady-state conditions, the conservation of mass dictates that the same flow rate of vapor ( $Q_g$ ) from the upper plenum simultaneously enters the region “b” through the gaps around the plastic elbow. Note that while the vapor is flowing through the upper plenum, heat is transferred from the motor compartment. The

leaving temperature of the vapor circulating through the motor is higher than that which flows past the deflector and through the elbow. The fluid mechanics model is used to determine the fraction of the total vapor flowing from the suction pipe ( $Q_t$ ) which passes through the bottom hole of the deflector plate.

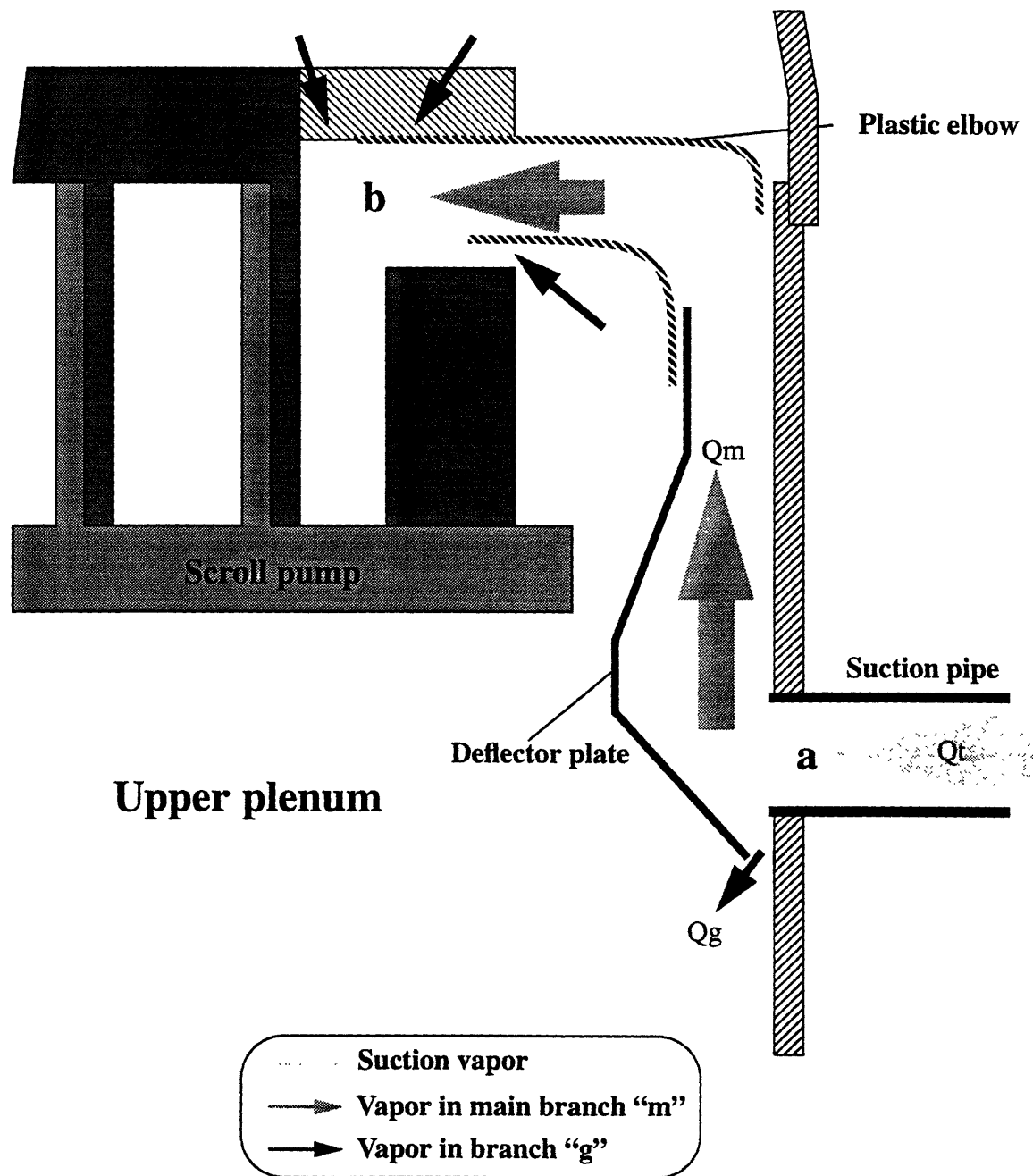


**Figure 2.1:** Flow path from the suction pipe to the scroll pump

## 2.2.2 Flow paths circulating through the motor

For the vapor flow paths circulating through the motor, it is assumed that certain amount of the vapor in the upper plenum flows downward through the two outer gaps (the two “big” semi-circular gaps, one is directly below the deflector plate and the other one is 180° off phase) between the stator core and the shell into the lower plenum and returns by flowing up through the inner gap (the annulus gap between the rotor and the stator), as shown in Figure 2.2. The whole circulation of the vapor is propelled by a radial pressure rise across the upper plenum. This pressure rise is generated by the spinning of the shaft’s counterweight in the upper plenum. The mechanism is described in Section 2.3.

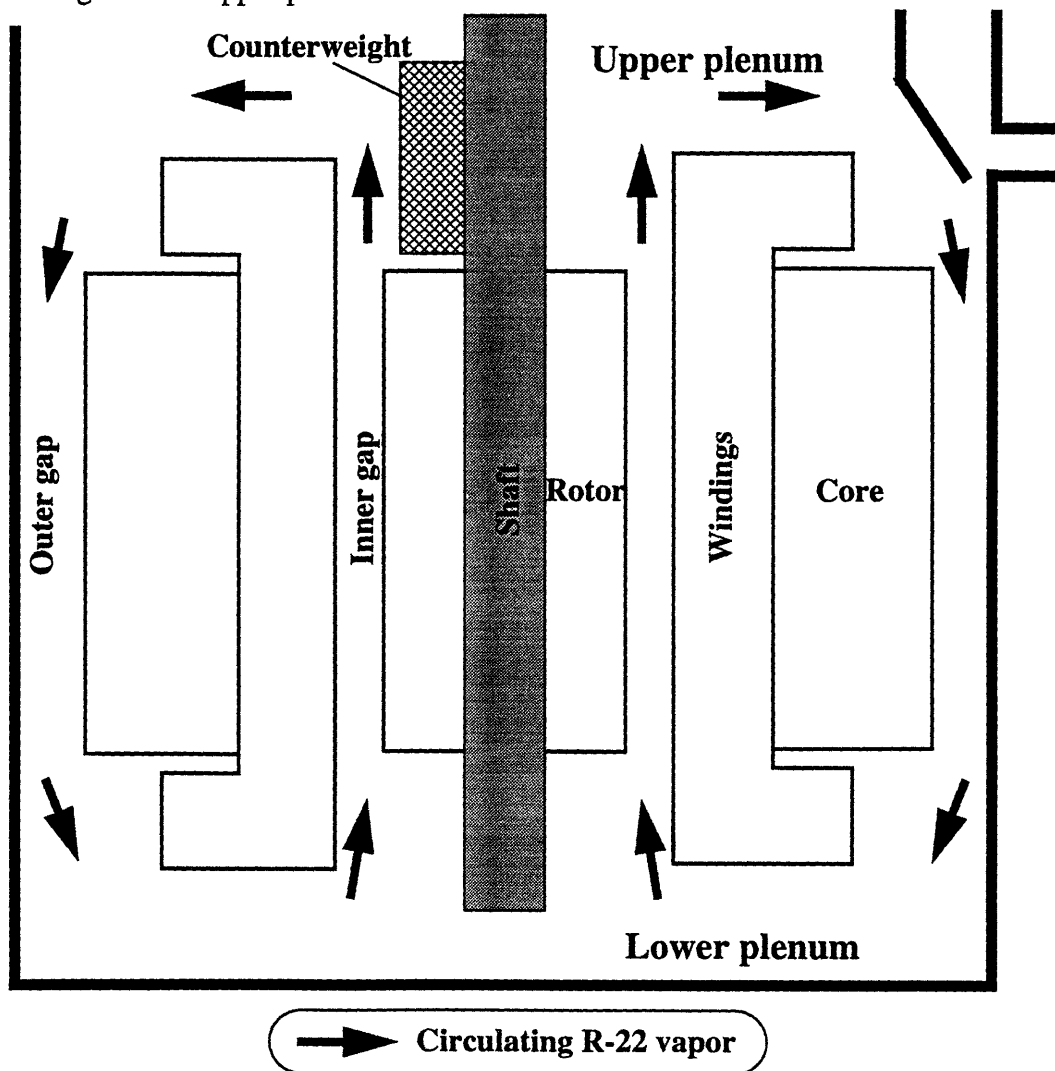


Figure 2.2: Flow paths circulating through the motor

## 2.3 Elements of the model: Fluid resistance and the “pump”

### 2.3.1 Fluid resistance

The fluid resistance as used in the model is defined as the magnitude of the slope of the curve of pressure versus flow rate. It reflects the head loss<sup>1</sup> in the fluid due to wall friction, abrupt change in cross-sectional area, and fittings. The expression for the fluid resistance is developed from the definition of the head loss coefficient:

$$\Delta P \equiv C_f \frac{\rho Q^2}{2A^2} \quad (2.1)$$

where  $C_f$  is the head loss coefficient

$\Delta P$  is the pressure loss

$\rho$  is the density of the vapor

$Q$  is the volume flow rate of the vapor

$A$  is the cross-sectional area

Then the expression for the fluid resistance ( $R$ ) is:

$$R \equiv \frac{dP}{dQ} = C_f \frac{\rho |Q|}{A^2} \quad (2.2)$$

Note that the value of  $C_f$  is determined by the geometric characteristics of the region. For each type of fitting, its value is different.

Using the analogy between an electrical network and a flow system with multiple paths, the head losses can be converted into a fluid resistance network with the characteristics which are similar to an electrical network. Table 2.1 shows the comparison of the elements between the fluid resistance network and the electrical network.

---

1. The detailed definition of fluid head loss can be found in Marks' Standard Handbook for Mechanical Engineers by Avallone and Baumeister III. [2].

**Table 2.1:** Comparison of the elements between the fluid resistance and electrical network

Electrical Network	Fluid Resistance Network
Potential difference V	Pressure difference $\Delta P$
Current A	Flow rate Q
Resistance $R \equiv V/A$	Resistance $R = C_f \frac{\rho  Q }{A^2}$ (2.2)

With the transformation of the problem into fluid resistance network, the volume flow rates of a flow path and its multiple branches in series or parallel can be solved using techniques similar to those used in solving electrical networks.

### 2.3.2 The “pump”

The circulation of the vapor around the motor compartment, as described in section 2.2.2, is propelled by a radial pressure rise. It is generated by the spinning of the shaft’s counterweight at the upper plenum, which acts as the “pump”. From Euler’s equation for radial equilibrium, the pressure gradient normal to a streamline is defined as follows:

$$\frac{dP}{dr} \equiv \frac{\rho v^2}{r} \quad (2.3)$$

where P is the radial pressure, r is the radial distance from the shaft’s center at the upper plenum, and v is the velocity of the flow. Due to the spinning of the counterweight, the vapor at the upper plenum is stirred up. Assuming that the vapor next to the outer radius of the counterweight has the same velocity as the counterweight at that radius and that  $vr$  is a constant from there out, the above Euler’s equation (EQ 2.3) becomes:

$$\frac{dP}{dr} = \frac{\rho C^2}{r^3} \quad (2.4)$$

where  $C$  is a constant equal to the tip velocity of the counterweight ( $V_i$ ) times the outer radius of the counterweight ( $R_i$ ), i.e.  $C = V_i \cdot R_i$ . See Figure 2.3 for the schematic of the upper plenum. Integrating EQ 2.4 over the region of the upper plenum, from outer radius of the counterweight to the inner radius of the shell ( $R_o$ ), the pressure rise ( $\Delta P_0$ ) is calculated as follows:

$$\Delta P_0 = \frac{\rho}{2} \cdot (V_i \cdot R_i)^2 \cdot \left( \frac{1}{R_i^2} - \frac{1}{R_o^2} \right) \quad (2.5)$$

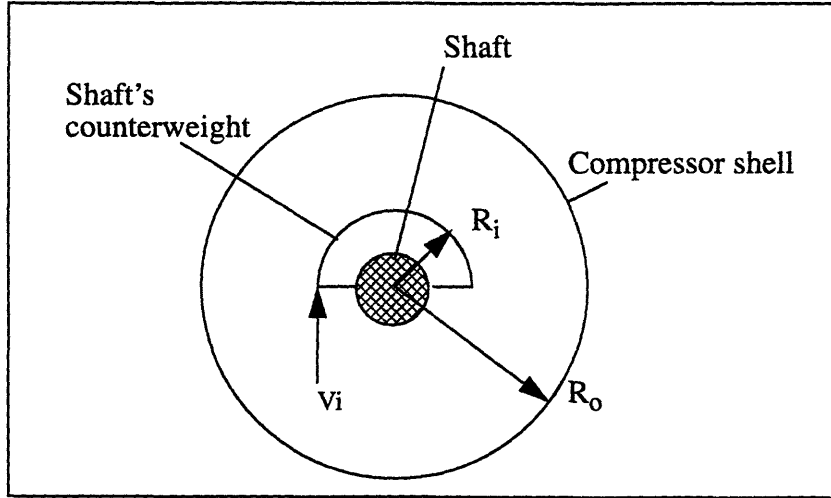


**Figure 2.3:** Schematic of the upper plenum, with counterweight

## 2.4 Fluid resistance network

Using the fluid resistance and the “pump”, described in Section 2.3, two fluid resistance networks are formed for the two systems of flow paths. Head loss coefficient for each fluid resistance can be found in the reference books [3] and [4].

### 2.4.1 Flow path from the suction pipe to the scroll pump

Figure 2.4 shows the fluid network of the flow path from the suction pipe to the scroll pump. It consists two fluid resistances parallel to each other.

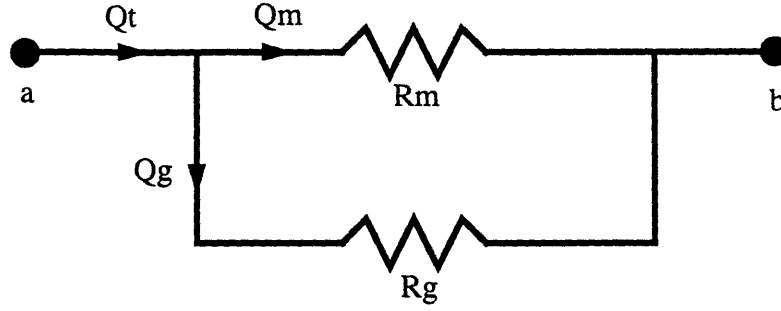


**Figure 2.4:** Fluid network for the flow path from the suction pipe to the scroll pump

Fluid resistance ( $R_m$ ) represents the fluid resistance in the main flow path m and includes both the head losses due to the duct friction along the plate and the 90° elbow, which is:

$$R_m = \left(f \cdot \frac{L}{D_h}\right) \cdot \frac{\rho Q_m}{A_m^2} + C_{B90} \cdot \frac{\rho Q_m}{A_m^2} \quad (2.6)$$

where  $\left(f \cdot \frac{L}{D_h}\right)$  = head loss coefficient for duct friction along the plate

$L$  = duct length

$D_h$  = hydraulic diameter

$f$  = friction factor of the duct

$C_{B90}$  = head loss coefficient for the 90° elbow

$Q_m$  = volume flow rate of the vapor in the main flow path

$A_m$  = average horizontal cross-sectional area of the duct along the plate

The other fluid resistance ( $R_g$ ) represents the fluid resistance through the bottom hole of the deflector plate, which is:

$$R_g = K_e \cdot \frac{\rho Q_g}{A_g^2} \quad (2.7)$$

where  $K_e$  = head loss coefficient for the orifice (the bottom hole)

$A_g$  = cross-sectional area of the orifice

It is assumed that the fluid resistance of the bottom hole of the deflector plate dominates in this flow branch with its relatively small cross-sectional area compared with other regions (e.g., the annular gap between the scroll pump and the shell).



Using the technique similar to that used in solving an electrical network (Kirchhoff's Voltage Law), an equation can be obtained by summing all the pressure differences of the close loop of the network:

$$\left(f \cdot \frac{L}{D_h} \cdot \frac{\rho}{A_m^2} + C_{B90} \cdot \frac{\rho}{A_m^2}\right)(Q_t - Q_g)^2 - K_e \cdot \frac{\rho Q_g^2}{A_g^2} = 0 \quad (2.8)$$

where  $Q_t = Q_g + Q_m$

The above equation can be simplified and leads to an equation of  $Q_g$  in terms of  $Q_t$ :

$$Q_g = \frac{Q_t}{1 + \left(\frac{A_m}{A_g}\right) \sqrt{\frac{K_e}{f \cdot \frac{L}{D_h} + C_{B90}}}} \quad (2.9)$$

With knowledge of the fluid properties for the vapor, the fraction  $Q_g/Q_t$  can be found.

#### 2.4.2 Flow paths circulating through the motor

A similar procedure can be used to determine the volume flow rates of the flow paths circulating through the motor. Figure 2.5 shows the fluid network for this system. It consists of two paths flowing down the two outer gaps and one flowing up the inner gap.

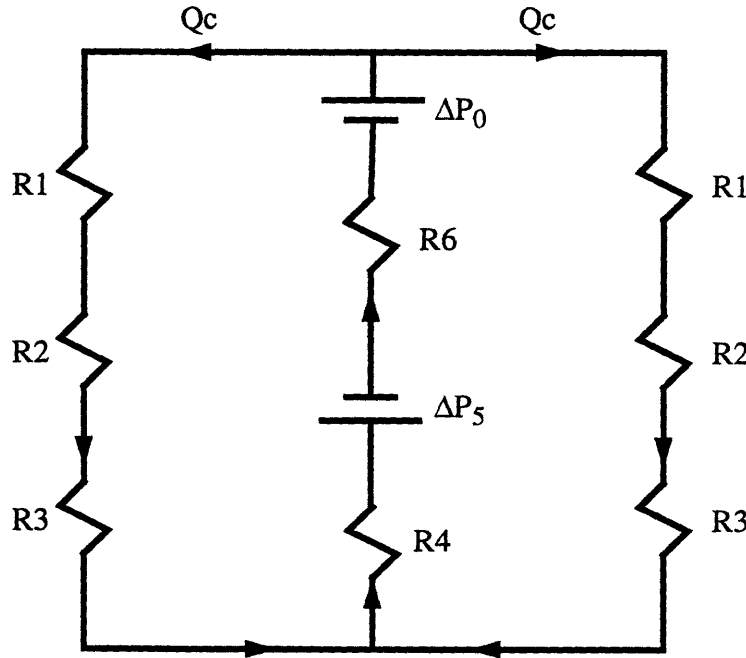


**Figure 2.5:** Fluid network for the flow paths circulating through the motor

The value of each fluid resistance is based on the geometric characteristics for each element along the path. These are described as follows:

- $\Delta P_0$ : pressure difference normal to the streamlines, as shown in EQ 2.5
- $R_1$ : fluid resistance due to duct contraction at the entrance of each outer gap

$$R_1 = K_{c1} \cdot \frac{\rho Q_c}{A_{c1}^2} \quad (2.10)$$

where  $K_{c1}$  = head loss coefficient for duct contraction at the entrance

$Q_c$  = volume flow rate of the vapor circulating down in each outer gap

$A_{c1}$  = cross-sectional area of the outer gap

- $R_2$ : fluid resistance due to wall friction along each outer gap between the stator and the shell

$$R_2 = f_2 \cdot \frac{L}{D_h} \cdot \frac{\rho Q_c}{A_{c2}^2} \quad (2.11)$$

where  $f_2 \cdot \frac{L}{D_h}$  = head loss coefficient for duct friction along the outer gap

$L$  = length of the outer gap

$D_h$  = hydraulic diameter of the outer gap

$f_2$  = friction factor of the duct along the outer gap

$A_{c2}$  = cross-sectional area of the outer gap

- $R_3$ : fluid resistance due to duct expansion at the exit of each outer gap

$$R_3 = K_{e3} \cdot \frac{\rho Q_c}{A_{c3}^2} \quad (2.12)$$

where  $K_{e3}$  = head loss coefficient for duct expansion at the exit

$A_{c3}$  = cross-sectional area of the outer gap

- $R_4$ : fluid resistance due to duct contraction at the entrance of the inner gap

$$R_4 = K_{c4} \cdot \frac{\rho (2 \cdot Q_c)}{A_{c4}^2} \quad (2.13)$$

where  $K_{c4}$  = head loss coefficient for duct contraction at the entrance

$A_{c4}$  = cross-sectional area of the inner gap

- $\Delta P_5$ : pressure loss due to the windage along the inner gap

$$\Delta P_5 = \frac{\tau_w \cdot \sin \left( \left( \tan \left( \frac{2 \cdot Q_c}{V_T \cdot A_{c5}} \right) \right) \right) \cdot A_w}{A_{c5}} \quad (2.14)$$

where  $\tau_w$  = shear stress generated because of the windage

$A_w$  = cylindrical surface area of the rotor along the inner gap

$A_{c5}$  = cross-sectional area of the inner gap

$V_T$  = velocity of the rotor

- $R_6$ : fluid resistance due to duct expansion at the exit of the inner gap

$$R_6 = K_{e6} \cdot \frac{\rho (2 \cdot Q_c)}{A_{c6}^2} \quad (2.15)$$

where  $K_{e6}$  = head loss coefficient for duct expansion at the exit

$A_{c6}$  = cross-sectional area of the inner gap

Using the similar procedure in solving for  $Q_g$  (KVL), an equation can be obtained by summing all the pressure differences around one of the closed loops of the network:

$$(R_1 + R_2 + R_3) \cdot Q_c + R_4 \cdot (2 \cdot Q_c) + \Delta P_5 + R_6 \cdot (2 \cdot Q_c) - \Delta P_0 = 0 \quad (2.16)$$

for which leads to an equation can be solved for  $Q_c$ :

$$\left( K_c \cdot \frac{\rho Q_c}{A_{c1}^2} + f \cdot \frac{L}{D_h} \cdot \frac{\rho Q_c}{A_{c2}^2} + K_e \cdot \frac{\rho Q_c}{A_{c3}^2} \right) \cdot Q_c + \left( K_c \cdot \frac{\rho (2 \cdot Q_c)}{A_{c4}^2} \right) \cdot (2 \cdot Q_c) + \frac{\tau_w \cdot \sin \left( \left( \tan \left( \frac{2 \cdot Q_c}{V_T \cdot A_{c5}} \right) \right) \right) \cdot A_w}{A_{c5}} \quad (2.17)$$

$$+ \left( \left( K_e \cdot \frac{\rho (2 \cdot Q_c)}{A_{c6}^2} \right) \cdot (2 \cdot Q_c) \right) - \frac{\rho}{2} \cdot (V_i \cdot R_i)^2 \cdot \left( \frac{1}{R_i^2} - \frac{1}{R_o^2} \right) = 0$$

Note that the total mass flow rate of the R-22 vapor circulating through the motor equals  $2 \cdot Q_c$ .

## 2.5 Circulation of the Lubricating Oil

As shown in Figure 2.6, the lubricating oil is treated as being in closed circulation around the motor compartment. It flows down under the influence of gravity along the outer gaps to the oil sump at the bottom of the lower plenum. While the oil is flowing

down the outer gaps, it forms thin films along either the core or the shell surface. The accumulated oil at the oil sump flows up through the inclined tube in the shaft which acts as an oil pump. The oil exits through the top of the shaft or the side holes and flows into the upper plenum. The oil disperses across the upper plenum and lands on the top of the core. The oil disperses across the upper plenum and lands on the top of the core. Finally, the oil flows down the outer gaps and the process repeats itself.

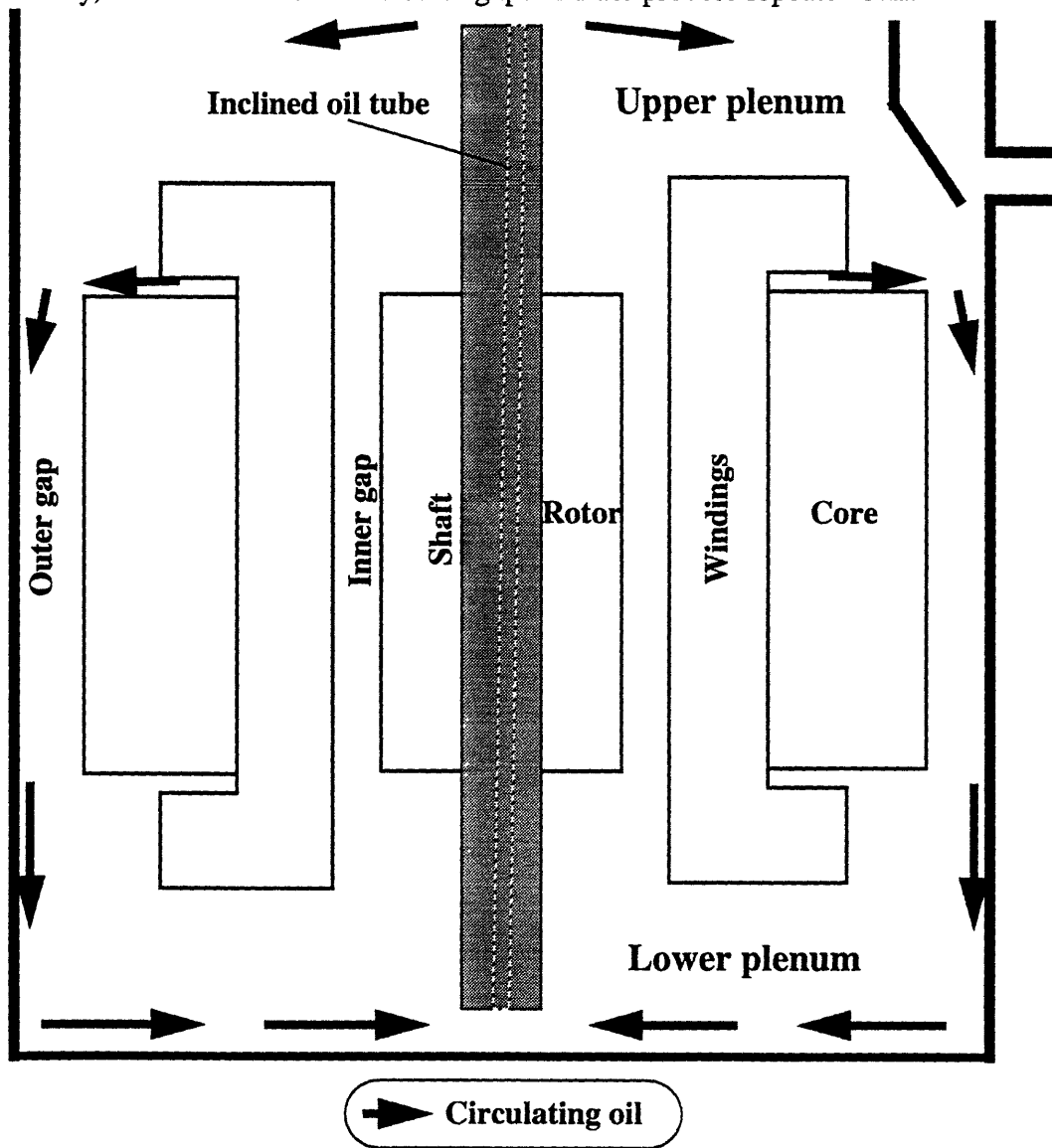


**Figure 2.6:** Circulation of the lubricating oil

With the conditions  $\dot{m}_{OIL}$  equaled 110 lbm/hr,  $\rho_{OIL}$  equaled 54.8 lbm/ft<sup>3</sup> and  $\mu_{OIL}$  equaled 16.5 lbm/ft-hr<sup>1</sup>, the thickness of the oil film<sup>2</sup> flowing down due to the gravity along the outer gaps inside the compressor shell was estimated to be 0.018 in. The film thickness was small compared with space of the outer gap (0.4 in maximum for the outer gaps). This result validated the present fluid mechanics model, which doesn't include a contribution to the pressure drop due to the flowing lubricating oil film. The effects on the motor heat transfer due to the oil circulating through the motor will be included in the motor heat transfer model, however.

## 2.6 Numerical calculations

Appendix A shows the calculation of each individual fluid resistance used in EQ 2.5-2.15. The dimensions inside the SC37 compressor were obtained from the Carrier Corporation. The thermophysical properties of the R-22 vapor were evaluated at the pressure and the average temperatures measured in the UTRC's testing report on a SC37 scroll compressor [7] at the cycle condition 45/110/65 [45°F  $T_{se}$ ; 110°F  $T_{sc}$ ; 65°F  $T_{suct}$ ].

Using EQ 2.9,  $Q_g/Q_t$  was found to be 20% at the specified cycle condition. Note that the density term has been cancelled out in EQ 2.9 and the fraction is dictated by the velocity and geometry only. It is not very temperature dependent. Thus the fraction 20% will be about the same at different cycle conditions as long as the geometry doesn't change inside the compressor. Also note that not all the cold vapor, which is discharged through the bottom hole of the deflector, flows down the outer gap (beneath the bottom hole) to the lower plenum under the motor. In fact, the cold vapor is partially diverted with a portion flowing down the outer gap and the remainder mixing with the hot vapor in the upper

- 
1. The values were obtained from Raymond DeBlois of UTRC.
  2. The calculation was based on the falling film flow of vertical annular flow without shear.

plenum. The amount of the cold vapor, which flows down the outer gap, has been measured and controlled in the dynamometer test.

Solving EQ 2.17, the volume flow rate of the vapor circulating around the motor ( $=2Q_c$ ) was found to be  $0.0170 \text{ ft}^3/\text{sec}$ . It is equivalent to a mass flow rate ( $M_c$ ) of  $81.0 \text{ lbm/hr}$  at  $140^\circ\text{F}$  and a pressure of  $90 \text{ psia}$ . The value of ( $2Q_c$ ) is dictated by the motor speed and the geometry of the motor compartment. It is not very temperature dependent. Therefore this value can be used for different cycle conditions for the same motor speed and dimensions of the motor compartment. Calculation of the mass flow rate of the circulating vapor will be required for compressors of different sizes since the values of the fluid resistances will be different. However, the same fluid mechanics model is still valid.

## Chapter 3

### Analytical Model 2: The Motor Heat Transfer Model

#### 3.1 Introduction

The motor heat transfer model is used to predict the steady state temperature distribution in the motor compartment at different suction conditions and motor loads. In the model, the whole motor compartment, including the upper and lower plenums, is divided into several control volumes. Using the steady state conservation of energy principle for each control volume, the temperatures of each motor component as well as those of the surrounding regions are assembled into a thermal network in the form of a system of equations. The heat generated from each motor component due to motor losses<sup>1</sup> and the suction vapor temperature are the inputs and the interior component temperatures are the unknowns. The temperature unknowns are determined by solving the system of equations simultaneously.

#### 3.2 Thermal network

From the steady state energy balance on a control volume with multiple inlet and outlet flow streams<sup>2</sup>:

$$\dot{Q} - \dot{W} = \sum_{OUT} \dot{m} \cdot h - \sum_{IN} \dot{m} \cdot h \quad (3.1)$$

where  $\dot{Q}$  = the rate of heat transfer into the system

$\dot{W}$  = the rate of work done by the system

$\dot{m}_{IN}, \dot{m}_{OUT}$  = mass flow rate of each inlet and exit flow stream respectively

$h_{IN}, h_{OUT}$  = enthalpies corresponding to the each inlet and exit flow stream respectively

---

1. Motor losses are estimated using the motor model by Umans. [1]

2. In the equation, potential- and kinetic-energy changes are assumed negligible and their terms are dropped.

$\dot{Q}$  is the net heat transfer across the boundary of the control volume and the volume heating due to the losses of in the motor components and of the bearings. Note that for a vapor (or oil) stream, the change in energy term can be simplified to:

$$\left( \sum_{OUT} \dot{m} \cdot h - \sum_{IN} \dot{m} \cdot h \right)_{vapor} = (\dot{m} \cdot C_p \cdot (T_{OUT} - T_{IN}))_{vapor} \quad (3.2)$$

where  $T_{IN}$ ,  $T_{OUT}$  = temperatures of the vapor stream entering and exiting the control volume respectively

$C_p$  = specific heat of the vapor at constant pressure

For the SC37 compressor, nine circumferential control volumes (CV1 to CV9) were defined in the model, as shown in Figure 3.1, along with the vapor flow path from the suction pipe to the scroll pump, the vapor flow paths circulating through the motor, and the flow path of the circulating oil. The description of the split zone, the oil circulation, and the detailed energy balance for each control volume are presented in the following subsections.



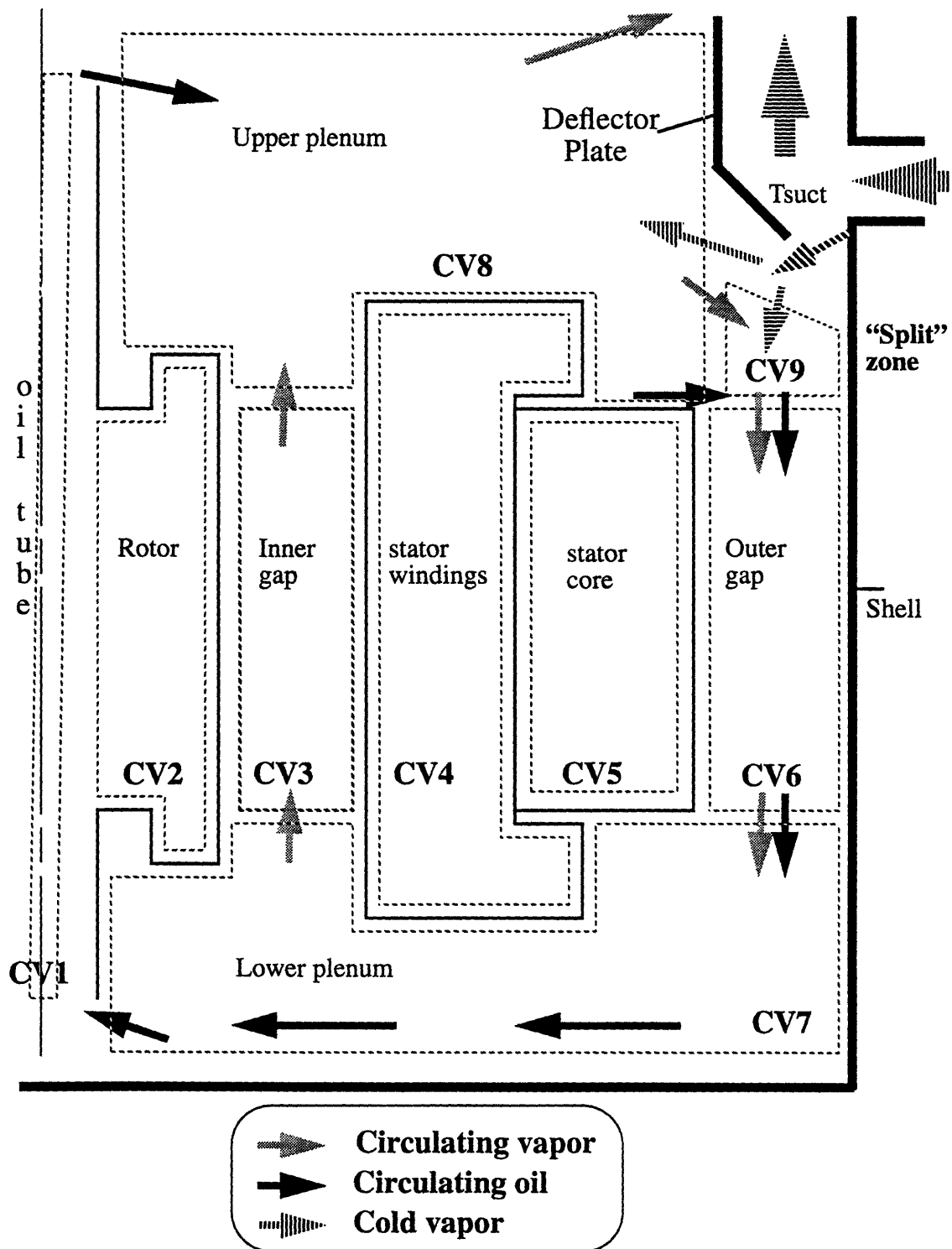


**Figure 3.1:** Schematic of the control volumes defined for SC compressor

### 3.2.1 The “split” zone

The “split” zone is the control volume below the hole at the bottom of the deflector plate (CV9). The following mechanism is assumed for partitioning the cold vapor which is discharged from the bottom hole of the deflector plate between that circulated through the motor and that immediately mixed in the upper plenum. Of the amount of  $\dot{m}_2$ <sup>1</sup> being discharged through the bottom hole of the deflector plate, a fraction of it ( $= \text{frac}_2 \cdot \dot{m}_2$ ) is mixed with the warm vapor and the circulating oil leaving the upper plenum and flowing into CV9. The resultant mixture flows down the outer gap (CV6). The fraction,  $\text{frac}_2$ , is determined by the geometry of the mixing zone. The conservation of mass of the R-22 vapor in CV9 leads to the following equation:

$$\text{frac}_2 \cdot \dot{m}_2 + \text{frac}_1 \cdot \dot{m}_1 = \dot{m}_1 \quad (3.3)$$

where  $\dot{m}_1$  = the mass flow rate of the R-22 vapor circulating through the motor<sup>2</sup>

$\text{frac}_1$  = fraction of  $\dot{m}_1$  flowing from CV8

Note that same amount of circulating oil flows in and out of the control volume. The remaining cold vapor ( $(1 - \text{frac}_2) \cdot \dot{m}_2$ ) flows directly into CV8. Figure 3.2 is a schematic of the flow splitting and mixing mechanism mentioned above.

- 
1. The fluid mechanics model, described in Chapter 2, predicted 20% of the cold vapor was discharged through the hole at the condition of 90 psia and 60 °F.
  2. The fluid mechanics model predicted  $\dot{m}_1$  was 81.0 lbm/hr at a condition of 90 psia and 140 °F.

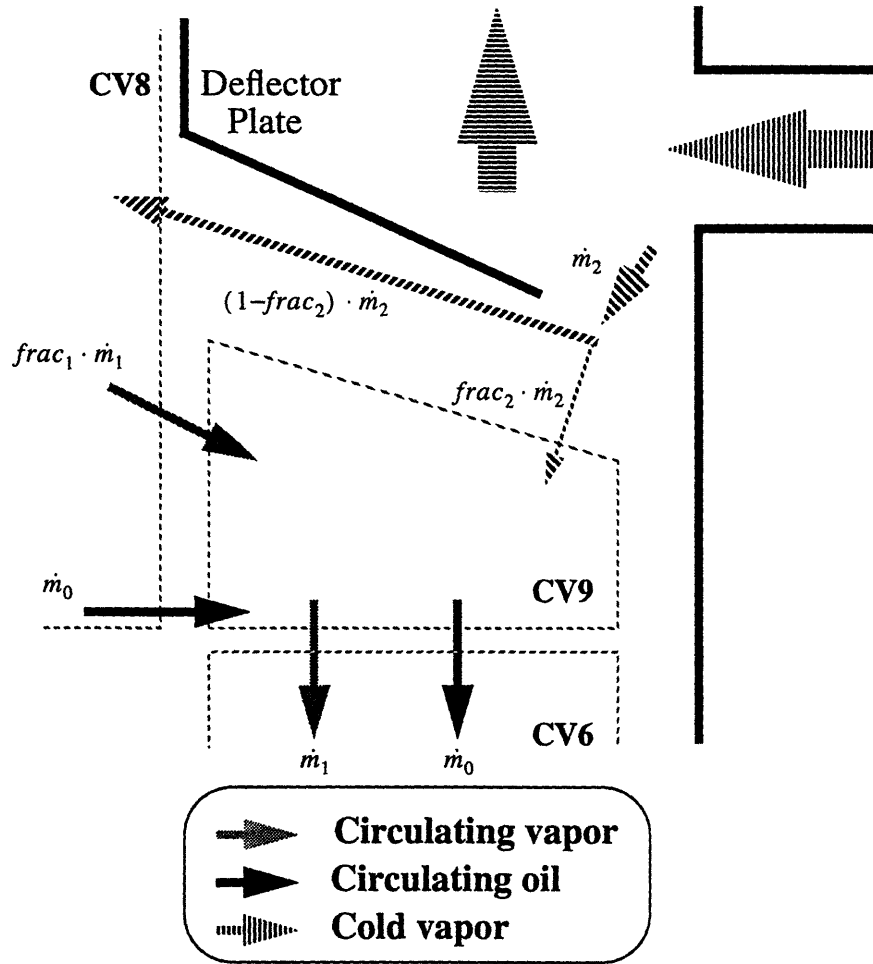


**Figure 3.2:** Schematic of the flow splitting and mixing mechanism in CV9

### 3.2.2 Thermal influence of the lubricating oil

As described in Section 2.5, the lubricating oil is assumed to be in a closed circulation path around the motor compartment. Here, it is further assumed that the oil exits CV8 at the same temperature as the core. The thin oil film on the top of the core has high thermal conductivity and is assumed to reach a thermal equilibrium with the core while it flows towards the outer gaps. When the oil flows across the entrance to the outer gaps, part of the oil stream crosses the warm R-22 vapor stream. Because of this intimate contact, both streams are assumed to be equal in temperature. Furthermore, it is assumed that this oil temperature is the same as the R-22 vapor in the outer gaps and in the lower plenum.

### 3.2.3 Control volumes

Refer to Figure 3.3, where the temperatures for various regions around the motor are defined. For each control volume, a steady state energy balance is provided.

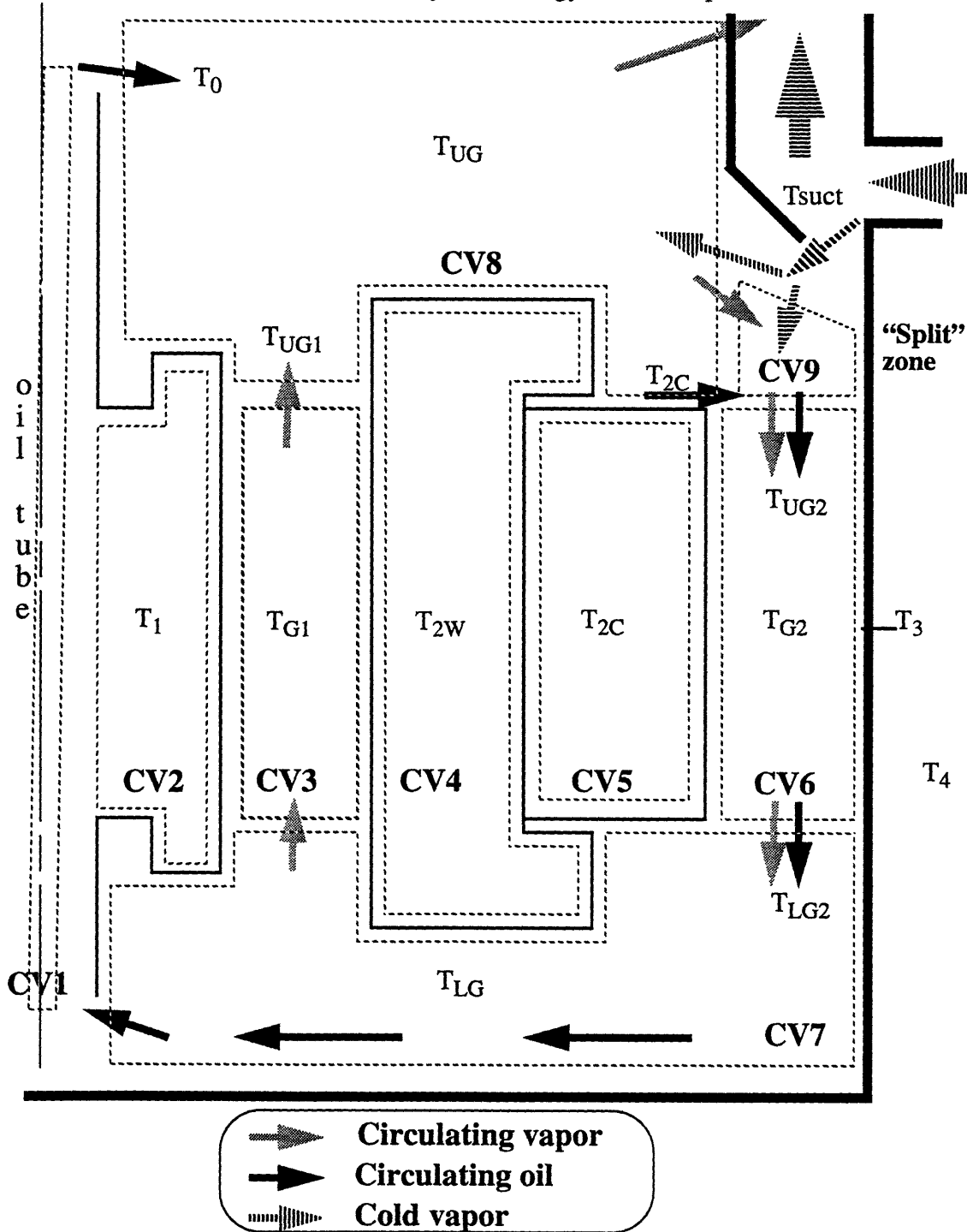


**Figure 3.3:** Schematic of the control volumes with defined temperatures

• CV1:

CV1 includes the oil in the inclined oil tube inside the shaft in the rotor. It is bounded a plane just above the lower journal bearing and one just above the upper bearing. Oil flows in from the lower plenum at  $T_{LG}$ . While the oil flows up, heat is transferred between the oil and the rotor. Heat generated from the upper bearing ( $Q_{u\_bearing}$ ) is assumed to be added to the oil in this control volume. The oil leaves the control volume at  $T_o$ . The energy balance is:

$$Q_{u\_bearing} + h_o A_o \left( T_1 - \left( \frac{T_o + T_{LG}}{2} \right) \right) = \dot{m}_o C_o (T_o - T_{LG}) \quad (3.4)$$

where  $\dot{m}_o$  = the mass flow rate of the R-22 vapor circulating around the motor

$C_o$  = specific heat capacity of the circulating oil

$h_o$  = heat transfer coefficient between the rotor and the oil stream

$A_o$  = cylindrical area of the oil tube for heat transfer

• CV2:

CV2 is the rotor. It is assumed to be at a uniform temperature of  $T_1$  due to its high axial thermal conductivity and the relatively small rotor losses,  $Q_{ROTOR}$ . The rotor exchanges heat with the circulating oil in the oil tube at the temperature of  $\left( \frac{T_o + T_{LG}}{2} \right)$  and also exchanges heat with the R-22 vapor in the inner gap at  $T_{G1}$ . The heat transfer from the top and the bottom of the rotor is neglected in this model. The energy balance is:

$$Q_{ROTOR} - h_1 A_1 (T_1 - T_{G1}) = h_o A_o \left( T_1 - \left( \frac{T_o + T_{LG}}{2} \right) \right) \quad (3.5)$$

where  $h_1$  = heat transfer coefficient in the inner gap

$A_1$  = cylindrical surface area of the rotor for heat transfer

• CV3:

CV3 is the inner gap between the rotor and the stator in which the R-22 vapor flows from the lower plenum (CV7) at  $T_{LG}$ . While the vapor is flowing up along the gap, heat is

transferred between the vapor at  $T_{G1}$  and the rotor at  $T_1$  and also between the vapor and the stator windings at a uniform temperature,  $T_{2W}$ . The vapor leaves at  $T_{UG1}$  and flows into the upper plenum (CV8). The energy balance is:

$$Q_{FRIC} + h_1 A_1 (T_1 - T_{G1}) - h_1 A_1 (T_{G1} - T_{2W}) = \dot{m}_1 C_g (T_{UG1} - T_{LG}) \quad (3.6)$$

where  $Q_{FRIC}$  = windage loss due to shear

$\dot{m}_1$  = the mass flow rate of the R-22 vapor circulating around the motor

$C_g$  = specific heat of the R-22 vapor

It is assumed that the heat transfer coefficients between the vapor and the rotor and between the vapor and the stator windings are the same. Furthermore, it is assumed that the vapor temperature within the gap,  $T_{G1}$ , is the average of the temperature entering and exiting the gap, i.e.:

$$T_{G1} = \frac{1}{2} (T_{LG} + T_{UG1}) \quad (3.7)$$

• CV4:

CV4 includes the stator windings. It is assumed the windings are at a uniform temperature,  $T_{2W}$ . The heat generated in the windings ( $Q_{WINDINGS}$ ) is either conducted to the stator core or convected to the inner gap as well as both the upper and lower plenums.

The energy balance is:

$$Q_{WINDINGS} - h_{WC} A_{WC} (T_{2W} - T_{2C}) + h_1 A_1 (T_{G1} - T_{2W}) - h_{W1} A_{W1} (T_{2W} - T_{UG}) - h_{W2} A_{W2} (T_{2W} - T_{LG}) = 0 \quad (3.8)$$

where  $h_{WC}$  = heat transfer coefficient between the windings and the core

$A_{WC}$  = effective contact area for heat transfer

$h_{W1, W2}$  = convective heat transfer coefficients of the top and bottom stator winding end turns respectively

$A_{W1, W2}$  = corresponding areas of the top and bottom winding end turns which are exposed to the upper and lower plenums for heat transfer

• CV5:

CV5 is the stator core. It experiences a net electrical losses of  $Q_{CORE}$  and is at a uniform temperature of  $T_{2C}$ . Heat is transferred through the core, the windings at  $T_{2W}$ , the shell at  $T_3$  and the vapor/oil streams in the two outer gaps which are at  $T_{G2}$ . It is assumed that the core transfers heat to the shell both through the direct contact and across the thin gaps (other than the two “big” outer gaps) which are filled with R-22 vapor. It is assumed that there is negligible axial flow in those thin gaps. The heat transfer across the narrow gaps is modelled as heat conduction through a thin layer of R-22 vapor. The energy balance is:

$$Q_{CORE} + h_{WC}A_{WC}(T_{2W} - T_{2C}) - h_2A_2(T_{2C} - T_{G2}) - h_{2C}A_{2C}(T_{2C} - T_3) = 0 \quad (3.9)$$

where  $h_2$  = heat transfer coefficient between the core and the oil/vapor in the outer gap

$h_{2C}$  = heat transfer coefficient between the core and the shell (combined heat transfer through direct contact and across the thin gaps)

$A_{2,2C}$  = effective areas for heat transfer of the corresponding heat transfer coefficients

• CV6:

CV6 consists of the two outer gaps. Circulating oil and R-22 vapor at  $T_{UG2}$  flow in from CV9 and flow out at  $T_{LG2}$  to CV 7 after heat is transferred between the mixture, the core, and the shell. The energy balance is:

$$h_2A_2(T_{2C} - T_{G2}) - h_{2C}A_{2C}(T_{G2} - T_3) = \dot{m}_o C_o (T_{LG2} - T_{UG2}) + \dot{m}_1 C_g (T_{LG2} - T_{UG2}) \quad (3.10)$$

It is assumed that the vapor temperature,  $T_{G2}$ , is the average of the temperature entering and exiting the gap, i.e.:

$$T_{G2} = \frac{1}{2} (T_{LG2} + T_{UG2}) \quad (3.11)$$

• CV7:

CV7 is the lower plenum, below the motor. Circulating oil and R-22 vapor flow in from CV6 at  $T_{LG2}$  and flow out at  $T_{LG}$ , the average lower plenum temperature. Heat is transferred from the windings to the control volume and from the control volume to the shell. Also, heat generated from the lower bearings ( $Q_l$ ) is added to the control volume. The energy balance is:

$$Q_l + h_{w2}A_{w2}(T_{2w} - T_{LG}) - h_lA_l(T_{LG} - T_3) = \dot{m}_oC_o(T_{LG} - T_{LG2}) + \dot{m}_1C_g(T_{LG} - T_{LG2}) \quad (3.12)$$

where  $h_l$  = heat transfer coefficient between the lower plenum and the shell

$A_l$  = effective area for heat transfer

• CV8:

CV8 is the upper plenum. It includes the region above the motor and below the separating plate but excludes the scroll pump and the main suction duct inside the deflector plate. The cold R-22 vapor ( $(1 - \text{frac}_2) \cdot \dot{m}_2$ ) at  $T_{SUCT}$  and the hot R-22 vapor at  $T_{UG1}$  from CV3 flow into the control volume and are assumed to reach an equilibrium temperature of  $T_{UG}$  because of the mixing facilitated by the spinning counterweight. The circulating oil at  $T_0$  flows from CV1 and enters CV9 at  $T_{2C}$  (as described in Section 3.2.2). A fraction of the warm vapor ( $\text{frac}_1 \cdot \dot{m}_1$ ) enters CV9 along with the warm circulating oil. The remaining warm vapor ( $\dot{m}_2$ ) leaves the control volume and enters the scroll pump suction port to be compressed. Heat transfer from the discharge port, as well as from the bottom of the scroll pump is represented as  $Q_u$ . Heat transferred also occurs between the control volume, the stator windings, and the shell. The energy balance is:

$$\begin{aligned} & Q_u + h_{w1}A_{w1}(T_{2w} - T_{UG}) - h_uA_u(T_{UG} - T_3) \\ & = \dot{m}_oC_o(T_{2C} - T_0) + \dot{m}_2C_gT_{UG} + \dot{m}_1C_g \cdot \text{frac}_1T_{UG} \\ & \quad - \dot{m}_1C_gT_{UG1} - \dot{m}_2C_g(1 - \text{frac}_2)T_{SUCT} \end{aligned} \quad (3.13)$$

where  $h_u$  = heat transfer coefficient between the upper plenum and the shell

$A_u$  = effective area for heat transfer



Using EQ 3.3 (conserving the mass in the vapor streams), EQ 3.13 yields a simplified form:

$$\begin{aligned} & Q_u + h_{w1}A_{w1}(T_{2w} - T_{UG}) - h_uA_u(T_{UG} - T_3) \\ &= \dot{m}_o C_o (T_{2C} - T_0) + \dot{m}_1 C_g (T_{UG} - T_{UG1}) + \dot{m}_2 C_g (1 - \text{frac}_2) (T_{UG} - T_{SUCT}) \end{aligned} \quad (3.14)$$

• CV9:

CV9 is the split zone described in the previous section (3.2.1). Its energy balance is:

$$0 = \dot{m}_o C_o (T_{2C} - T_{UG2}) + \dot{m}_2 \text{frac}_2 C_g T_{SUCT} + \dot{m}_1 \text{frac}_1 C_g T_{UG} - \dot{m}_1 C_g T_{UG2} \quad (3.15)$$

An additional energy balance is applied to the shell of the compressor to obtain the following equation:

$$h_2 A_2 (T_{G2} - T_3) + h_{2C} A_{2C} (T_2 - T_3) + h_l A_l (T_{LG} - T_3) + h_u A_u (T_{UG} - T_3) - h_3 A_3 (T_3 - T_4) = 0 \quad (3.16)$$

where  $h_3$  = total ( sum of convective and radiative) heat transfer coefficient

$A_3$  = effective shell area for heat transfer

$T_4$  = ambient temperature

Appendix B shows the calculation of the heat transfer coefficients used in the model for a SC37 compressor.

### 3.2.4 Resulting system of equations

EQ 3.4 to 3.16 constitutes a system of 12 equations and 13 unknowns. Using  $\text{frac}_2$  as a parameter that is adjusted on the basis of Experiment 2 described in Chapter 5, the system of equations becomes soluble and the unknowns can be evaluated simultaneously. The resulting system of equations, in a 12x12 matrix format, is shown in Figure 3.4.

33

**Figure 3.4:** The system of equations of the heat transfer model (continues on the next page)

$$\begin{array}{c}
 T_0 \\
 T_1 \\
 T_{2W} \\
 T_3 \\
 T_{G1} \\
 * T_{G2} \\
 T_{UG} \\
 T_{UG1} \\
 T_{UG2} \\
 T_{LG} \\
 T_{LG2} \\
 T_{2C}
 \end{array}
 =
 \begin{array}{c}
 Q_{u\_bearings} \\
 Q_{ROTOR} \\
 -Q_{FRIC} \\
 Q_{WINDINGS} \\
 0 \\
 -Q_l \\
 -Q_u - m_2 C_g (1 - frac_2) T_{SUCTION} \\
 -m_2 C_g frac_2 T_{SUCTION} \\
 -Q_{CORE} \\
 0 \\
 0 \\
 -h_3 A_3 T_4
 \end{array}
 \begin{array}{c}
 (3.4) \\
 3.5 \\
 3.6 \\
 3.8 \\
 3.10 \\
 3.12 \\
 3.13 \\
 3.14 \\
 3.15 \\
 3.9 \\
 3.7 \\
 3.11 \\
 3.16
 \end{array}
 \quad EQ:$$

**Figure 3.4:** The system of equations of the heat transfer model (continued from the previous page)

### 3.3 Cooling mechanism for the motor

In the motor heat transfer model, part of the heat generated from the motor compartments is carried away by the cold suction vapor drawn into the upper plenum. The cold suction vapor which is discharged into the plenum (CV8) then mixes with hot vapor already in the plenum. The mixed vapor then leaves the plenum and enters the scroll pump for compression, as described in Section 2.2.1. For this reason, supplying more cold vapor means increasing the cooling capacity of the vapor stream passing through the plenum and its ability to extract heat from the motor compartment. Heat is transferred to the upper plenum by convection from the top of the core and the top winding end turns. Heat is conducted upwards from the various parts of the motor by the windings with their relatively high thermal conductivity. It is then convected to the vapor in the plenum. The circulating vapor and oil streams (described in Section 2.2.2) also “transport” part of the heat generated from the motor to the upper plenum as these fluids circulate through the motor.

Additional cooling of the motor is done by convection across the outer gaps through the shell and to the ambient air. Heat generated in the stator is also conducted to the shell through the direct contact between the core and the shell surface.

### **3.4 Implementation of the model using a Fortran computer program**

A Fortran computer program<sup>1</sup>, as shown in Appendix C, was written to solve the system of equations. This program facilitates the calculation of the solution for different suction conditions and motor loads. For a fixed geometry configuration and all heat transfer coefficients determined, the model can determine the steady state temperature distribution and the amount of heat being transferred to the cold vapor at different input conditions. The input variables are:

1. Suction temperature ( $T_{\text{SUCT}}$ )
2. System mass flow rate into the compressor ( $m_0$ )
3.  $\text{Frac}_0$ , the fraction of the cold R-22 vapor which is discharged into the upper plenum
4.  $\text{Frac}_2$ , the fraction of the cold R-22 vapor flows down the outer gaps
5. Ambient temperature ( $T_4$ )
6. Losses from each motor's component ( $Q_{\text{ROTOR}}$ ,  $Q_{\text{WINDINGS}}$ , and  $Q_{\text{CORE}}$ )

This program is also capable of predicting the effect of any physical dimension change inside the compressor. It is useful as an analytical tool for examining future design changes. For example, to examine the effect of changing the direct contact area between the stator core and the shell can be done by adjusting the value of the variable  $A_{2C}$  in the program.

---

1. In the computer program, two subroutines used, ludcmp and lubksb, were copied from the computer files of Numerical Recipes by Press. [8]

## Chapter 4

### Experiment 1: Measurement of the Outside Convective Heat Transfer Coefficient of the SC37 Compressor Shell in a 38 TKB Outdoor Condenser

#### 4.1 Introduction

In this chapter, an experiment is described in which the outside convective heat transfer coefficient from the SC37 compressor shell to the surroundings in a 38TKB condenser was measured. The coefficient was determined by measuring the condensate formed inside an empty SC37 shell while it was supplied with saturated steam. Empirical correlations of the measured data are provided for the calculation of the coefficient for this system and other, geometrically similar, systems.

Figure 4.1 shows the schematic of the system. The SC37 compressor shell is roughly bullet-shaped. The shell is placed on stubby legs inside the 38TKB outdoor condenser with air flowing in from 3 sides. The air passes through a set of heat exchanger coils and then flows out through the top opening. The air flow is propelled by the condenser's fan at the top opening of the casing. Heat released inside the shell will be transferred to the air stream because of the temperature difference between the shell and the air stream. The outside convective and radiative heat transfer coefficients ( $\bar{h}_{conv}$  and  $\bar{h}_{rad}$ ) from the compressor shell to the surroundings are defined below.

$$q = \bar{h}_{Total} A (T_s - T_o) \quad (4.1)$$

$$\text{and} \quad \bar{h}_{Total} = \bar{h}_{conv} + \bar{h}_{rad} \quad (4.2)$$

where  $q$  = the total heat transfer from the shell

$A$  = the area

$T_s$  = the shell temperature

$T_o$  = the surrounding temperature outside the shell.

While  $\bar{h}_{rad}$  can be estimated using the Stefan-Boltzmann Law, the uniqueness of the air flow pattern for this system requires measurements to determine  $\bar{h}_{conv}$ .

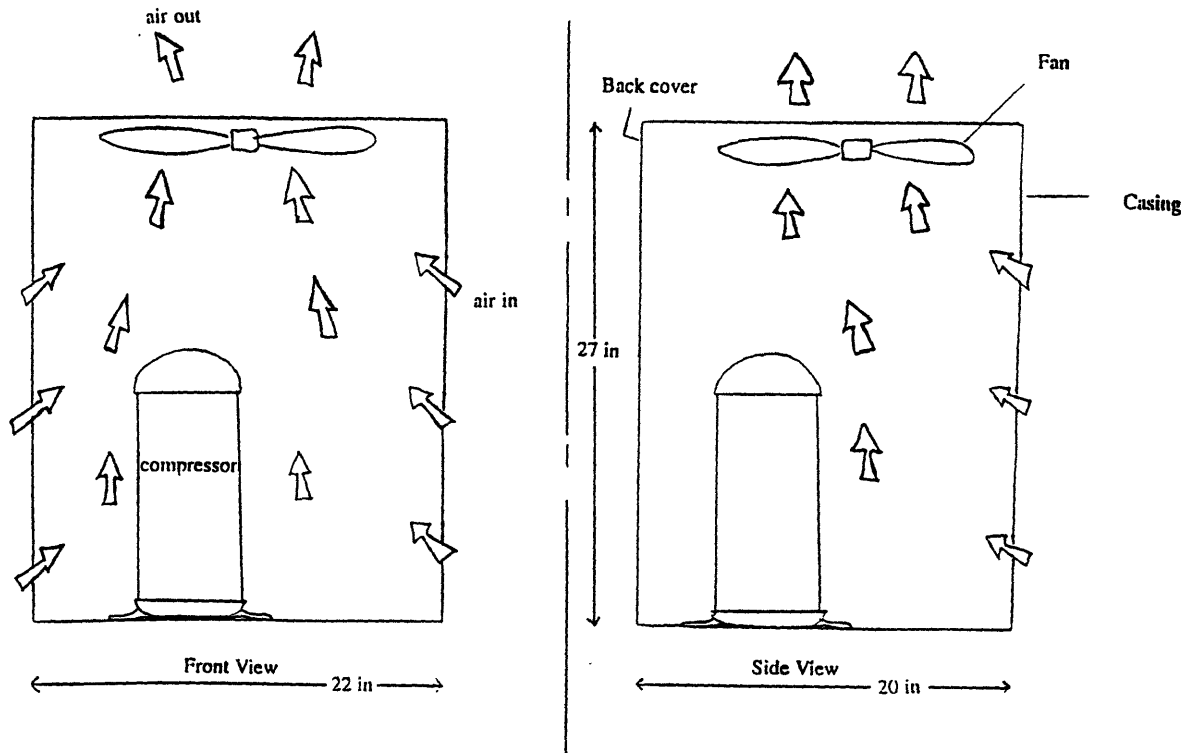


**Figure 4.1:** Schematic of the system

## 4.2 Procedure

### 4.2.1 Setup

In this experiment, an empty shell replaces the hermetic compressor in the condenser unit casing. With the fan blowing as usual, the interior of the shell is injected with saturated steam at a pressure very close to atmospheric pressure. The heat transfer from the shell surface causes condensate to form on the inside wall of the shell. The heat transfer rate ( $q$ ) can be inferred from the condensation rate ( $\dot{m}$ ):

$$q = \dot{m} \cdot h_{fg} = \bar{h}_{Total} A (T_s - T_o) \quad (4.3)$$

where  $h_{fg}$  is the latent heat of vaporization of the steam.

Thus, by measuring the area of the shell (A), the temperatures ( $T_s$  &  $T_o$ ), and the rate at which condensate accumulates,  $\bar{h}_{Total}$  can be calculated. Inside the empty shell, several condensate collectors (gutters) and rubber tubes have been installed to collect the water condensed from four separate sections: the top dome, the upper vertical section, the middle vertical section, and the lower section. The top dome corresponds to the region inside the shell where the hot R-22 vapor is discharged from the scroll pump. The upper vertical section corresponds to the region outside the scroll pump. The middle vertical section corresponds to the region outside the motor. The lower section includes the oil sump and the stubby legs. See Figure 4.2 for the setup.

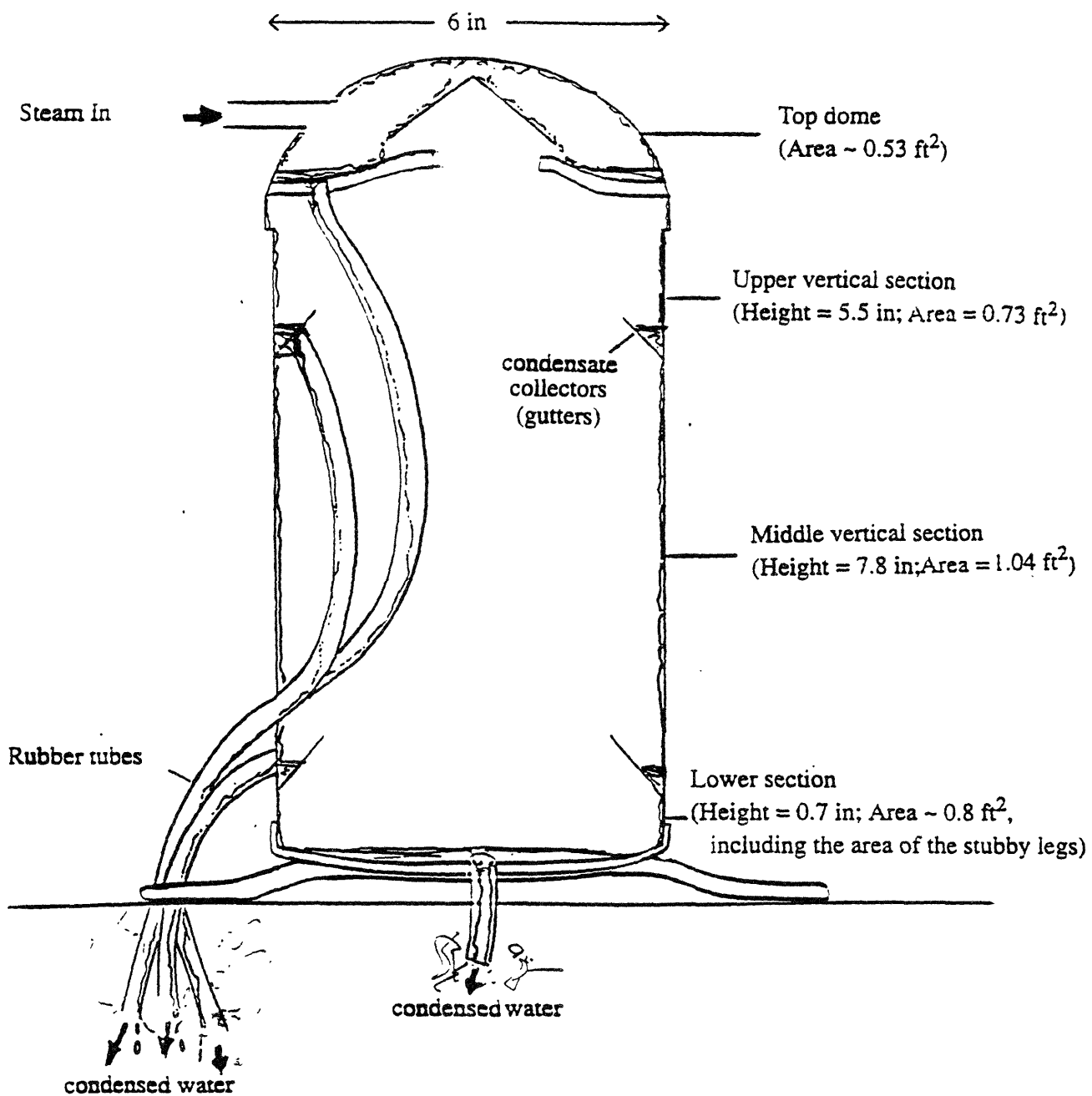


Figure 4.2: Setup of the experiment



#### 4.2.2 Assumptions

Several assumptions are made in reducing the data from this experiment. The temperature inside the empty shell as well as at the shell surface is taken to be 672 °R (212 °F), which is the saturation temperature of water at atmospheric pressure. In essence we are assuming that the thermal resistances of the shell material and the condensing film are negligible compared to the air film on the outside surface<sup>1</sup>. In addition, the steam is supplied slightly in excess until vapor comes out of the rubber tubes. This insures that the entire shell is active in transferring heat at the nominal inside temperature. It also insures the removal of any non-condensable gas which enters with the steam.

#### 4.2.3 Measurement

In the experiment, the time (t) it takes for the condensate from each section to be collected in container of volume (v) is measured. Then the condensation rate ( $\dot{m}$ ) is calculated as follows:

$$\dot{m} = v \rho / t \quad (4.4)$$

where  $\rho$  = the density of the condensate which saturated water in this case

The reduced form of the Stefan-Boltzmann Law gives an expression for the radiation heat transfer coefficient  $\bar{h}_{rad}$ :

$$\bar{h}_{rad} = \epsilon \sigma (T_s + T_o) (T_s^2 + T_o^2) \quad (4.5)$$

where  $\sigma = 0.1714 \times 10^{-8}$  Btu/hr-ft<sup>2</sup>-R<sup>4</sup> (the Stefan-Boltzmann constant)

$\epsilon = 0.9$  (the emissivity of the painted shell)

$T_s = 672$  °R (212 °F)

$T_o = 540$  °R (80 °F)

yielding  $\bar{h}_{rad} = 1.40$  Btu/hr-ft<sup>2</sup>-F°. After  $\bar{h}_{rad}$  is found,  $\bar{h}_{conv}$  can be calculated using EQ

4.2.

---

1. The estimated thermal resistance (1/h) for the shell material and the condensing film for the steam are  $0.8 \times 10^{-3}$  and  $2.70 \times 10^{-4}$  [(Btu/hr-ft<sup>2</sup>-F)<sup>-1</sup>] respectively while the outside resistance is in the order of  $10^{-1}$  [(Btu/hr-ft<sup>2</sup>-F)<sup>-1</sup>]

#### 4.2.4 Empirical correlations calculation

The empirical correlations for calculating the convective heat transfer coefficient are based on the general form for external flow over a surface<sup>1</sup>:

$$\overline{Nu}_L = C Re_L^m Pr^{1/3} \quad (4.6)$$

$$\text{or} \quad \frac{\bar{h}_{conv} L}{k} = C \left( \frac{VL}{\nu} \right)^m Pr^{1/3} \quad (4.7)$$

where  $\overline{Nu}_L$ ,  $Re$ , and  $Pr$  are the Nusselt, Reynolds, and Prandtl Numbers respectively.

The values of  $C$  and  $m$  depend on the characteristic of the flow and the geometry of the surface. All fluid properties are evaluated at the film temperature ( $T_f = \frac{T_s + T_\infty}{2}$ ). Note that EQ 4.6 and 4.7 do not account for natural convection as it is assumed that the effects of the natural convection are small compared to the forced convection from the shell's surface.

Using the results from these measurements, three correlations are constructed. The regions are the top dome, the vertical section, and the lower section. In the correlations, the vertical section includes both the upper and middle sections and the calculated  $\bar{h}_{conv}$  is the area average of the two. The union of the upper and middle sections in the correlation is needed in order to facilitate and simplify the usage of the correlation. For each section that is distinguished, a type of flow field must be assumed in order to define the appropriate characteristic length ( $L$ ) and velocity ( $V$ ). While the air velocity over the shell surface increases with elevation,  $V$  for each section is calculated based on the following formula:

$$V = \frac{\dot{Vol}}{Area_{AR}} = \frac{\dot{Vol}_{total} \cdot \left( \frac{\text{Average elevation of the section}}{\text{Elevation of the fan}} \right)}{Area_{AR}} \quad (4.8)$$

where  $\dot{Vol}$  = average air volume flow rate flowing over each section

---

1. Validity of the general form is explained in many heat transfer textbooks. The suggested reference is Introduction to Heat Transfer by Incropera and DEWitt [6].

$\dot{Vol}_{total}$  = total air volume flow rate flowing through the fan (specified by the fan capacity)

Area<sub>AR</sub> = Area of the annular ring formed by the compressor shell and the casing

In above formula, air is assumed to be flowing into the casing uniformly through the condenser's coil. Thus the ratio  $\dot{Vol}$  of a section to  $\dot{Vol}_{total}$  is proportional to the average elevation of the section to the elevation of the fan (the height of the casing). For the 38TKB condenser,  $\dot{Vol}_{total}$  is 1900 cfm, the elevation of the fan is 16 in, and Area<sub>AR</sub> is 2.86 ft<sup>2</sup>. Over the top dome, the flow is believed to separate, leaving as a wake. The diameter of the shell is the characteristic dimension of the dome and thus should be used as L. For the vertical section, the air flows approximately as it would in parallel flow over a flat plate, where both the velocity and the thermal boundary layers develop from the base of the vertical section of the shell. So L is length of the vertical section, measured from the base where the section and the stubby legs intersect. The heat transfer over the lower section is more complex than that for the vertical section and the top dome. There are several modes of convective heat transfer present: forced convection at the bottom region of the shell, heat transfer enhancement through the stubby legs acting as fins, and natural convection in the gap beneath the shell. Nevertheless, the general form of EQ 4.6 and the procedures to find m and C will be used as a first approximation for the empirical correlation. The length of the stubby leg is used as L. See Figure 4.3 for the schematic drawing of the shell with the location of L's indicated.

In order to find m, the speed of the fan<sup>1</sup> was varied and the resulting  $\bar{h}_{conv}$  determined. Taking the ratio of EQ 4.7 for the 2 sets of conditions:

$$\frac{\bar{h}_{conv1}}{\bar{h}_{conv0}} = \left( \frac{V_i}{V_o} \right)^m \quad (4.9)$$

---

1. Different fan speeds are achieved by using a variable frequency AC power generator.

Assuming the air velocity flowing inside is directly proportional to the fan speed ( $\omega$ ), EQ 4.9 becomes:

$$\frac{\bar{h}_{conv1}}{\bar{h}_{conv0}} = \left( \frac{\omega_i}{\omega_o} \right)^m \quad (4.10)$$

Using a stroboscopes to determine the fan speeds,  $m$  can be calculated from EQ 4.10.  $C$  can then be calculated using EQ 4.7 and the measured value of  $\bar{h}_{conv}$ . Note that for the vertical section, the average  $\bar{h}_{conv}$  of the upper and middle vertical sections were used to calculate  $m$  and  $C$ .

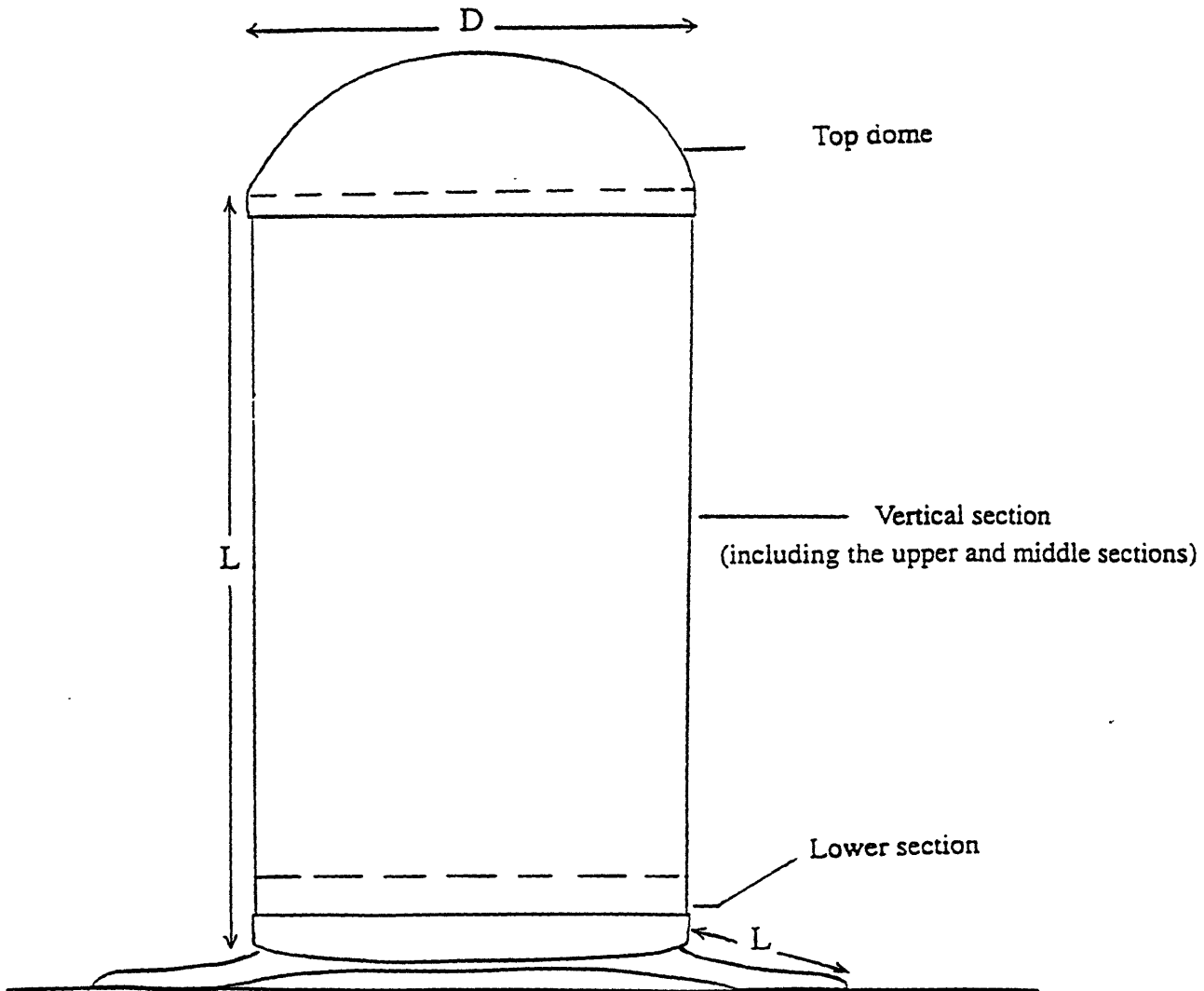


**Figure 4.3:** Schematic drawing of the compressor's shell

### 4.3 Results and Discussions

A total of 9 runs were completed in the experiment at  $T_f = 606^\circ\text{R}$  ( $146^\circ\text{F}$ ). Run# 1 and 3 were done at the normal fan speed of 1100 rpm. Other runs were done at different fan speeds, varying between 525 and 1100 rpm. The condensation rate data acquired are listed in Appendix D. For each section, the average condensation rate values were used to determine  $\bar{h}_{Total}$  and  $\bar{h}_{conv}$  using EQ 2.2, EQ 2.3, and the value of  $\bar{h}_{rad}$ <sup>1</sup>. The calculations are detailed in Appendix D. Table 4.1 shows the average measured values of  $\bar{h}_{Total}$  and  $\bar{h}_{conv}$  at normal fan speed (1100 rpm) and Figure 4.4 show the average  $\bar{h}_{conv}$  versus different fan speeds.

**Table 4.1:** Average measured values of  $h_{total}$  and  $h_{conv}$  at Normal fan speed

	$h_{total}$ [Btu/hr-ft <sup>2</sup> -F]	$h_{conv}$ [Btu/hr-ft <sup>2</sup> -F]
Top dome	8.56	7.16
Upper vertical section	6.08	4.68
Middle vertical section	5.53	4.13
Lower section	4.32	2.92

---

1.  $\bar{h}_{rad} = 1.40 \text{ Btu/hr-ft}^2\text{-F}$  (calculated in Procedure section).

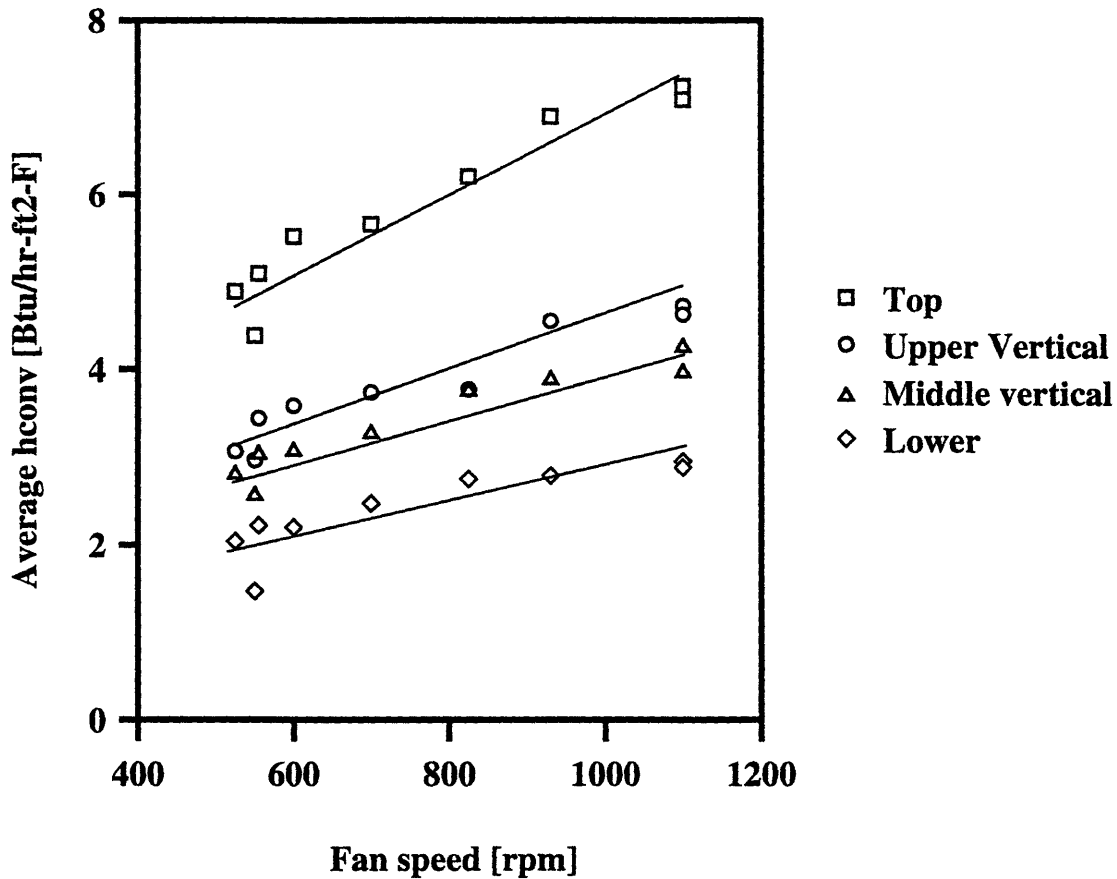


**Figure 4.4:** Average  $\bar{h}_{conv}$  versus fan speed

From Figure 4.4,  $\bar{h}_{conv}$  increases monotonically with the speed of the fan and the elevation of the shell, except in Run# 2. The relatively high values for  $\bar{h}_{conv}$  at normal fan speed suggests that forced convection is the dominant mode of the heat transfer from the shell, compared with radiation (1.4 Btu/hr-ft<sup>2</sup>-F) and natural convection (~ 1 Btu/hr-ft<sup>2</sup>-F).

After Run# 2 was completed, a trace of steam was found coming out the crack between the top dome and the vertical section. This could have increased the local effective air temperature and reduced the amount of condensate formed. The crack was sealed using silicon sealant before Run# 3 was performed. From the plotted data shown in Figure 4.4, a lower than expected  $\bar{h}_{conv}$  was measured in Run# 2 probably because of the significant effect of the escaped steam to the heat transfer at low fan speed. For this reason,

the data of Run# 2 were not used in the calculation of coefficients “m” and “C”.

The exponent m and the coefficient “C” for each section were calculated using the equations described in the Procedure section (EQ 4.8, 4.9, and 4.10).  $\bar{h}_{conv}$  and  $\omega$  at the normal fan speed had been used as the fixed  $h_{conv0}$  and  $\omega_0$  in EQ 4.10 while  $\bar{h}_{conv}$  and  $\omega$  data at other fan speeds were treated as numerous  $h_{convi}$  and  $\omega_i$ . Figure 4.5 shows the graph of Log (hi/ho) versus Log (wi/wo). A least square calculation was used to obtain the exponent m for each section. The results are shown in Table 4.2. See Appendix D for the detailed calculations.

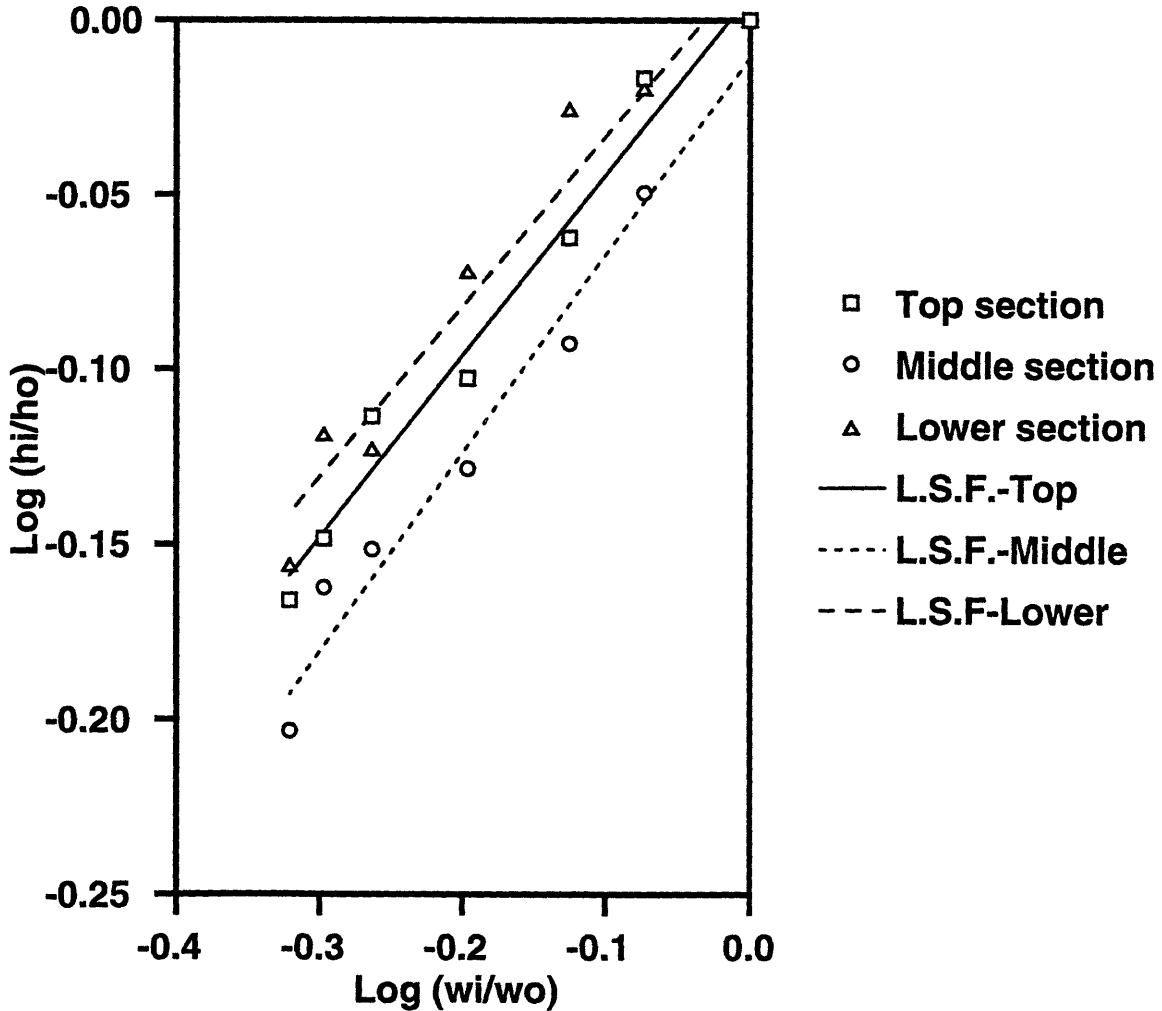


Figure 4.5: Graph of Log (hi/ho) versus Log (wi/wo)

**Table 4.2:** Calculated values of m and C

	m	C
Top dome	0.517	1.64
Vertical section	0.573	1.21
Lower section	0.486	2.41

The values of m of the top dome and the vertical section are within the expected ranges of a typical wake flow and a parallel flow over a flat plate respectively. The values of m indicate that the air stream is in the transition state between laminar and turbulent flow despite low length or diameter Re numbers calculated for both sections. It is believed that this is due to the turbulence which is induced when air flows through the condenser coils. The wakes due to the tubes passing through the fins increase the free stream turbulence and enhance the heat transfer from the shell. The value of C of each section is higher than that of a typical wake flow or parallel flow over a flat plate because of the choice of the characteristic velocity used for calculation and the unique flow field inside the condenser casing.

Table 4.3 shows the summary of the correlations found with the defined characteristics lengths and velocities. When applying the correlations, the fluid properties have to be scaled appropriately for different shell and ambient temperatures. Also,  $\bar{h}_{rad}$  has to be re-calculated using EQ 4.5. The correlations will be valid for the fan speed between 525 to 1100 rpm, where forced convection is the dominant mode of heat transfer. The correlations can also be used as an approximation to other geometrically similar systems such as the different sizes of the TKB outdoor condensers.



**Table 4.3:** Summary of Correlation expressions

	Char. Length	Empirical Correlation
Top dome	D = Diameter of the dome	$\overline{Nu}_D = \frac{\bar{h}_{conv}D}{k} = 1.64Re_D^{0.517}Pr^{1/3}$
Vertical section	L = Length of the vertical section of the shell	$\overline{Nu}_L = \frac{\bar{h}_{conv}L}{k} = 1.21Re_L^{0.573}Pr^{1/3}$
Lower section	L = Length of the stubby leg	$\overline{Nu}_L = \frac{\bar{h}_{conv}L}{k} = 2.41Re_L^{0.486}Pr^{1/3}$

$$\text{Char. velocity} \quad (V) = \frac{\dot{Vol} \cdot \frac{\text{Average elevation of the section}}{\text{Elevation of the fan}}}{\text{Area}_{AR}} \quad (4.8)$$

where  $\dot{Vol}$  = air volume flow rate through the fan (specified as the fan capacity)

$\text{Area}_{AR}$  = Area of the annular ring formed by the compressor shell and the casing

Elevation of the fan = 16 in (for 38TKB condenser)

## **Chapter 5**

### **Experiment 2: The Dynamometer Test**

#### **5.1 Introduction**

The purpose of the dynamometer test was to measure the steady state temperature distribution inside a SC37 compressor at different suction conditions and motor loads. In this experiment, the roles of the R-22 vapor and the circulating oil for the motor cooling as well as the mixing mechanism in the upper plenum were studied. The results were also compared to the simulations from the motor heat transfer model as a verification of the model.

#### **5.2 Procedures**

##### **5.2.1 Setup**

Figure 5.1 shows the schematic of the experiment setup. The basic components include an instrumented compressor, a DC motor, and a de-superheat loop. The compressor is actually a modified SC37 compressor in which the top and bottom domes are bolted to the cylindrical section. The scroll pump was removed and replaced with a coupling connecting the shaft of the rotor to the DC motor which simulates the load from the scroll pump. Inside the compressor, thermocouples were placed at various locations, including both the rotor and the stator of the motor, to determine the temperature distribution. Figure 5.2 shows the map of the thermocouples locations. The description of the locations is provided in Appendix E.

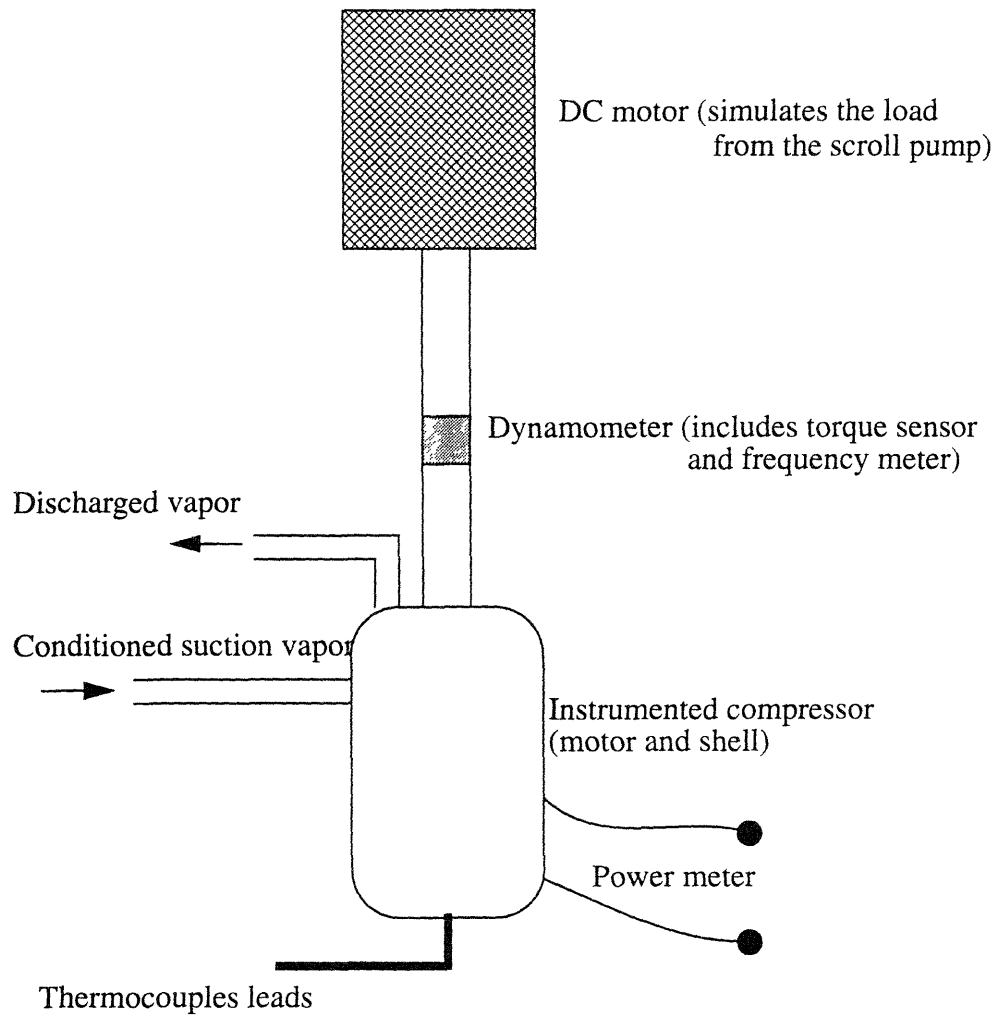


**Figure 5.1:** The setup of the dynamometer test

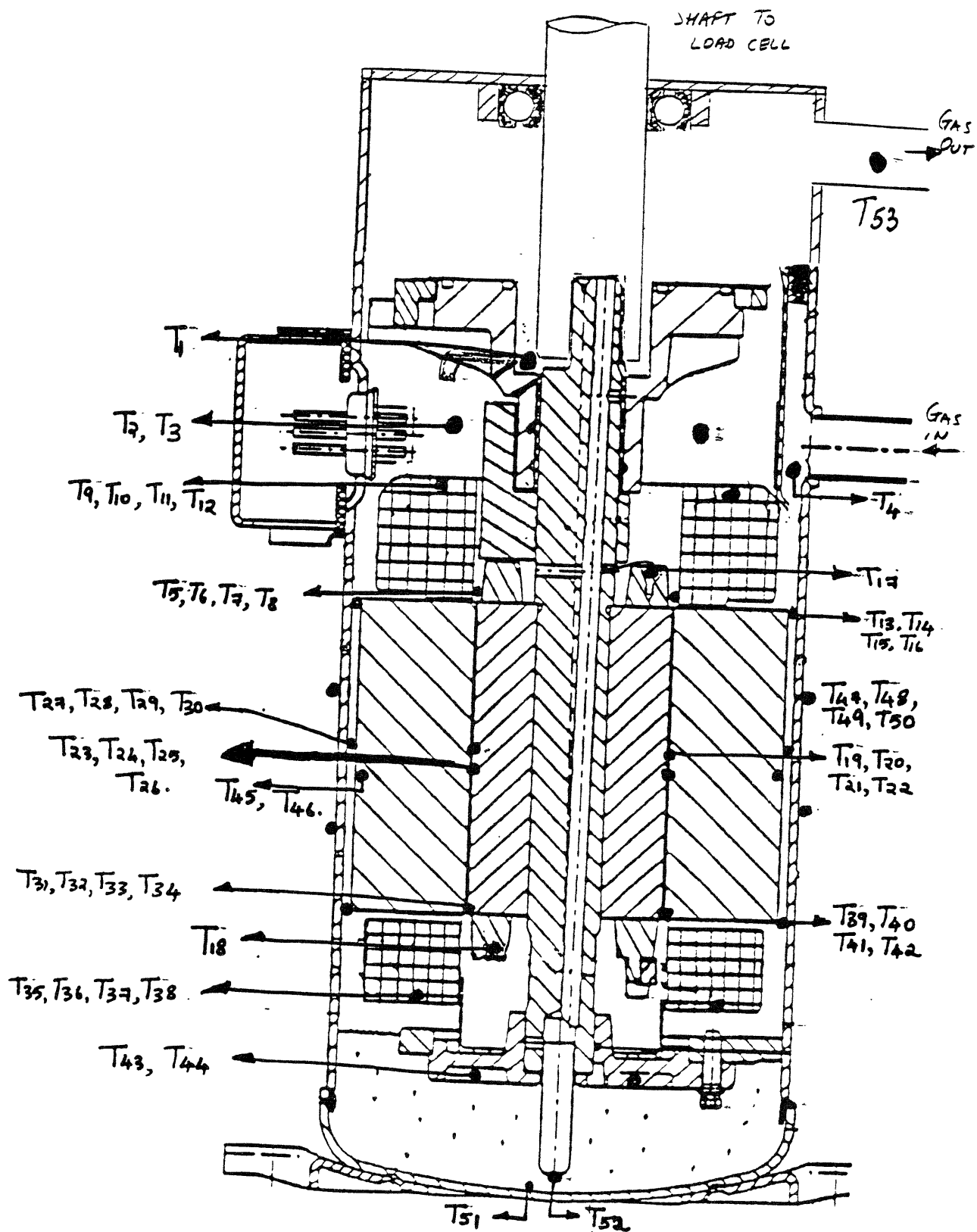
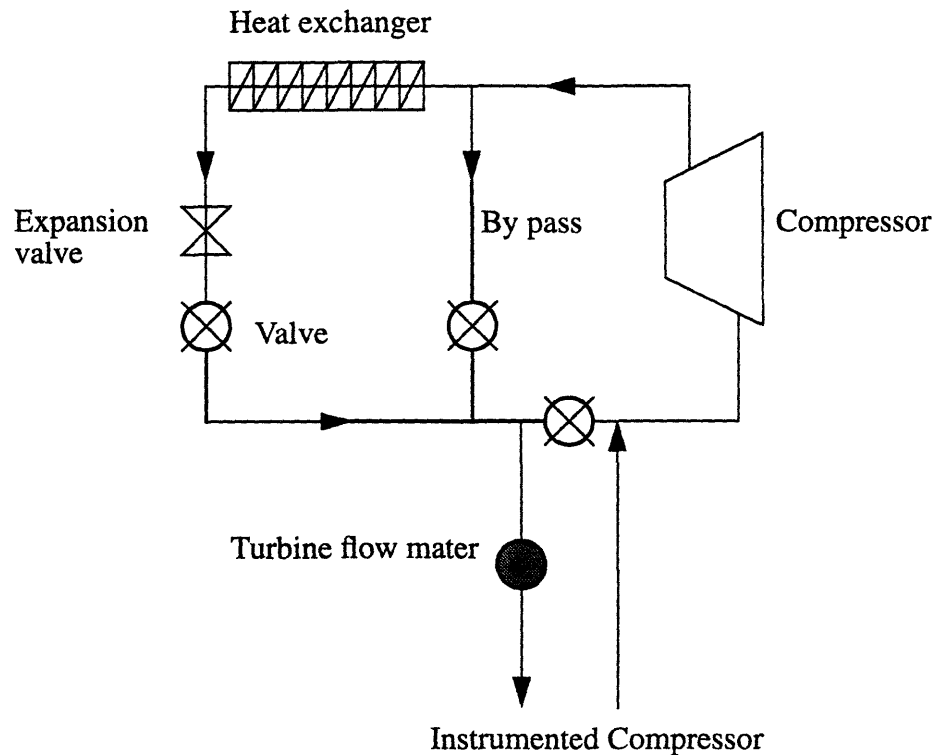


Figure 5.2: The map of the thermocouples locations

The de-superheat loop is used to reproduce different states of the R-22 vapor supplied to the compressor. Possible variations include pressure, temperature and flow rate. Figure 5.3 shows the schematic of the loop.



**Figure 5.3:** Schematic of the de-superheat loop

### 5.2.2 Measurement

In each test, the de-superheat loop was started first. The valves in the loop were adjusted until the desired state for the R-22 vapor flowing to the instrumented compressor was reached. Then, the DC motor was connected to a variable power supply and was brought up, along with the rotor in the instrumented compressor, to the normal operating speed for the compressor<sup>1</sup>. Then the compressor motor was turned on. After the variable

1. The normal speed of the SC37 compressor is slightly less than 3600 rpm.

power supply was turned off, a field current was applied to the DC motor until the specified load on the motor, in terms of the input power to the motor, was reached. The whole setup was left running until a steady state was observed. In the experiment, the temperature of the bottom winding end turns, which was expected to have highest temperature, was monitored until its temperature stopped rising. When a steady state had been reached, measurements were made and recorded. In general, it took three hours for a steady state to be reached.

The power input to the compressor ( $P_{in}$ ) was measured by an electric power meter and the power output from the motor ( $P_{out}$ ) was measured by the dynamometer placed in between the compressor and the DC motor. The accuracies of both meters were within 3% full scale. Thus for meter readings above 3000 W, an uncertainty of 100 W was expected. The power loss from the compressor, which was set equal to power input minus power output, was expected to have the same magnitude of variation.

The mass flow rate of the cold R-22 vapor supplied to the compressor was measured by the turbine flow meter, which was placed up stream in the suction pipe. Fluctuations of  $\pm 5\%$  in readings was observed during trials due to the disturbances generated inside the de-superheat loop.

The thermocouple readings, in terms of mV, were measured by a multimeter. Cold-junction-compensated circuits were used to calibrate the measurement with the thermocouple junction at room temperature. The thermocouple readings were then converted to the corresponding temperatures with the conversion equation provided by the manufacturer. Note that all temperature measurements, except those on the rotor, were made after the steady state was reached. The thermocouple leads attached to the rotor were spinning with the rotor during the test. Thus the measurements had to be done after the motor was stopped.

Total bearing losses was the power measured by the dynamometer when the compressor motor was spinning at 3500 rpm which was loaded by the DC motor. The values was found to be in the range of 420 W to 500 W at various pressures (50 to 90 psia) and at the vapor temperature of about 100 °F inside the compressor. The average value, 460 W, was used in the simulations of the motor heat transfer model.

Heat loss through the shell ( $Q_{shell}$ ) for each test was calculated by measuring the temperature at the various locations of the heated shell surface and using appropriate heat transfer coefficients for each surface. The setup was placed in a air-conditioned laboratory with negligible air movement. Heat transfer from the shell to the ambient air ( $T_{amb}$ ) was natural convection and radiation. An separate test was done using the setup of Experiment 1, described in Chapter 3, without the condenser fan blowing and the calculated combined convection and radiation heat transfer coefficient for the vertical section ( $h$ ) was 2.3 Btu/hr-ft<sup>2</sup>-F. Heat transfer coefficients for the heated horizontal plated were found to be 2.4 and 1.7 Btu/hr-ft<sup>2</sup>-F for the upper and lower surfaces respectively using the empirical correlations for external free convection flow suggested by Incropera [5].  $Q_{shell}$  could be calculated using the heat transfer rate equation:

$$Q_{shell} = \sum_i h_i A_i (T_i - T_{amb}) \quad (5.1)$$

where  $h_i$ ,  $A_i$ ,  $T_i$  = the heat transfer coefficient, the area, and, the temperature of every heated surface (i) of the instrumented compressor and the supporting stand being heated up.

Every surface temperature was measured and its area was determined to calculate  $Q_{shell}$ .

## 5.3 Results and Discussions

### 5.3.1 Results from the experiment

In the experiment, a total of six tests were completed at different suction conditions and different loads on the motor. The first five tests were done with different pressures and mass flow rates. Test# 7.13.94-1 was done with fiber-glass insulation covered the whole compressor to minimize the heat loss through the shell.<sup>1</sup> Table 5.1 is a the summary of the results, including the energy balance and the motor losses calculations. Figure 5.4 shows the temperature distribution of Test# 7.5.94-1. The temperature distributions of other tests are shown in Appendix E. Note that the temperatures shown in Table 5.1 are the average circumferential temperatures. The average temperatures will be used to compare with the simulations of the motor heat transfer model.

**Table 5.1: Summary of the results from the dynamometer test**

Date	7/1/94	7/5/94	7/6/94	7/10/94	7/12/94	7/13/94
Test #	7.1.94-1	7.5.94-1	7.6.94-1	7.10.94-1	7.12.94-1	7.13.94-1
<b>Conditions</b>						
Suction pressure [psia]	90	90	90	65	65	100
Suction temperature [F]	60	61.7	58.4	64	58	62.6
$\dot{m}$ [lbm/hr] (mass flow rate into the compressor)	59	132	264	118	194	143
$P_{in}$ [W] (Power input, measured from power meter)	2.51e+03	3.22e+03	3.2e+03	3.17e+03	3.11e+03	3.12e+03
$T_{amb}$ [F] (Ambient temperature)	80	80	77	77	79	78
Insulation	no	no	no	no	no	yes
<b>Temperature measurements</b>						
$T_{wind\_m}$ [F] (ave. windings temp)	220	187	150	202	181	214
$T_{out\_m}$ [F] (exit gas stream temp)	189	157	108	149	120	159
$T_{rotor\_m}$ (ave. rotor temp) [F]	224	189	157	209	192	224
<b>Energy balance calculations</b>						
$P_{out}$ [W] (Power output, measured from dynamometer)	1.74e+03	2.28e+03	2.29e+03	2.28e+03	2.28e+03	2.28e+03
$P_{loss1}$ (= $P_{in} - P_{out}$ ) [W]	770	940	910	890	830	840
$\dot{m}h_m$ [W] (= $\dot{m}(h_{out} - h_{suct})$ )	408	674	704	518	618	750
$Q_{shell\_m}$ [W]	307	260	189	281	233	35
$P_{loss2}$ [W] (= $\dot{m}h_m + Q_{shell\_m}$ )	715	934	893	799	851	785
$P_{loss1} - P_{loss2}$ [W]	55	6	17	91	-21	55
$((P_{loss1} - P_{loss2}) / P_{loss1}) * 100\%$ [%]	7.14	0.638	1.87	10.2	-2.53	6.55
<b>Motor losses calculations</b>						
Total bearing losses (measured at no load condition)	460	460	460	460	460	460
Motor losses [W] (= $P_{loss1} - \text{total bearing losses}$ )	310	480	450	430	370	380
(Motor losses / $P_{in}$ ) * 100% [%]	12.4	14.9	14.1	13.6	11.9	12.2

1. With the presence of the 1 in fiber glass insulation (with heat transfer coefficient of 0.25 Btu/hr-ft<sup>2</sup>-F), the overall heat transfer coefficient outside the compressor dropped to 0.23 Btu/hr-ft<sup>2</sup>-F.



Date: 7/5/94

Time: 12:10 pm

Test #: 7.5.94-1

Notes:

\* = below the bottom hole of the deflector plate

- = bad thermocouple

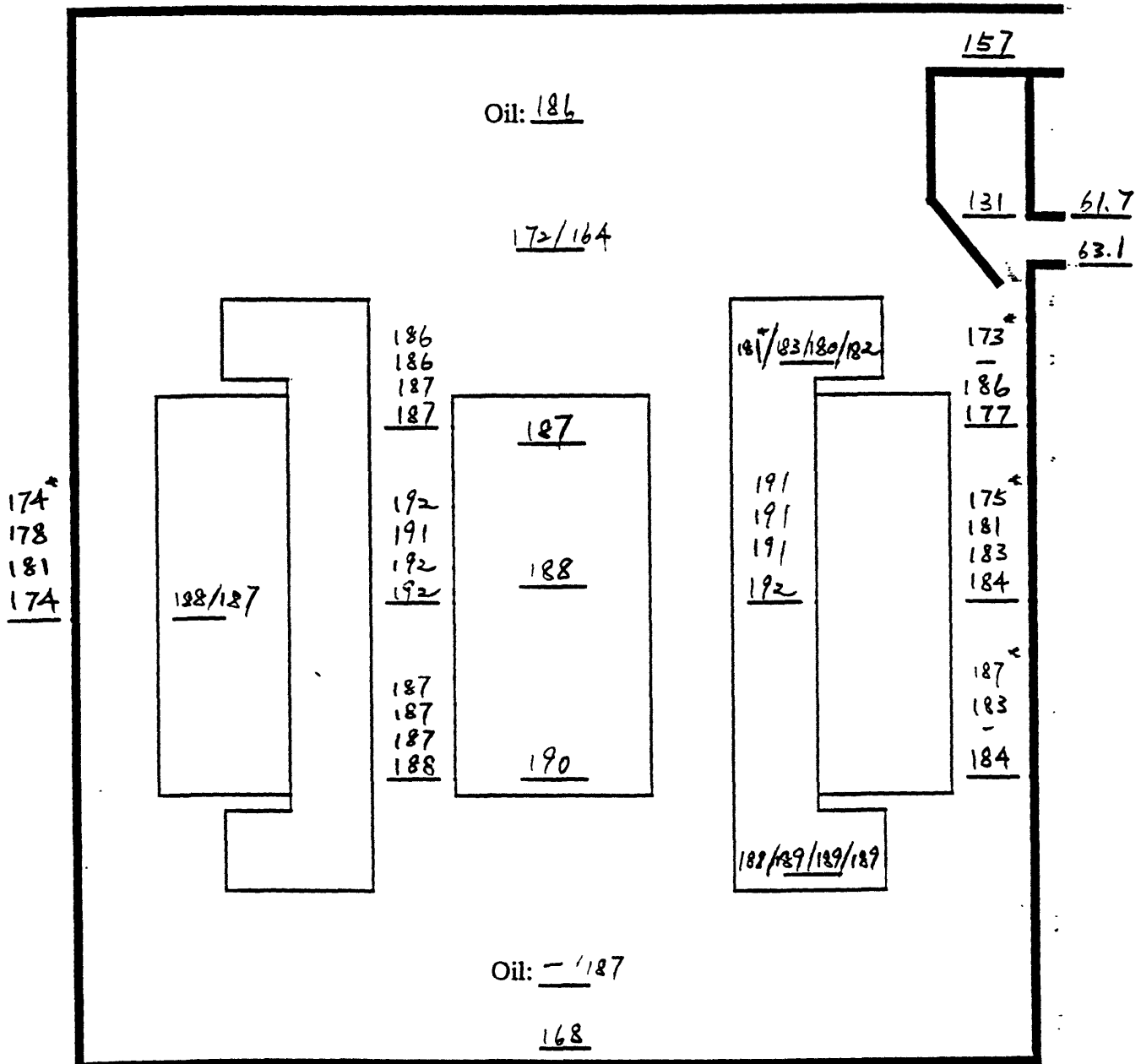


Figure 5.4: Temperature distribution of Test# 7.5.94-1

Two major heat transfer resistances of the motor cooling appear in the present motor configuration: the conduction temperature drop in the metal that constitutes the motor and the convective heat transfer coefficient on the top winding end turns and the top of the core. Observing the winding's temperature distribution for each test, the average temperature of the bottom winding end turns (T9-12) is always higher than that of the top winding end turns (T35-38). The decrease in temperature from the bottom to top winding end turns showed significant amount of heat from the motor was conducted upwards. The heat conducted to the top winding end turns was then convected to the vapor in the upper plenum. The convective heat transfer coefficient<sup>1</sup> (based on the exposed area of the end turns of 0.272 ft<sup>2</sup>) is 37.5 Btu/hr-ft<sup>2</sup>-F when the motor is operating at 3600 rpm. As the circulation and the mixing in the upper plenum is largely induced by the shaft's counterweight, the heat transfer coefficient is expected to be a strong function of the motor speed.

The temperature drop from the circulating R-22 vapor stream<sup>2</sup> at the exit of the inner gap (T5-8) to the entrance of the outer gaps (T13-16) indicated motor heat was also transferred through the circulating vapor stream. On the other hand, a negligible temperature rise of the oil was observed from the lower plenum (T43-44) to the exit of the inclined oil tube (T1) for all six tests. This showed that no significant heat was transferred from the lower plenum, the rotor, and the upper bearing to the upper plenum by the lubricating oil. Most of the heat was either transferred through heat convection from the top winding end turns or the R-22 vapor stream circulating through the motor.

Additional motor cooling was done by heat convection through the shell to the ambient air (high shell temperature versus low ambient temperature). The fraction of the

---

1. The calculation of the heat transfer coefficient ( $h_{w1}$ ) is shown in Appendix C.

2. The flow paths circulating through the motor compartment were described in Section 2.2.2.

heat carried away through heat convection from the shell varied from 20 to 40% (first five tests only), depending on the shell temperature which increased with motor temperature. Thus when the motor was operating at a high temperature, motor cooling through the shell could be an important factor.

Observing the temperature data for the outer gap right below the bottom hole of the deflector plate for all six tests (T13, T19, and T39), there was almost no trace of the jet of the cold R-22 vapor flowing down the gap. Mixing was so good that  $\text{frac}_2$  in the motor heat transfer model was set to zero for this motor configuration. However, the values of  $\text{frac}_2$  could be non-zero for high by-pass flows or a different geometry.

The difference in the energy balance calculations between the power meter measurement (Ploss1) and the energy gain of the suction vapor<sup>1</sup> plus heat loss from the shell (Ploss2) were within 100W for all six tests. The difference was within the expected uncertainties in the power and the mass flow rate measurements.

### **5.3.2 Comparison with simulations of Motor Heat Transfer Model**

When applying the heat transfer model, all the input variables, listed in Section 3.4, had to be assigned. Note that for this experiment,  $\text{frac}_0$ , the fraction of the cold R-22 vapor is discharged from the suction pipe to the upper plenum, was set to one because all the cold vapor was put into the plenum.  $\text{frac}_2$ , the fraction of the cold R-22 vapor flows directly down the outer gaps, was set to zero (discussed in Section 5.3.1). The convective heat transfer coefficient of the vertical section ( $1.3 \text{ Btu/hr-ft}^2\text{-F}$ ) was used as  $h_{3c}$  in the model. The area of the compressor shell plus the modified top and the stubby legs ( $3.98 \text{ ft}^2$ ) was used as  $A_3$  in the model. The radiative heat transfer coefficient ( $h_{3r}$ ) was assumed to be  $1.0 \text{ Btu/hr-ft}^2\text{-F}$ . For Test# 7.13.94-1, the overall outside heat transfer coefficient ( $h_3$ )

---

1. Energy gain of the suction vapor was set equal to the mass flow rate of the suction vapor times the change of enthalpies from the vapor from the suction temperature to discharged temperature.

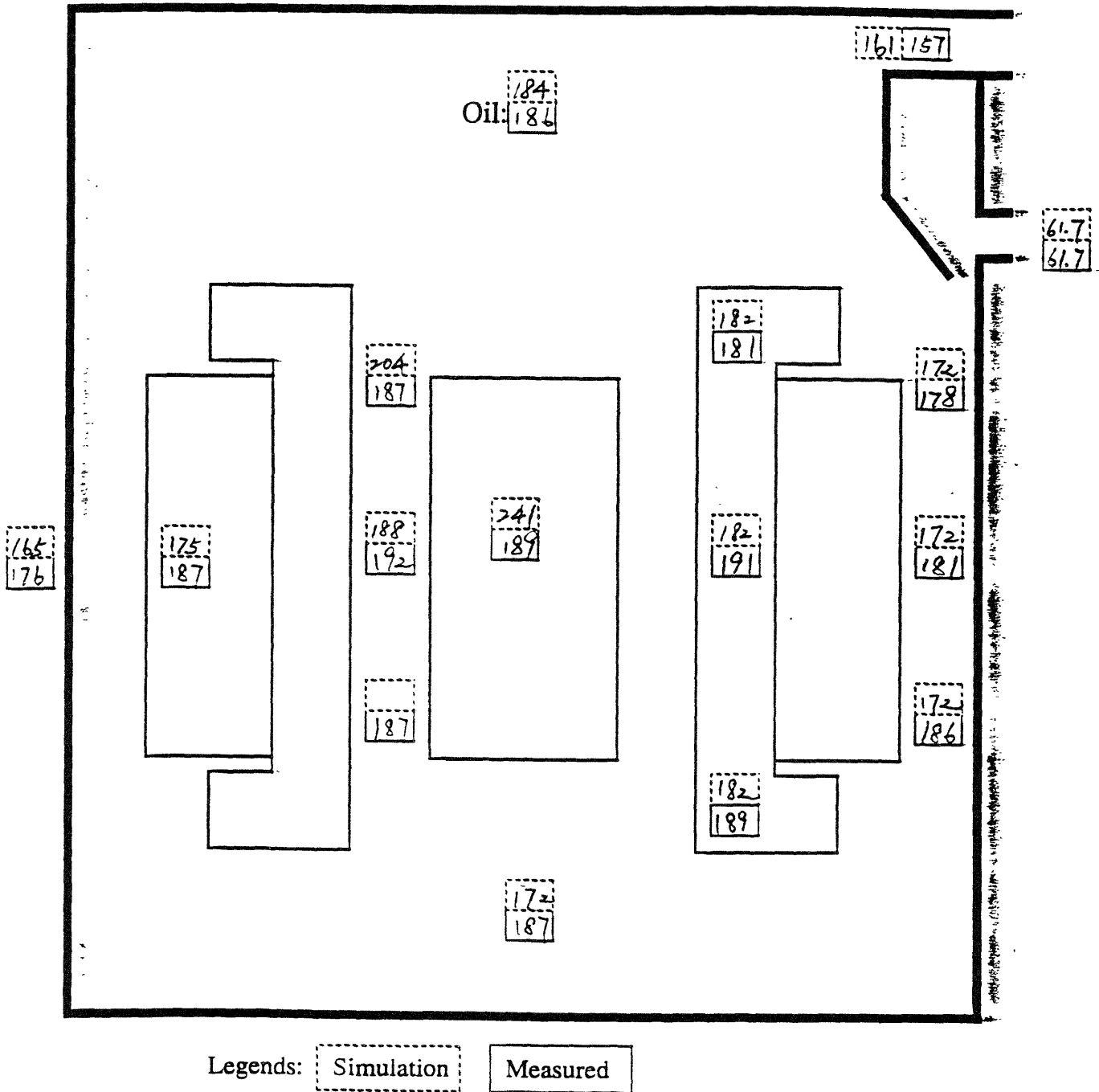
was 0.23 Btu/hr-ft<sup>2</sup>-F (see Footnote 1 at page 55) when the compressor was covered with the fiber glass insulation.

Figure 5.7 shows the simulated temperature distribution of Test# 7.5.94-1 using the Fortran program, along the measured temperature from the experiment. The simulation results of the five other tests are provided in Appendix F. Note that the temperatures compared were the average circumferential temperatures. The summary of the comparison of the results from the dynamometer test and the simulations from the model is shown in Table 5.2.

**Table 5.2:** Comparison of results between the motor heat transfer model and the dynamometer test

Test #	7.1.94-1	7.5.94-1	7.6.94-1	7.10.94-1	7.12.94-1	7.13.94-1
<b>Energy balance calculations</b>						
Motor losses [W] (from motor model by Umans [1])	385	482	461	479	469	478
Total bearing losses [W] (measured at no load condition)	460	460	460	460	460	460
Ploss3 [w] (=motor losses + total bearing losses)	845	942	921	939	929	938
(Ploss1-Ploss3) [W]	-75	-2	-11	-49	-99	-98
%Diff = (Ploss1-Ploss3)/Ploss1*100%	9.74	-0.2123	-1.209	-5.506	-11.93	-11.67
(Ploss2-Ploss3) [W]	-130	-3	-23	-140	-78	-153
%Diff = (Ploss2-Ploss3)/Ploss2*100%	-18.18	-0.8365	-3.135	-17.52	-9.165	-19.49
<b>Simulations</b>						
mdh_p [W] (=mdot*Cp*(Tout-Tsuct), predicted from model)	497	714	796	682	769	907
(mdh_m - mdh_p) [W]	-89	-40	-91	-134	-151	-157
%Diff = ((mdh_m - mdh_p)/mdh_m)*100%	-21.81	-6.935	-12.57	-21.66	-24.43	-20.93
Qshell_p [W] (=hA*(Tshell-Tamb), predicted from model)	348	229	125	257	160	31.5
(Qshell_m - Qshell_p) [W]	-41	31	64	24	73	3.5
%Diff = ((Qshell_m - Qshell_p)/Qshell_m)*100%	-13.36	11.92	33.86	8.541	31.33	10
<b>Temperature predictions</b>						
Twind_p [F]	226	182	139	190	155	210
(Twind_m - Twind_p) [F]	-6	5	11	12	26	4
%Diff = (Twind_m-Twind_p)/(Twind_m-Tsuct)*100%	3.75	3.99	12.01	8.696	21.14	2.642
Tout_p [F]	215	161	114	171	131	180
(Tout_m - Tout_p) [F]	16	4	6	22	11	21
%Diff = (Tout_m-Tout_p)/(Tout_m-Tsuct)*100%	-20.16	-4.197	-12.11	-25.88	-17.74	-11.78
Trotor_p [F]	260	241	194	246	210	265
(Trotor_m - Trotor_p) [F]	-36	-42	-57	-57	-18	-41
%Diff = (Trotor_m-Trotor_p)/(Trotor_m-Tsuct)*100%	21.95	10.85	27.53	25.52	13.43	25.4

$Q_{\text{ROTOR}} = 161 \text{ W}$ ;  $Q_{\text{CORE}} = 28.3 \text{ W}$ ;  $Q_{\text{WINDINGS}} = 233 \text{ W}$   
 $Q_{\text{FRIC}} = 1 \text{ W}$ ;  $Q_l = 9 \text{ W}$ ;  $Q_{u\_bearing} = 175 \text{ W}$ ;  $Q_u = 275 \text{ W}$   
 frac2 (fraction to go down to lower plenum): 0  
 All temp. values are in [°F]



**Figure 5.5:** Simulated temperature distribution of Test# 7.5.94-1

Comparing the simulations with the measured data, the model demonstrated correct prediction of the overall temperature distribution and the adjustment with the changes in mass flow rate and the temperature of the suction vapor. The maximum percentage difference in temperature prediction was 41%<sup>1</sup> over the wide test matrix.

The predictions of the rotor temperature in the simulations were always higher than that from the measurements. This indicated that the rotor was cooled by other means in addition to the heat transfer to the oil stream and through the inner gap suggested in the motor heat transfer model. Certain amount of heat from the rotor is probably transferred to the R-22 vapor in the upper plenum through heat convection on the top and the shaft which acts as a fin. Further analysis is needed and work is continuing.

The discharged vapor temperature ( $T_{out}$ ) and energy gain of the suction vapor ( $\dot{m}_{dh\_m}$ )<sup>2</sup> predicted for each test was higher than measured because the total power loss used in the model ( $P_{loss3}$ ) was higher than that measured from power meter ( $P_{loss1}$ ) and that calculated from energy gain of the suction vapor plus heat loss through the shell ( $P_{loss2}$ ). The uncertainties in the bearing losses, the power meter, and the mass flow rate measurements could also account the disagreement. The difference in power loss calculations also contributes the large percentage difference in the temperature predictions.

---

1. The percentage difference was the combined error of the motor heat transfer model and the motor model by Umans [1].

2. In the model,  $\dot{m}_{dh\_m} \approx \dot{m}_2 C_p (T_{out} - T_{suct})$ .

# Chapter 6

## Conclusions

### 6.1 Summary of results

Based on the fluid mechanical model, about 20% of the cold R-22 vapor that flows from the suction pipe was discharged through the bottom hole of the deflector plate into the upper plenum for the SC37 compressor. The mass flow rate of the R-22 vapor circulating through the motor due the spinning counterweight was estimated to be about 81.0 lbm/hr at the average temperature of 140°F and at a pressure of 90 psia. The fraction and the mass flow rate of circulation are dictated by the geometry and the motor or more precisely the counterweight-spinning speed. The amount of circulated R-22 vapor is not very temperature dependent.

With the motor losses and suction conditions specified, the motor heat transfer model can be used to determine the steady state temperature distribution in the motor compartment and estimate the amount of heat transferred from the motor which is to the suction vapor as well as to the ambient air through the shell. The model is also capable of predicting the effects of physical dimension changes inside the compressor in terms of temperature distribution and the amount of heat being transferred to the cold vapor. A Fortran compressor program was written to facilitate the calculation of the temperatures unknowns.

From the experimental measurement of the outside convective heat transfer coefficient of the SC37 compressor in a 38TKB condenser, the convective heat transfer coefficient was determined for different section of the compressor, as shown in Table 4.1. Empirical correlations for each section were also determined, as shown in Table 4.3. The use of these correlations is recommended for geometrically similar systems.

From the results of the dynamometer test, the motor was evidently cooled by the cold suction vapor in the upper plenum. Motor heat was conducted to the top winding end turns and then convected to the R-22 vapor in the upper plenum. Additional motor cooling were done by the mixing of the hot R-22 vapor stream circulating through the motor and the cooler suction vapor in the upper plenum and heat convection through the compressor shell to the ambient air. The results also showed that the circulating oil had little effect in the overall motor cooling.

Comparing the results of the dynamometer test and the simulations of the motor heat transfer model, the model demonstrated the correct predictions of the overall temperature distribution and the adjustment with the changes in the mass flow rate and the temperature of the suction vapor. The maximum error in a component temperature prediction was found to be 41% over the wide test matrix. The uncertainties in the bearing losses, the power and the mass flow rate measurements appear to be important contributors to these errors. Work is continuing.

## **6.2 Recommendations for future work**

The study showed that the heat convection from the top winding end turns to the vapor in the upper plenum was the major cooling mechanism for the motor. It is recommended that a detailed fluid analysis of the upper plenum to be conducted to determine the heat transfer coefficient from the top winding end turns to the R-22 vapor in the plenum. The analysis can also identifies the heat transfer process from the rotor to the vapor in the plenum.

At present, most of the heat generated by the motor is transferred to the suction vapor. This is thermodynamically undesirable in its effect on the compression process. It reduces the volumetric efficiency and increases the compressor work. To cool the motor better, it



would be desirable to have more coolant, either the oil or the R-22 vapor, circulates through the motor and then transfers that heat directly to the ambient air. With the heat capacity of the oil about three times more than that of the R-22 vapor, oil is the better choice for the motor coolant. One possible improved cooling scheme is to increase the flow of the circulating oil and then directs the oil by pouring it over the motor. The heated oil is then pumped through an external oil cooling circuit for cooling before returning back to the motor.

## References

- [1] Umans, Steve, "Steady-State, Lumped-Parameter Model for Capacitor-Run, Single-Phase Induction Motors", paper to be presented at the 1994 IEEE-IAS Annual Meeting, Denver, Co., October, 1994
- [2] Avallone, E. and Baumeister III, T., Marks' Standard Handbook for Mechanical Engineers, 9th ed., New York:McGraw-Hill, 1987.
- [3] Fox, Robert W. and McDonald, Alan T., Introduction to Fluid Mechanics, 3rd ed., New York: Wiley, 1985.
- [4] Kaminski, Deborah, ed., Heat Transfer and Fluid Flow Data Book, Schenectady, New York: General Electric, 1943- .
- [5] Marchese, A., "SC37NB010 Scroll Compressor Test Results", Copyright © UTRC, 1992.
- [6] Incropera, F. and DEWitt, D., Introduction to Heat Transfer, 2nd ed., New York: Wiley, 1990.
- [7] Beker, K. M. and Kaye, J., "Measurements of Diabatic Flow in an Annulus With an Inner Rotating Cylinder", *Journal of Heat Transfer*, Vol. 84, p.97, New York: ASME, 1962.
- [8] Press, W., Numerical recipes in FORTRAN, 2nd ed., New York: Cambridge University Press, 1992

## Appendix A

### Calculation of the fluid resistance of the SC 37 compressor

#### Flow path from the suction pipe to the scroll pump

Note: All R-22 vapor properties were evaluated at 90 °F and 90 psia. Head loss coefficients were obtained from the reference books [3] and [4].

$$\begin{aligned}\text{EQ 2.6: } R_m &= f \cdot \frac{L}{D_h} \cdot \frac{\rho Q_m}{A_m^2} + C_{B90} \cdot \frac{\rho Q_m}{A_m^2} \\ &= 93.6 Q_m [\text{psi/ft}^3/\text{sec}]\end{aligned}$$

where

$f=0.054$  (friction factor: conservative value for turbulent flow)

$L=1$  in (duct length)

$D_h=0.47$  in (hydraulic dia. of the duct inside the deflector plate)

$\rho=1.48$  lbm/ft<sup>3</sup>

$A_m=0.338$  in<sup>2</sup> (cross-sectional area of the duct)

$C_{B90}=1.5$  (head loss coeff. for 90 deg. elbow)

$$\begin{aligned}\text{EQ 2.7: } R_g &= K_e \cdot \frac{\rho Q_g}{A_g^2} \\ &= 1.38 \times 10^3 Q_g [\text{psi/ft}^3/\text{sec}]\end{aligned}$$

where

$K_e=0.9$  (head loss coeff. for the orifice with area ratio~0.05))

$A_g=0.0658$  in<sup>2</sup> (cross-sectional area of the orifice)

#### Flow paths circulating through the motor compartment

Note: All R-22 vapor properties were evaluated at 140 °F and 90 psia. Head loss coefficients were obtained from the reference books [3] and [4].

$$\begin{aligned}\text{EQ 2.5: } \Delta P_0 &= \frac{\rho}{2} \cdot (V_i \cdot R_i)^2 \cdot \left( \frac{1}{R_i^2} - \frac{1}{R_o^2} \right) \\ &= 0.149 [\text{psi}]\end{aligned}$$

where

$\rho=1.32$  lbm/ft<sup>3</sup>

$V_i=33.4$  ft/sec (tip velocity of the counterweight)

$R_i=1.046$  in (outer rad. of the counterweight or inner rad. of the plenum)

$R_o=2.926$  in (inner rad. of the shell or outer rad. of the plenum)

$$\text{EQ 2.10-2.12: } R_1 + R_2 + R_3 = K_{c1} \cdot \frac{\rho Q_c}{A_{c1}^2} + f_2 \cdot \frac{L}{D_h} \cdot \frac{\rho Q_c}{A_{c2}^2} + K_{e3} \cdot \frac{\rho Q_c}{A_{c3}^2}$$

$$= 0.436 Q_c \text{ [psi/ft}^3\text{/sec]}$$

where

$$\rho = 1.32 \text{ lbm/ft}^3$$

$$A_{c1} = A_{c2} = A_{c3} = 1.25 \text{ in}^2 \text{ (cross-sectional area of each outer gap)}$$

$$K_{c1} = 0.05 \text{ (head loss coeff. for duct contraction with area ratio} \sim 0.9)$$

$$f_2 = 0.054 \text{ (friction factor: conservative value for turbulent flow)}$$

$$K_{e3} = 0.05 \text{ (head loss coeff. for duct expansion with area ratio} \sim 0.9)$$

$$D_h = 0.865 \text{ in (hydraulic dia. of each outer gap with semi-circular shape)}$$

$$L = 4.32 \text{ in (length of each outer gap)}$$

$$\text{EQ 2.13: } R_4 = K_{c4} \cdot \frac{\rho (2 \cdot Q_c)}{A_{c4}^2}$$

$$= 274 Q_c \text{ [psi/ft}^3\text{/sec]}$$

where

$$\rho = 1.32 \text{ lbm/ft}^3$$

$$A_{c4} = 0.144 \text{ in}^2 \text{ (cross-sectional area of the inner gap)}$$

$$K_{c4} = 0.48 \text{ (head loss coeff. for duct contraction with area ratio} \sim 0.05)$$

$$\text{EQ 2.14: } R_5' (= \Delta P_5) = \frac{\tau_w \cdot \sin \left( \left( \tan^{-1} \left( \frac{2 \cdot Q_c}{V_T \cdot A_{c5}} \right) \right) \right) \cdot A_w}{A_{c5}}$$

$$= 0.112 \cdot \sin \left( \tan^{-1} \left( \frac{2 \cdot Q_c}{0.041} \right) \right) \text{ [psi]}$$

where

$$\tau_w = 0.0621 \text{ lbf/ft}^2 \text{ (Shear stress generated because of the windage}^1)$$

$$A_w = 37.5 \text{ in}^2 \text{ (cylindrical surface area of the rotor along the inner gap)}$$

$$A_{c5} = 0.144 \text{ in}^2 \text{ (cross-sectional area of the inner gap)}$$

$$V_T = \omega r = 41.1 \text{ ft/sec (velocity of the rotor)}$$

$$\text{EQ 2.15: } R_6 = K_{e6} \cdot \frac{\rho (2 \cdot Q_c)}{A_{c6}^2}$$

$$= 228 Q_c \text{ [psi/ft}^3\text{/sec]}$$

where

$$\rho = 1.32 \text{ lbm/ft}^3$$

$$K_{e6} = 0.8 \text{ (head loss coeff. for duct expansion with A.R.} \sim 0.05)$$

$$A_{c5} = 0.144 \text{ in}^2 \text{ (cross-sectional area of the inner gap)}$$

---

1. The shear stress was calculated based on the correlation of drag-rotating (windage torque) for enclosed cylinder with zero axial flow in Reference [4].

## Appendix B

### Calculations of the heat transfer coefficients of the SC37 Compressor

Note: All correlations, unless otherwise indicated, were obtained from Reference [6].

All R-22 vapor properties are evaluated at 90 psia and  $T_f$  (film temp.) = 180 °F.

- $h_o$  (heat transfer coefficient between the rotor and the oil stream):  
-modeled as internal laminar flow with constant surface temperature assuming the oil fills the whole tube (upper limit)

$$\overline{Nu} = \frac{h_o D}{k} = 3.66$$

$$h_o = 17.6 \text{ Btu/ft}^2\text{-hr-F}$$

where

$D = 0.25$  in (diameter of the tube)

$V_o = 1.83$  ft/s (axial oil stream velocity; based on oil flow rate of 110 lbm/hr)

$\rho = 54.8$  lbm/ft<sup>3</sup> (density of the oil)

$\mu = 16.5$  lbm/hr-ft (absolute viscosity of the oil)

$Re = \left(\frac{\rho V_o}{\mu}\right) = 431$  (Reynolds number; laminar flow)

$k = 0.1$  Btu/hr-ft-F (thermal conductivity of oil)

- $h_i$  (heat transfer coefficient in the inner gap):  
-modeled as annular turbulent flow and assumed high Critical Taylor number with no vortex formed (Reference [7])

$$\overline{Nu} = \frac{(h_i/2) D}{k} \approx 7$$

$$h_i = 40.2 \text{ Btu/ft}^2\text{-hr-F}$$

where

$D = 0.035$  in (2\*radial clearance in the inner gap)

$V_g = 17.0$  ft/s (axial vapor velocity)

$\rho = 1.19$  lbm/ft<sup>3</sup> (density of the R-22 vapor)

$\mu = 0.0369$  lbm/hr-ft (absolute viscosity of the R-22 vapor)

$Re = \left(\frac{\rho V_g}{\mu}\right) = 5766$  (Reynolds Number; turbulent flow)

$k = 0.00838$  Btu/hr-ft-F (thermal conductivity of the R-22 vapor)

- $h_2$  (convective heat transfer coefficient in the two outer gaps):  
-modeled as internal turbulent flow

$$\overline{Nu} = \frac{h_2 D_h}{k} = 0.023 Re_L^{0.8} Pr^{0.4}$$

$$h_2 = 3.43 \text{ Btu/ft}^2\text{-hr-F}$$

where

$$D_h = 0.865 \text{ in (hydraulic diameter of each outer gap with semi-circular shape)}$$

$$V_g = 0.983 \text{ ft/s}$$

$$Re = \left( \frac{\rho V_g}{\mu} \right) = 8230 \text{ (turbulent flow)}$$

$$Pr = 0.87 \text{ (Prandtl Number)}$$

- $h_{2C}$  (combined heat transfer coefficient between the stator core and the shell):

$$h_{2C} = \frac{(h_{2c-1} A_{2c-1} + h_{2c-2} A_{2c-2})}{A_{2c-1} + A_{2c-2}}$$

where

$$A_{2c-1} = 0.304 \text{ ft}^2 \text{ (total surface area of the "thin" outer gaps for heat transfer)}$$

$$A_{2c-2} = 0.127 \text{ ft}^2 \text{ (total surface area which the core is in direct contact with the shell)}$$

$$h_{2c-1} = \text{heat transfer coefficient in the two "thin" gaps between the stator core and the shell}$$

$$h_{2c-2} = \text{contact heat transfer coefficient between the stator core and the shell in direct contact}$$

- $h_{2c-1}$  (heat transfer coefficient in the two "thin" gaps between the stator core and the shell):

-modeled as heat conduction across the gap of 0.01 filled with R-22 vapor

$$h_{2c-1} = \frac{k}{L} = 10.1 \text{ Btu/ft}^2\text{-hr-F}$$

where

$$L = 0.01 \text{ in (average length of the "thin" gaps)}$$

$$k = 0.00838 \text{ Btu/hr-ft-F (thermal conductivity of the R-22 vapor)}$$

- $h_{2c-2}$  (contact heat transfer coefficient between the stator core and the shell in direct contact):

-modeled as contact heat transfer with a pressure of 488 psia, assuming at shrink fit of 0.001 in negative interference)

$$h_{2c-2} = \frac{1}{R_c} \\ = 714 \text{ Btu/ft}^2\text{-hr-F}$$

where

$R_c = 0.0014 \text{ ft}^2\text{-hr-F/Btu}$  (contact resistance of carbon steel with pressure 488 psia and high surface roughness (3320 rms) from Reference [3])

- $h_{wc}$  (contact heat transfer coefficient between the windings and the core):

-modeled as direct contact conducted through a layer of plastic wrap (0.02 in) and assumed the copper wires are closed packed against the core

$$h_{wc} = \frac{K_{pl}}{L} \\ = 240 \text{ Btu/ft}^2\text{-hr-F}$$

where

$L = 1.67 \times 10^{-3} \text{ ft}$  (thickness of the plastic wrap between the windings and the core)

$K_{pl} = 0.4 \text{ Btu/ft-hr-F}$  (thermal conductivity of the plastic material)

- $h_3$  (combined heat transfer coefficient between the shell and the ambient air):

$$h_3 = h_{3c} + h_{3r}$$

where

$h_{3c}$ ,  $h_{3r}$  = convective and radiative heat transfer coefficient respectively

- $h_{3c}$  (convective heat transfer coefficient between the shell and the ambient air outside)

-the value was obtained from Experiment 1

$$h_{3c} = 4.13 \text{ Btu/ft}^2\text{-hr-F}$$

- $h_{3r}$  (radiative heat transfer coefficient between the shell and the ambient air outside)

-modeled at radiation between two surfaces at two different temperatures and used reduced form of the Stefan-Boltzmann Law

$$h_{3r} = \epsilon \sigma (T_s + T_o) (T_s^2 + T_o^2) \\ h_{3r} = 1.25 \text{ Btu/ft}^2\text{-hr-F}$$

where

$\sigma = 1.73 \times 10^{-9}$  (the Stefan-Boltzmann constant)

$\epsilon = 0.9$  (emissivity of the painted surface)

$T_g = 570^\circ\text{R}$  (surrounding temperature)

$T_s = 600^\circ\text{R}$  (shell temperature)

- $h_{w1}$  (convective heat transfer coefficient from the top winding end turns to the vapor)  
-modeled as internal turbulent flow with the vapor spinning stirred by the counterweight

$$\overline{Nu} = \frac{h_{w1} D_h}{k} = 0.023 Re_L^{0.8} Pr^{0.4}$$

$$h_{w1} = 37.5 \text{ Btu/ft}^2\text{-hr-F}$$

where

$D_h = 1.71 \text{ in}$  (hydraulic diameter of the vertical cross section of the upper plenum)

$V_g = 22.8 \text{ ft/s}$  (average spinning vapor velocity in the upper plenum)

$$Re = \left( \frac{\rho V_g}{\mu} \right) = 3.75 \times 10^5 \text{ (turbulent flow)}$$

- $h_{w2}$  (heat transfer coefficient from the bottom winding end turns to the vapor)  
-modeled as internal annular turbulent flow

$$\overline{Nu} = \frac{h_{w2} D}{k} = 0.023 Re_L^{0.8} Pr^{0.4}$$

$$h_{w2} = 1.60 \text{ Btu/ft}^2\text{-hr-F}$$

where

$D = 1.5 \text{ in}$  (radial clearance between the bottom winding end turns and the shell)

$V_g = 0.436 \text{ ft/s}$

$$Re = \left( \frac{\rho V_g}{\mu} \right) = 6327 \text{ (turbulent flow)}$$

- $h_u$  (heat transfer coefficient between the upper plenum and the shell)  
-assumed to be the same as  $h_{w1}$

$$h_u = 37.5 \text{ Btu/ft}^2\text{-hr-F}$$

- $h_l$  (heat transfer coefficient between the lower plenum and the shell)  
-assumed to be the same as  $h_{w2}$

$$h_l = 1.60 \text{ Btu/ft}^2\text{-hr-F}$$



Other related values to be used in the motor heat transfer model:

$A_0 = 0.0236 \text{ ft}^2$  (cylindrical surface area of the oil tube for heat transfer with the rotor)

$A_1 = 0.248 \text{ ft}^2$  (cylindrical surface area of the rotor for heat transfer with the vapor in the inner gap)

$A_2 = 0.165 \text{ ft}^2$  (total surface area of the core for heat transfer with the vapor in the two outer gaps)

$A_3 = 1.3 \text{ ft}^2$  (outside surface area (vertical section) of the shell for heat transfer)

$A_{w1} = A_{w2} = 0.272 \text{ ft}^2$  (effective surface area of the exposed winding end turns)

$A_{wc} = 0.381 \text{ ft}^2$  (effective area of windings-to-core for heat transfer approximated by the cylindrical area enclosed by the middle windings)

$A_u = 0.654 \text{ ft}^2$  (surface area of the shell in contact with the upper plenum)

$A_l = 0.590 \text{ ft}^2$  (surface area of the shell in contact with the lower plenum, including the oil sump)

$\dot{m}_1 = 81.0 \text{ lbm/hr}$  (mass flow rate of the R-22 vapor circulating through the motor, obtained from the fluid mechanics model)

$C_g = 0.19 \text{ Btu/lbm-F}$  (average specific heat of the R-22 vapor)

$\dot{m}_o = 110 \text{ lbm/hr}$  (mass flow rate of the oil flowing up the included oil tube inside the shaft, obtained from Ray DeBlois of UTRC)

$C_o = 0.47 \text{ Btu/lbm-F}$  (specific heat of the oil)

$Q_l = 10 \text{ W}$  (heat generated from the lower bearing; data obtained from the Carrier Corporation)

$Q_{u\_bearing} = 175 \text{ W}$  (data obtained from the Carrier Corporation)

## Appendix C

### Fortran computer program for the motor heat transfer model

```
c *****
c *
c *
c *
c *
c *
c *
c * MIT-Carrier Project
c *
c *
c * Motor Heat Transfer
c * Model (Version 19)
c *
c *
c * Patrick Leung
c *
c *
c * August 8, 1994
c *
c *****
c This is a Fortran program for the motor heat transfer model. With the
c input of loss of each motor's component and T-suction,
c the program can compute the temperature distribution of the motor
c compartment.
c The subroutine format of this program is written to be implemented to the
c compressor system model main2e.
c
c   program prog19
c
c Define variables:
c
c INPUTS:
c
c q0 = heat generated from the upper bearings to the oil in CV1 [Btu/hr]
c q1 = heat generated from the rotor loss [Btu/hr]
c q2 = heat generated from the core loss [Btu/hr]
c q3 = heat generated from the windings loss [Btu/hr]
c q4 = heat generated between the rotor and the stator - windage [Btu/hr]
c q5 = additional heat input to the lower plenum (CV7) [Btu/hr]
c q6 = additional heat input to the upper plenum (CV8) [Btu/hr]
c tsuct = temp. of the suction vapor [F]
c frac0 = fraction of cold vapor which is discharged through the bottom hole
c of the deflector [%]
c frac2 = fraction of the cold vapor (after being discharged through
c the bottom hole of the deflector) to be mixed in CV9
c m0 = mass flow rate of the vapor flowing from the suction pipe [lbm/hr]
c m1 = mass flow rate of the vapor circulating through the motor [lbm/hr]
c m2 = mass flow rate of the suction vapor flows through the bottom hole
c of the deflector [lbm/hr]
c cg = specific heat of the R-22 vapor [Btu/lbm-F]
c h0 = heat transfer coefficient between the rotor and the oil stream
c h1 = heat transfer coefficient in the inner gap [Btu/hr-F ft^2]
```

c h2 = heat transfer coefficient in the outer gaps [Btu/hr-F ft<sup>2</sup>]  
 c h2c1 = heat transfer coefficient in the outer "thin" gap  
 c the stator's core and the shell [Btu/hr-F ft<sup>2</sup>]  
 c h2c2 = contact heat transfer coefficient between the stator's core  
 c and the shell which is in closed contact [Btu/hr-F ft<sup>2</sup>]  
 c h2c = heat transfer coefficient between the stator's core and  
 c the shell [Btu/hr-F ft<sup>2</sup>]  
 c  $(= (h2c1*a2c1+h2c2*a2c2)/a2c)$   
 c h3c = convective heat transfer coefficient between the shell and  
 c the ambient surrounding the compressor [Btu/hr-F ft<sup>2</sup>]  
 c h3r = radiative heat transfer coefficient between the shell and  
 c the ambient surrounding the compressor [Btu/hr-F ft<sup>2</sup>]  
 c h3 = equ. heat transfer coefficient in the region between the shell and  
 c the ambient air surrounding the compressor [Btu/hr-F ft<sup>2</sup>]  
 c  $(= h3c+h3r)$   
 c a0 = cylindrical are of the oil tube for heat transfer  
 c a1 = eff. area of the rotor and the stator in contact with the gas  
 c in the inner gap [ft<sup>2</sup>]  
 c a2 = total surface area of the core for heat transfer with the vapor  
 c in the two outer gaps [ft<sup>2</sup>]  
 c a2c1 = total surface area of the "thin" outer gaps for heat transfer  
 c [ft<sup>2</sup>]  
 c a2c2 = total surface area which the core in direct contact with the  
 c shell [ft<sup>2</sup>]  
 c a2c = total surface area between the core and the shell for heat transfer  
 c [ft<sup>2</sup>]  
 c  $(= a2c1+a2c2)$   
 c a3 = surface area of the shell in contact with the ambient air  
 c hw1 = heat transfer coefficient from the top winding end turns to the vapor in  
 c the upper plenum [Btu/hr-F ft<sup>2</sup>]  
 c hw2 = heat transfer coefficient from the bottom winding end turns to the vapor in  
 c the lower plenum [Btu/hr-F ft<sup>2</sup>]  
 c aw1 = effective surface area of the exposed top winding end turns  
 c the upper plenum [ft<sup>2</sup>]  
 c aw2 = effective surface area of the exposed bottom winding end turns  
 c the lower plenum [ft<sup>2</sup>]  
 c hwc = contact heat transfer coefficient between the windings and  
 c the core [Btu/hr-F ft<sup>2</sup>]  
 c awc = effective area of windings-to-core interface: cylindrical area  
 c enclosed by the middle windings [ft<sup>2</sup>]  
 c hu = heat transfer coefficient between the upper plenum and the shell  
 c [Btu/hr-F ft<sup>2</sup>]  
 c hl = heat transfer coefficient between the lower plenum and the shell  
 c [Btu/hr-F ft<sup>2</sup>]  
 c au = surface area of the shell in contact with the upper plenum [ft<sup>2</sup>]  
 c al = surface area of the shell in contact with the lower plenum [ft<sup>2</sup>]  
 c mo = mass flow rate of lubricating oil [lbm/hr]  
 c co = specific heat of the lubricating oil [Btu/lbm-F]  
 c  
 c OUTPUTS:  
 c  
 c t0 = temp. of the oil coming out CV1 [F]  
 c t1 = ave. temp. of the rotor [F]  
 c t2w = ave. temp. of the stator's windings [F]

```

c t2c = ave. temp. of the stator's core [F]
c t3 = ave. temp. of the compressor's shell [F]
c t4 = temp. of the ambient air surrounding the compressor [F]
c tg1 = ave. temp. of the vapor in the inner gap [F]
c tg2 = ave. temp. of the vapor in the outer gaps [F]
c tug1 = ave. temp. of the gas coming out the inner gap to
c the upper plenum [F]
c tug2 = temp. of the vapor/oil leaving CV9 and flowing down the outer gaps [F]
c tug = ave. temp. of the vapor in the upper plenum (CV8) [F]
c tlg = ave. temp. of the vapor/oil in the lower plenum (CV7) [F]
c tlg2 = ave. temp. of the vapor/oil leaving the outer gap to the lower
c plenum [F]
c htg = total energy of the suction vapor [Btu/hr]
c htoc = heat convection from the shell to the outside ambient air [Btu/hr]
c htor = heat radiation from the shell to the outside ambient air [Btu/hr]

```

```

c Variables declarations
double precision q0,q1,q2,q3,q4,q5,q6,t1,t2w,t2c,t3,t4,
&tg1,tg2,tug,tlg,tsuct,m0,frac0,htg,htoc,htor

```

```

c Input the values for each known variables

```

```

q0=175*3.413
q1=97.0*3.413
q2=96.7*3.413
q3=191*3.413
q4=4.
q5=9*3.413
q6=275*3.413
t4=80.
tsuct=60.
m0=525.
frac0=0.2

```

```

c Calling subroutine mht to do the computation
call mht (q0,q1,q2,q3,q4,q5,q6,t4,tsuct,m0,frac0,
&t1,t2w,t2c,t3,tug,tlg,tg1,tg2,htg,htoc,htor)

```

```

c Print out results

```

```

write(*,*) "t1, t2w, t2c, t3 =",t1,t2w,t2c,t3
write(*,*) "tug tlg =",tug,tlg
write(*,*) "tg1 tg2 =",tg1,tg2
write(*,*) "htg htoc htor=", htg,htoc,htor
write(*,*) "fraction to the gas=", (htg/(htg+htoc+htor))
stop
end

```

```

c Subroutine mht: compute temperatures unknowns

```

```

subroutine mht (q0,q1,q2,q3,q4,q5,q6,t4,tsuct,m0,frac0,

```

```
&t1,t2w,t2c,t3,tug,tlg,tg1,tg2,htg,htoc,htor)
```

c More variables declarations

```
double precision q0,q1,q2,q3,q4,q5,q6,t1,t2w,t2c,t3,t4,tg1,tg2,  
&tug,tug1,tug2,tlg,tlg2,tsuct,m0,frac0,  
&frac2,mo,m1,m2,co,cg,h0,h1,h2,h2a,h2c1,h2c2,h2c,h3,h3c,h3r,  
&a0,a1,a2,a2a,a2c1,a2c2,a2c,a3,hw1,hw2,aw1,aw2,hu,au,hl,al,  
&hwc,awc,htg,htoc,htor,d  
integer n,np  
double precision a(12,12),b(12),indx(12)
```

c Additional input variables

```
m1=81.  
m2=m0*frac0  
frac2=0.  
cg=0.185  
h1=40.2  
h2=3.43  
h2c1=10.1  
h2c2=714  
h3c=1.3  
h3r=1.  
a1=0.248  
a2=0.165  
a2c1=0.304  
a2c2=0.127  
a3=3.98  
hw1=37.5  
hw2=1.9  
aw1=0.272  
aw2=0.272  
hu=37.5  
au=1.24  
hl=1.9  
al=.59  
mo=110  
co=0.47  
hwc=240  
awc=0.381  
h0=17.6  
a0=0.0236
```

c Compute h2c and h3

```
h2c=(h2c1*a2c1+h2c2*a2c2)/(a2c1+a2c2)  
a2c=a2c1+a2c2  
h3=h3c+h3r
```

c Transforms the system of equations into matrix format  
c and calculate all the unknowns by computing the inverse  
c of the matrix (subroutines ludcmp and lubksb were copied from

c Numerical Recipes in FORTRAN computer files by Press)

c Input the size of the matrix

```
n=12
np=12
```

c Initiate matrix a and y(identity matrix)

```
do 11 i=1,n
  b(i)=0.
  do 12 j=1,n
    a(i,j)=0.
  12 continue
11 continue
```

c Input coefficients for each a(i,j) based on the system of equations

```
a(1,1)=h0*a0/2.+mo*co
a(1,2)=-h0*a0
a(1,10)=-mo*co+h0*a0/2.
a(2,1)=-h0*a0
a(2,2)=h1*a1+h0*a0
a(2,5)=-h1*a1
a(3,2)=h1*a1
a(3,3)=h1*a1
a(3,5)=-2*h1*a1
a(3,8)=-m1*cg
a(3,10)=m1*cg
a(4,3)=h1*a1+hw1*aw1+hw2*aw2+hwc*awc
a(4,5)=-h1*a1
a(4,7)=-hw1*aw1
a(4,10)=-hw2*aw2
a(4,12)=-hwc*awc
a(5,4)=h2*a2
a(5,6)=-2*h2*a2
a(5,9)=mo*co+m1*cg
a(5,11)=-mo*co-m1*cg
a(5,12)=h2*a2
a(6,3)=hw2*aw2
a(6,4)=hl*al
a(6,10)=-mo*co-m1*cg-hw2*aw2-hl*al
a(6,11)=mo*co+m1*cg
a(7,1)=mo*co
a(7,3)=hw1*aw1
a(7,4)=hu*au
a(7,7)=-m2*cg*(1-frac2)-m1*cg-hw1*aw1-hu*au
a(7,8)=m1*cg
a(7,12)=-mo*co
a(8,7)=-m2*cg*frac2+m1*cg
a(8,9)=-m1*cg-mo*co
a(8,12)=mo*co
a(9,3)=hwc*awc
a(9,4)=h2c*a2c
a(9,6)=h2*a2
a(9,12)=-hwc*awc-h2c*a2c-h2*a2
a(10,5)=1.
```

```

a(10,8)=-0.5
a(10,10)=-0.5
a(11,6)=1.
a(11,9)=-0.5
a(11,11)=-0.5
a(12,4)=-h2*a2-h3*a3-h2c*a2c-hu*au-hl*al
a(12,6)=h2*a2
a(12,7)=hu*au
a(12,10)=hl*al
a(12,12)=h2c*a2c
b(1)=q0
b(2)=q1
b(3)=-q4
b(4)=q3
b(6)=-q5
b(7)=-q6-m2*cg*(1-frac2)*tsuct
b(8)=-m2*cg*frac2*tsuct
b(9)=-q2
b(12)=-h3*a3*t4

```

c Call subroutine ludcmp and lubksb to compute the unknowns b's  
c by finding the inverse of the system matrix  
call ludcmp(a,n,np,indx,d)  
call lubksb(a,n,np,indx,b)

c Get all the unknowns

```

t0=b(1)
t1=b(2)
t2w=b(3)
t3=b(4)
tg1=b(5)
tg2=b(6)
tug=b(7)
tug1=b(8)
tug2=b(9)
tlg=b(10)
tlg2=b(11)
t2c=b(12)
htg=m2*cg*(tug-tsuct)
htoc=h3c*a3*(t3-t4)
htor=h3r*a3*(t3-t4)

```

c Subroutine end and return to main program  
return  
end

c This is the subroutines to solve the system of equations by finding  
c the inverse of the system matrix  
c (copied from Numerical Recipes in FORTRAN computer files by Press)  
SUBROUTINE ludcmp(a,n,np,indx,d)  
INTEGER n,np,indx(n),NMAX  
double precision d,a(np,np),TINY

```

PARAMETER (NMAX=500,TINY=1.0e-20)
INTEGER i,imax,j,k
double precision aamax,dum,sum,vv(NMAX)
d=1.
do 12 i=1,n
aamax=0.
do 11 j=1,n
if (abs(a(i,j)).gt.aamax) aamax=abs(a(i,j))
11 continue
if (aamax.eq.0.) pause 'singular matrix in ludcmp'
vv(i)=1./aamax
12 continue
do 19 j=1,n
do 14 i=1,j-1
sum=a(i,j)
do 13 k=1,i-1
sum=sum-a(i,k)*a(k,j)
13 continue
a(i,j)=sum
14 continue
aamax=0.
do 16 i=j,n
sum=a(i,j)
do 15 k=1,j-1
sum=sum-a(i,k)*a(k,j)
15 continue
a(i,j)=sum
dum=vv(i)*abs(sum)
if (dum.ge.aamax) then
imax=i
aamax=dum
endif
16 continue
if (j.ne.imax)then
do 17 k=1,n
dum=a(imax,k)
a(imax,k)=a(j,k)
a(j,k)=dum
17 continue
d=-d
vv(imax)=vv(j)
endif
indx(j)=imax
if(a(j,j).eq.0.)a(j,j)=TINY
if(j.ne.n)then
dum=1./a(j,j)
do 18 i=j+1,n
a(i,j)=a(i,j)*dum
18 continue
endif
19 continue
return
END

```



c (copied from Numerical Recipes in FORTRAN computer files by Press)

```
SUBROUTINE lubksb(a,n,np,indx,b)
  INTEGER n,np,indx(n)
  double precision a(np,np),b(n)
  INTEGER i,ii,j,ll
  double precision sum
  ii=0
  do 12 i=1,n
    ll=indx(i)
    sum=b(ll)
    b(ll)=b(i)
    if (ii.ne.0)then
      do 11 j=ii,i-1
        sum=sum-a(i,j)*b(j)
      11 continue
    else if (sum.ne.0.) then
      ii=i
    endif
    b(i)=sum
  12 continue
  do 14 i=n,1,-1
    sum=b(i)
    do 13 j=i+1,n
      sum=sum-a(i,j)*b(j)
    13 continue
    b(i)=sum/a(i,i)
  14 continue
  return
END
```

# Appendix D

## Data of Experiment 1

Measurement of Outside Convective Heat Transfer Coefficient of the SC37 compressor in a 38TKB condenser										
Data and Detailed calculation										
Date	5/24/94		6/24/94					6/27/94		
Run #	1	2	3	4	5	6	7	8	9	
speed [rpm]	1.1e+03	550	1.1e+03	825	700	525	930	600	555	
Time to collect 10ml										
Top dome	1.93	3	2.05	2.2	2.43	2.77	2.13	2.55	2.58	
	2.17	-	1.97	2.37	2.48	2.75	2.05	2.47	2.77	
Upper Vertical	2.12	2.88	2.03	2.43	2.43	2.8	2.1	2.55	2.58	
	2	-	2.15	-	2.47	2.83	2.13	2.5	2.62	
Middle vertical	1.62	2.22	1.58	1.68	1.9	2.08	1.63	1.95	1.98	
	1.67	-	1.53	1.73	1.87	2.1	1.7	1.98	1.98	
Lower	2.55	4	2.62	2.78	2.97	3.3	2.7	3.18	3.08	
	2.73	-	2.75	2.75	-	3.38	2.78	3.2	3.27	
Rate of condensation [lbm/hr]										
Top dome	0.655	0.422	0.618	0.576	0.521	0.458	0.594	0.497	0.49	
	0.585	-	0.644	0.535	0.51	0.461	0.618	0.514	0.458	
Upper Vertical	0.599	0.439	0.623	0.521	0.521	0.453	0.603	0.497	0.49	
	0.633	-	0.589	-	0.514	0.447	0.594	0.507	0.484	
Middle vertical	0.784	0.572	0.8	0.753	0.667	0.608	0.776	0.65	0.639	
	0.76	-	0.826	0.731	0.679	0.603	0.745	0.639	0.639	
Lower	0.497	0.317	0.484	0.455	0.427	0.384	0.469	0.398	0.411	
	0.464	-	0.461	0.461	-	0.374	0.455	0.396	0.388	

Detailed calculation (cont')											Area [ft2]
<b>htotal [Stu/hr-ft2-F]</b>											
Top dome	8.97	5.78	8.46	7.88	7.13	6.27	8.13	6.8	6.71	0.53	
	8.01	-	8.82	7.33	6.98	6.31	8.46	7.03	6.27	0.53	
Upper Vertical	5.95	4.37	6.19	5.18	5.18	4.5	6	4.94	4.87	0.73	
	6.3	-	5.86	-	5.11	4.44	5.9	5.04	4.81	0.73	
Middle	5.47	3.99	5.58	5.25	4.65	4.24	5.41	4.53	4.46	1.04	
	5.3	-	5.76	5.1	4.74	4.21	5.2	4.46	4.46	1.04	
Lower	4.51	2.87	4.39	4.13	3.87	3.48	4.26	3.61	3.73	0.8	
	4.2	-	4.18	4.18	-	3.4	4.13	3.59	3.52	0.8	
<b>hconv = htotal - hrad(1.4) [Stu/hr-ft2-F]</b>											
Top dome	7.57	4.38	7.06	6.48	5.73	4.87	6.73	5.4	5.31		
	6.61	-	7.42	5.93	5.58	4.91	7.06	5.63	4.87		
-average:	7.09	4.38	7.24	6.21	5.66	4.89	6.9	5.52	5.09		
Upper vertical	4.55	2.97	4.79	3.78	3.78	3.1	4.6	3.54	3.47		
	4.9	-	4.46	-	3.71	3.04	4.5	3.64	3.41		
-average:	4.72	2.97	4.63	3.78	3.74	3.07	4.55	3.59	3.44		
Middle vertical	4.07	2.59	4.18	3.85	3.25	2.84	4.01	3.13	3.06		
	3.9	-	4.36	3.7	3.34	2.81	3.8	3.06	3.06		
-average:	3.99	2.59	4.27	3.78	3.29	2.83	3.91	3.09	3.06		
Lower	3.11	1.47	2.99	2.73	2.47	2.08	2.86	2.21	2.33		
	2.8	-	2.78	2.78	-	2	2.73	2.19	2.12		
-average:	2.96	1.47	2.89	2.75	2.47	2.04	2.79	2.2	2.22		

Detailed calculation (cont')									
hconv for correlations [Btu/hr-ft <sup>2</sup> -F]									
								(ave. of Run#1 & 3)	
Top dome	-	4.38	7.16	6.21	5.66	4.89	6.9	5.52	5.09
Vertical (ave. of Upper and	-	2.74	4.67	3.78	3.48	2.93	4.17	3.3	3.22
Lower	-	1.47	2.92	2.75	2.47	2.04	2.79	2.2	2.22
<b>log(hi/ho)</b>									
Top dome	-	-	0	-0.0623	-0.103	-0.166	-0.0266	-0.113	-0.148
Vertical	-	-	0	-0.0927	-0.128	-0.203	-0.0494	-0.151	-0.162
Lower	-	-	0	-0.0255	-0.0721	-0.156	-0.0194	-0.123	-0.119
<b>log(wi/wo)</b>									
Top dome	-	-	0	-0.125	-0.195	-0.321	-0.0729	-0.263	-0.297
Vertical	-	-	0	-0.125	-0.196	-0.321	-0.0729	-0.263	-0.297
Lower	-	-	0	-0.125	0.196	0.321	-0.0729	-0.263	0.297
<b>m (using least square fit)</b>									
Top dome	0.517								
Vertical	0.573								
Lower	0.486								
<b>char. length (L) [ft]</b>									
Top dome	-	0.53	0.53	0.53	0.53	0.53	0.53	0.53	0.53
Vertical	-	1.17	1.17	1.17	1.17	1.17	1.17	1.17	1.17
Lower	-	0.25	0.25	0.25	0.25	0.25	0.25	0.25	0.25
<b>char. vel (V) [ft/sec]</b>									
Top dome	-	3.54	7.09	5.31	4.51	3.38	5.99	3.87	3.58
Vertical	-	1.88	3.76	2.82	2.4	1.8	3.18	2.05	1.9
Lower	-	0.221	0.443	0.332	0.282	0.211	0.374	0.242	0.223
<b>Re number (=V*L/v where v=2.11E-4 ft<sup>2</sup>/sec)</b>									
Top dome	-	8.9e+03	1.78e+04	1.33e+04	1.13e+04	8.5e+03	1.5e+04	9.71e+03	8.98e+03
Vertical	-	1.04e+04	2.09e+04	1.57e+04	1.33e+04	9.96e+03	1.76e+04	1.14e+04	1.05e+04
Lower	-	262	525	394	334	250	444	286	265
<b>Ci</b>									
Top dome	-	-	1.61	1.62	1.61	1.61	1.69	1.7	1.63
Vertical	-	-	1.23	1.17	1.18	1.18	1.21	1.23	1.25
Lower	-	-	2.32	2.52	2.45	2.32	2.41	2.35	2.47
<b>Elevation[in]</b>									
									16
									8.5
									1
<b>Average Ci</b>									
									1.64
									1.21
									2.41

## **Appendix E**

### **Data of Experiment 2: measured temperature distributions**

TC#	LOCATION	HOW MOUNTED	LENGTH	ROUTE
1	PLATTEN OIL DRAIN -X=180	OPEN TO OIL STREAM	73	OUT BOTTOM
2	AT ELECT. FEED-THU 315	OPEN TO GAS STREAM	72	OUT BOTTOM
3	180 DEGREES FROM #2 135	OPEN TO GAS STREAM	72	OUT BOTTOM
4	CENTER OF INLET X=0	OPEN TO GAS STREAM	75	OUT BOTTOM
5	GAP ID A-A Z=7.00 X=0	OPEN TO GAS STREAM	66	OUT BOTTOM
6	GAP ID A-A Z=7.00 Y=90	OPEN TO GAS STREAM	66	OUT BOTTOM
7	GAP ID A-A Z=7.00 -X=180	OPEN TO GAS STREAM	66	OUT BOTTOM
8	GAP ID A-A Z=7.00 -Y=270	OPEN TO GAS STREAM	66	OUT BOTTOM
9	LRG TURN A-A Z=8.25 X=0	COVERED WITH GLUE	68	OUT BOTTOM
10	SML TURN A-A Z=8.25 Y=90	COVERED WITH GLUE	68	OUT BOTTOM
11	LRG TN A-A Z=8.25 -X=180	COVERED WITH GLUE	68	OUT BOTTOM
12	SML TN A-A Z=8.25 -Y=270	COVERED WITH GLUE	68	OUT BOTTOM
13	STAT OD A-A Z=7.00 X=0	OPEN TO GAS STREAM	70	OUT BOTTOM
14	STAT OD A-A Z=7.00 Y=90	OPEN TO GAS STREAM	70	OUT BOTTOM
15	STA OD A-A Z=7.00 -X=180	OPEN TO GAS STREAM	70	OUT BOTTOM
16	STA OD A-A Z=7.00 -Y=270	OPEN TO GAS STREAM	70	OUT BOTTOM
17	ROTOR TOP END	COVERED WITH GLUE	25	OUT ROTOR TOP
18	ROTOR LOWER END	COVERED WITH GLUE	30	OUT ROTOR TOP
19	STAT ID B-B Z=4.875 X=0	COVERED IN INSUL	75	OUT BOTTOM
20	STA ID B-B Z=4.875 Y=90	COVERED IN INSUL	75	OUT BOTTOM
21	STA ID B-B Z=4.87 -X=180	COVERED IN INSUL	75	OUT BOTTOM
22	STA ID B-B Z=4.87 -Y=270	COVERED IN INSUL	75	OUT BOTTOM
23	GAP ID B-B Z=4.875 X=0	OPEN TO GAS STREAM	76	OUT BOTTOM
24	GAP ID B-B Z=4.875 Y=90	OPEN TO GAS STREAM	76	OUT BOTTOM
25	GAP ID B-B Z=4.87 -X=180	OPEN TO GAS STREAM	76	OUT BOTTOM
26	GAP ID B-B Z=4.87 -Y=270	OPEN TO GAS STREAM	76	OUT BOTTOM
27	BG GAP B-B Z=4.875 X=0	OPEN TO GAS STREAM	76	OUT BOTTOM
28	SML GAP B-B Z=4.875 Y=90	OPEN TO GAS STREAM	76	OUT BOTTOM
29	BG GAP B-B Z=4.87 -X=180	OPEN TO GAS STREAM	76	OUT BOTTOM
30	SM GAP B-B Z=4.87 -Y=270	OPEN TO GAS STREAM	76	OUT BOTTOM
31	STA ID C-C Z=2.75 X=0	OPEN TO GAS STREAM	74	OUT BOTTOM
32	STA ID C-C Z=2.75 Y=90	OPEN TO GAS STREAM	74	OUT BOTTOM
33	STA ID C-C Z=2.75 -X=180	OPEN TO GAS STREAM	74	OUT BOTTOM
34	STA ID C-C Z=2.75 -Y=270	OPEN TO GAS STREAM	74	OUT BOTTOM
35	LRG TRN C-C Z=1.5 X=0	COVERED WITH GLUE	61	OUT BOTTOM
36	SM TURN C-C Z=1.5 Y=90	COVERED WITH GLUE	61	OUT BOTTOM
37	LRG TRN C-C Z=1.5 -X=180	COVERED WITH GLUE	61	OUT BOTTOM
38	SM TRN C-C Z=1.5 -Y=270	COVERED WITH GLUE	61	OUT BOTTOM
39	BG GAP C-C Z=2.75 X=0	OPEN TO GAS STREAM	60	OUT BOTTOM
40	SM GAP C-C Z=2.75 Y=90	OPEN TO GAS STREAM	60	OUT BOTTOM
41	BG GAP C-C Z=2.75 -X=180	OPEN TO GAS STREAM	60	OUT BOTTOM
42	SM GAP C-C Z=2.75 -Y=270	OPEN TO GAS STREAM	60	OUT BOTTOM
43	LOWER HGR HOS C-C Z=2.75	OPEN TO OIL STREAM	58	OUT BOTTOM
44	180 FROM #43 Z=2.75	OPEN TO OIL STREAM	58	OUT BOTTOM
45	OD STA B-B Z=4.87 -Y=270	COVERED WITH GLUE	65	OUT BOTTOM
46	OD STA B-B Z=4.875 Y=90	COVERED WITH GLUE	65	OUT BOTTOM
47	OUTSIDE B-B Z=4.875 X=0	COVERED WITH GLUE	56	OUTSIDE SHELL
48	OUTSIDE B-B Z=4.875 Y=90	COVERED WITH GLUE	56	OUTSIDE SHELL
49	OUTSID B-B Z=4.87 -X=180	COVERED WITH GLUE	56	OUTSIDE SHELL
50	OUTSID B-B Z=4.87 -Y=270	COVERED WITH GLUE	56	OUTSIDE SHELL
51	BOTTOM SUMP C-C Z=1.00	OPEN TO OIL STREAM	60	OUT BOTTOM
52	CL OF ROTOR B-B Z=4.875	COVERED WITH GLUE	66	OUT ROTOR TOP

53 Discharge Vapor

54 Suction vapor, next to flow meter

55 Suction vapor, next to compressor shell

283.91 FEET TOTAL  
 X=0 = vertical line below bottom  
 hole of deflector plate  
 X=180 = 180 degree off phase of X=0  
 Y=90 = 90 degree CW of X=0 (Top View)  
 Y=270 = 180 degree off phase of Y=90

The description of the thermocouple locations

MIT - Carrier Program  
Dynamometer Test

Temp Distribution Data Sheet

Date:

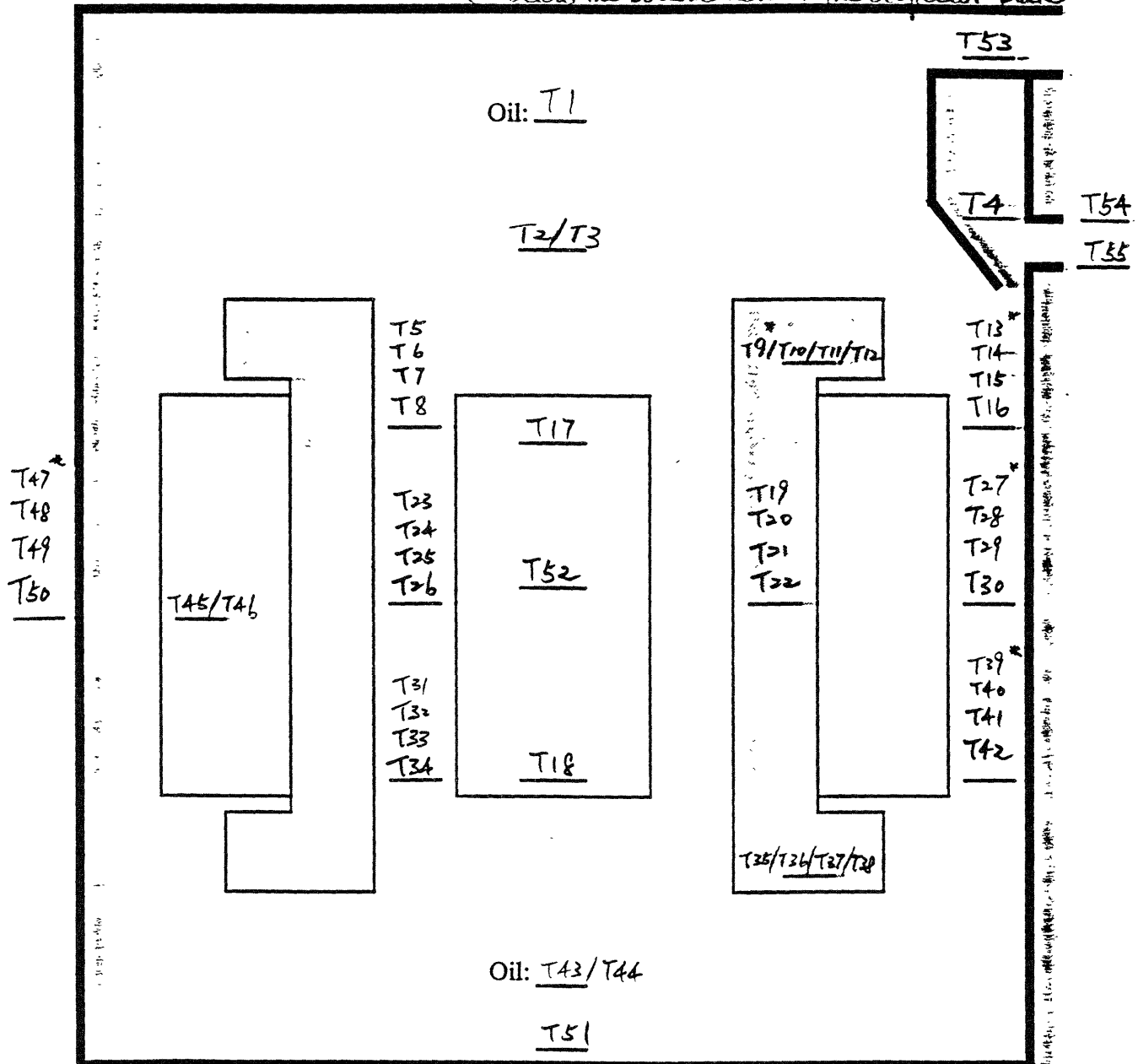
Time:

Test #:

Notes:

*Corresponding Thermocouples no. in the experiment*

*\* = below the bottom hole of the deflector plate*



## Dynamometer Test

### Comparison with the motor heat transfer model

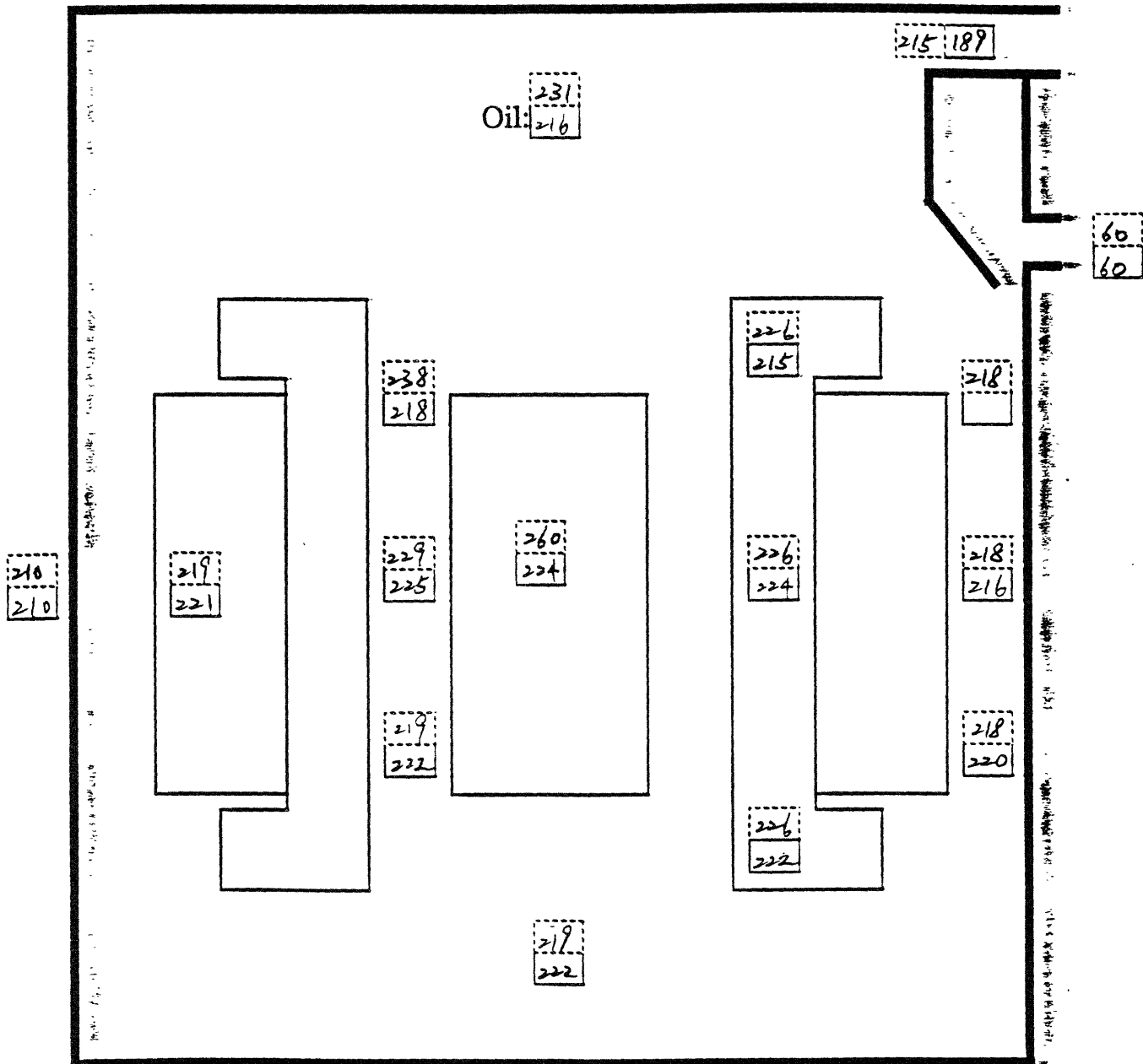
Test #: 7.1.94-1

Q<sub>ROTOR</sub>= 97.0 W; Q<sub>CORE</sub>= 96.7 W; Q<sub>WINDINGS</sub>= 191 W

$$Q_{\text{FRIC}} = 1 \text{ W}; Q_1 = 9 \text{ W}; Q_{u\_bearing} = 175 \text{ W}; Q_u = 275 \text{ W}$$

```
frac2 (fraction to go down to lower plenum): 0
```

All temp. values are in [°F]



Legends:	Simulation	Measured
----------	------------	----------



# MIT - Carrier Program Dynamometer Test

## Comparison with the motor heat transfer model

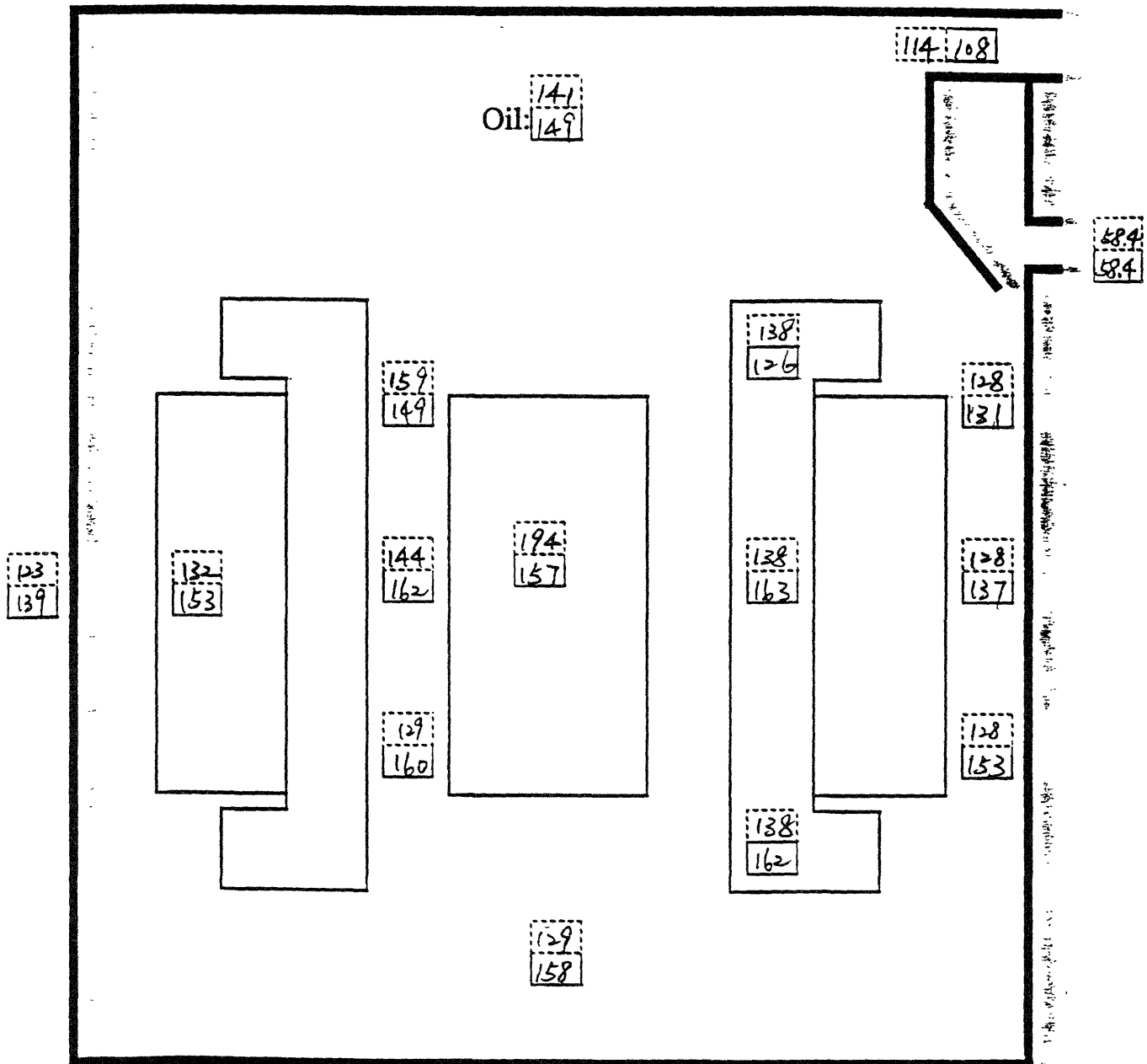
Test #: 7.6.94-1

$Q_{\text{ROTOR}} = 153 \text{ W}$ ;  $Q_{\text{CORE}} = 87.5 \text{ W}$ ;  $Q_{\text{WINDINGS}} = 220 \text{ W}$

$Q_{\text{FRIC}} = 1 \text{ W}$ ;  $Q_1 = 9 \text{ W}$ ;  $Q_{\text{u\_bearing}} = 175 \text{ W}$ ;  $Q_{\text{u}} = 275 \text{ W}$

frac2 (fraction to go down to lower plenum): 0

All temp. values are in [ $^{\circ}\text{F}$ ]



Legends: Simulation Measured

# MIT - Carrier Program Dynamometer Test

## Comparison with the motor heat transfer model

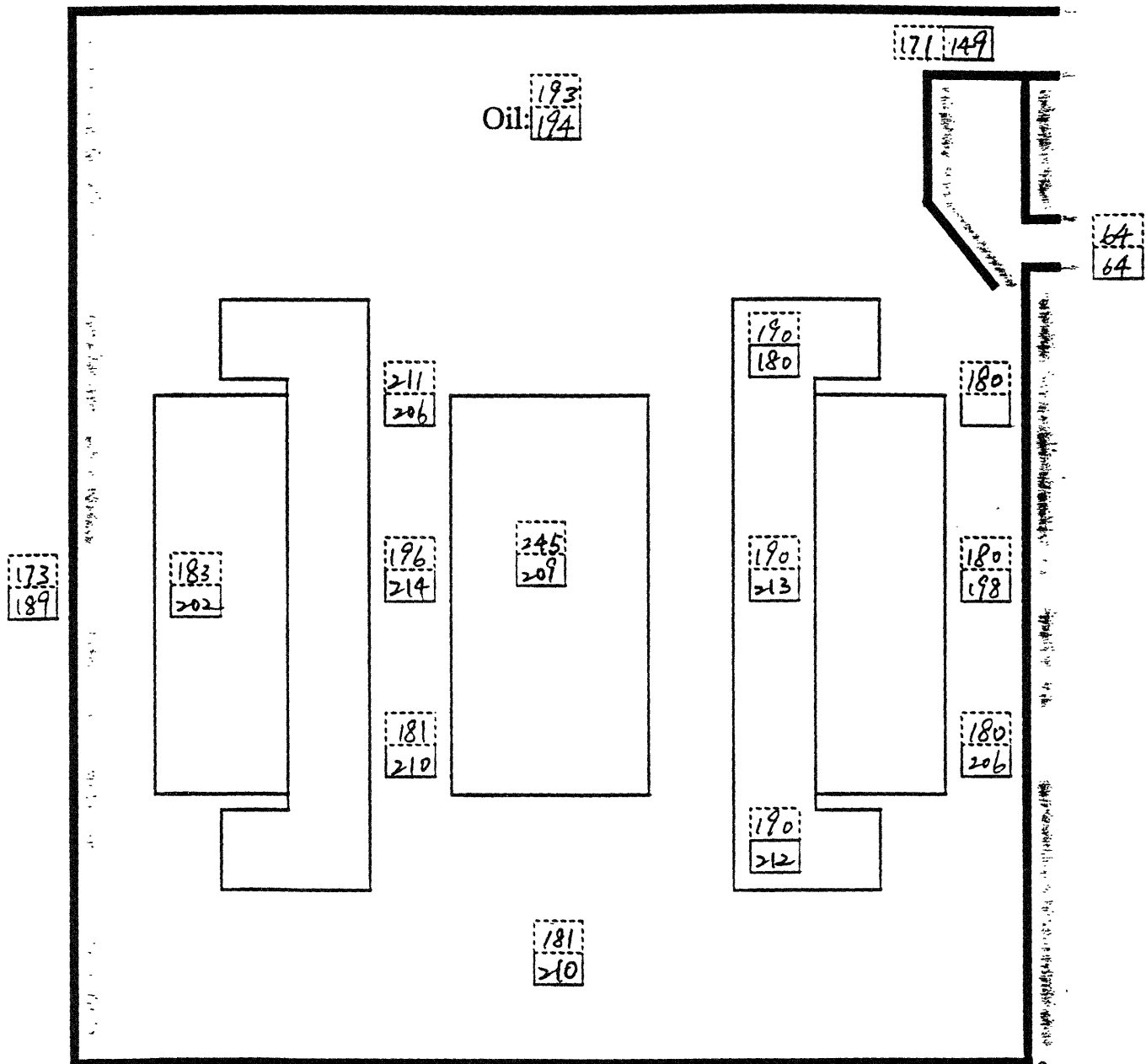
Test #: 7.10.94 - 1

$Q_{\text{ROTOR}} = 152 \text{ W}$ ;  $Q_{\text{CORE}} = 93.3 \text{ W}$ ;  $Q_{\text{WINDINGS}} = 234 \text{ W}$

$Q_{\text{FRIC}} = 1 \text{ W}$ ;  $Q_l = 9 \text{ W}$ ;  $Q_{u, \text{bearing}} = 175 \text{ W}$ ;  $Q_u = 275 \text{ W}$

frac2 (fraction to go down to lower plenum): 0

All temp. values are in [°F]



Legends: Simulation Measured

# MIT - Carrier Program Dynamometer Test

## Comparison with the motor heat transfer model

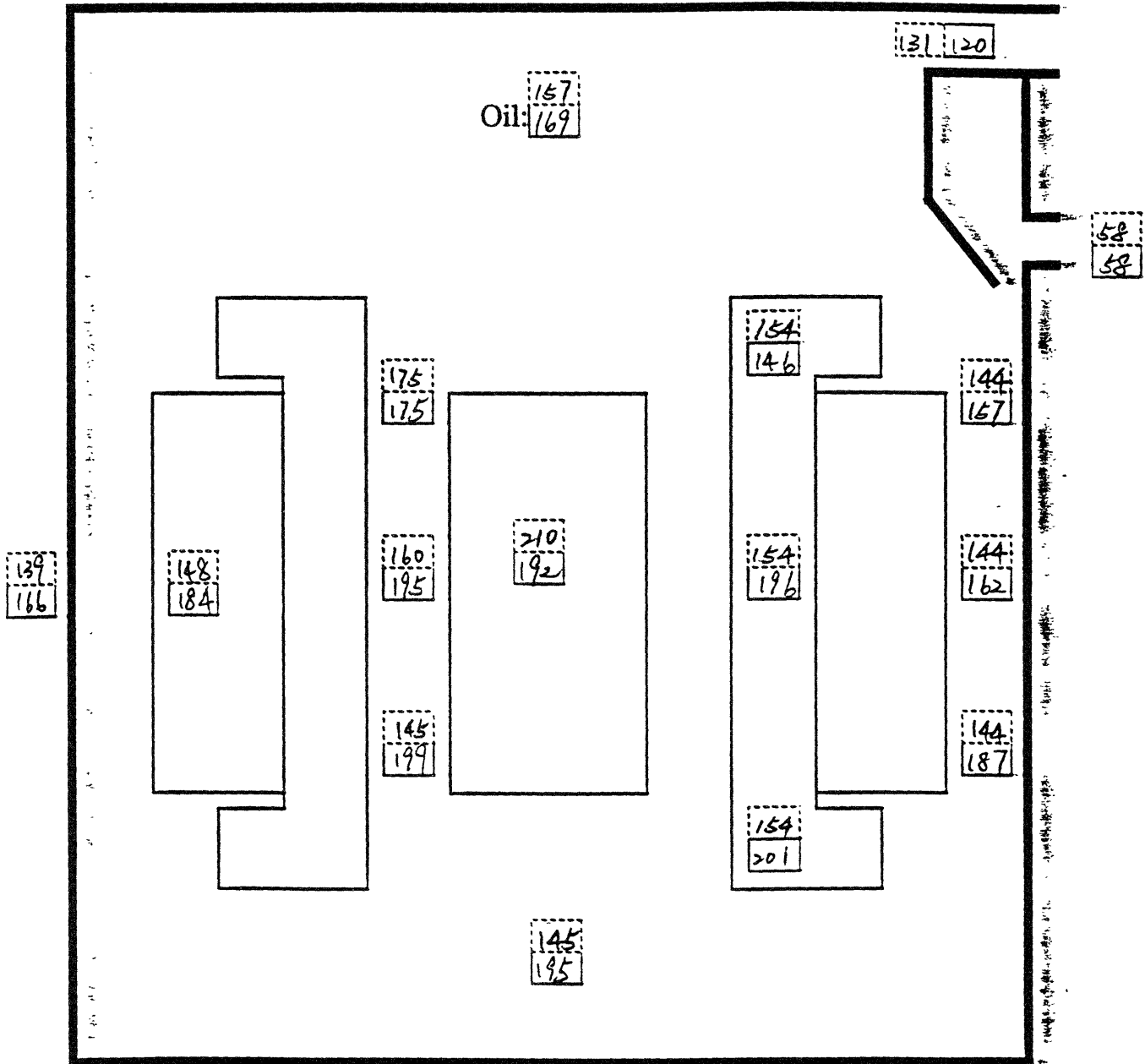
Test #: 7.12.94-1

$Q_{\text{ROTOR}} = 154 \text{ W}$ ;  $Q_{\text{CORE}} = 87.9 \text{ W}$ ;  $Q_{\text{WINDINGS}} = 227 \text{ W}$

$Q_{\text{FRIC}} = 1 \text{ W}$ ;  $Q_l = 9 \text{ W}$ ;  $Q_{u\_bearing} = 175 \text{ W}$ ;  $Q_u = 275 \text{ W}$

frac2 (fraction to go down to lower plenum): 0

All temp. values are in [°F]



Legends: Simulation Measured

# MIT - Carrier Program Dynamometer Test

## Comparison with the motor heat transfer model

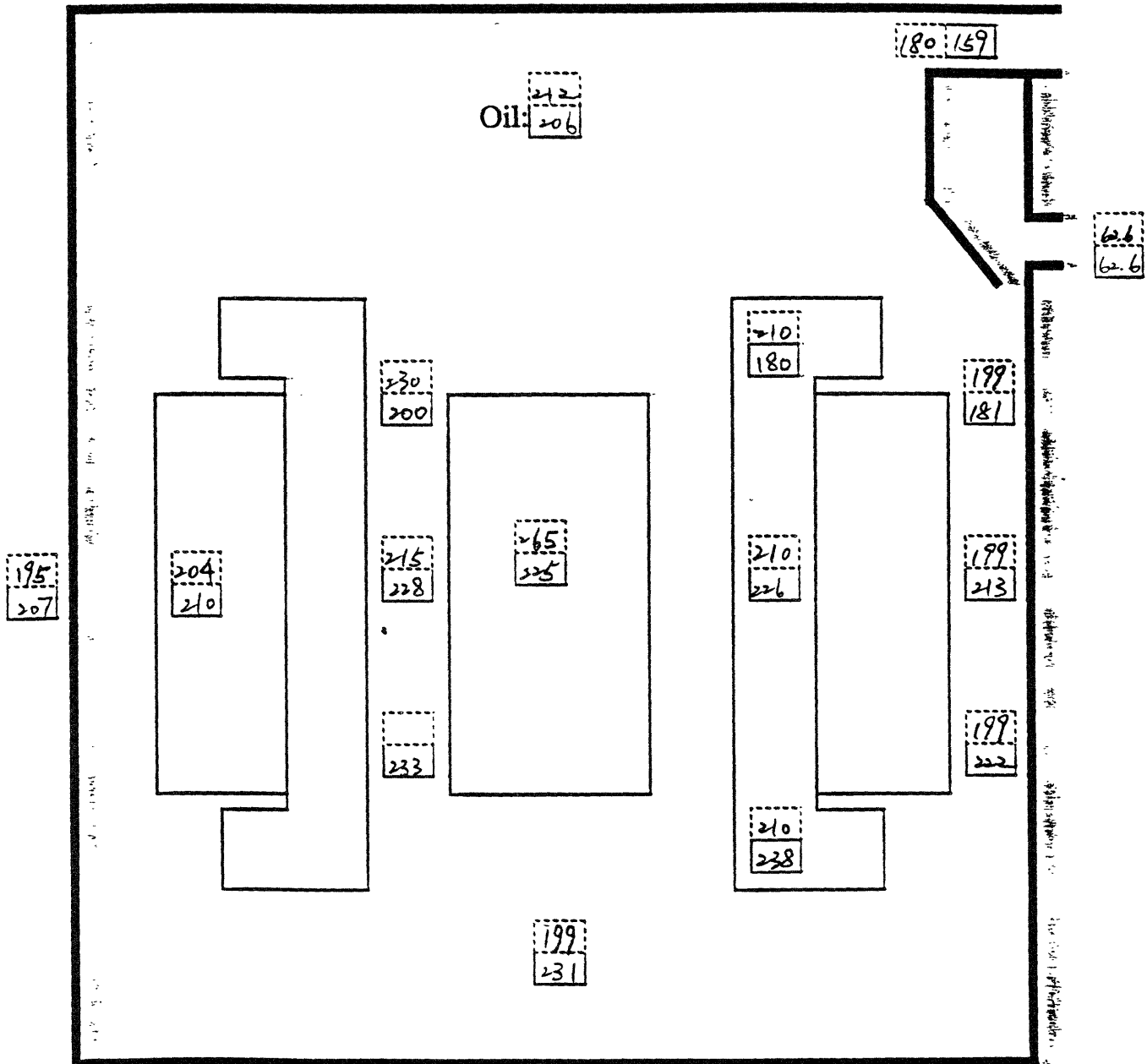
Test #: 7.13.94-1

$Q_{\text{ROTOR}} = 153 \text{ W}$ ;  $Q_{\text{CORE}} = 90.4 \text{ W}$ ;  $Q_{\text{WINDINGS}} = 235 \text{ W}$

$Q_{\text{FRIC}} = 1 \text{ W}$ ;  $Q_l = 9 \text{ W}$ ;  $Q_{u\_bearing} = 175 \text{ W}$ ;  $Q_u = 275 \text{ W}$

frac2 (fraction to go down to lower plenum): 0

All temp. values are in [°F]



Legends: Simulation Measured

## **Appendix F**

### **Data of Experiment 2: Comparison with the simulation results**

MIT - Carrier Program  
Dynamometer Test

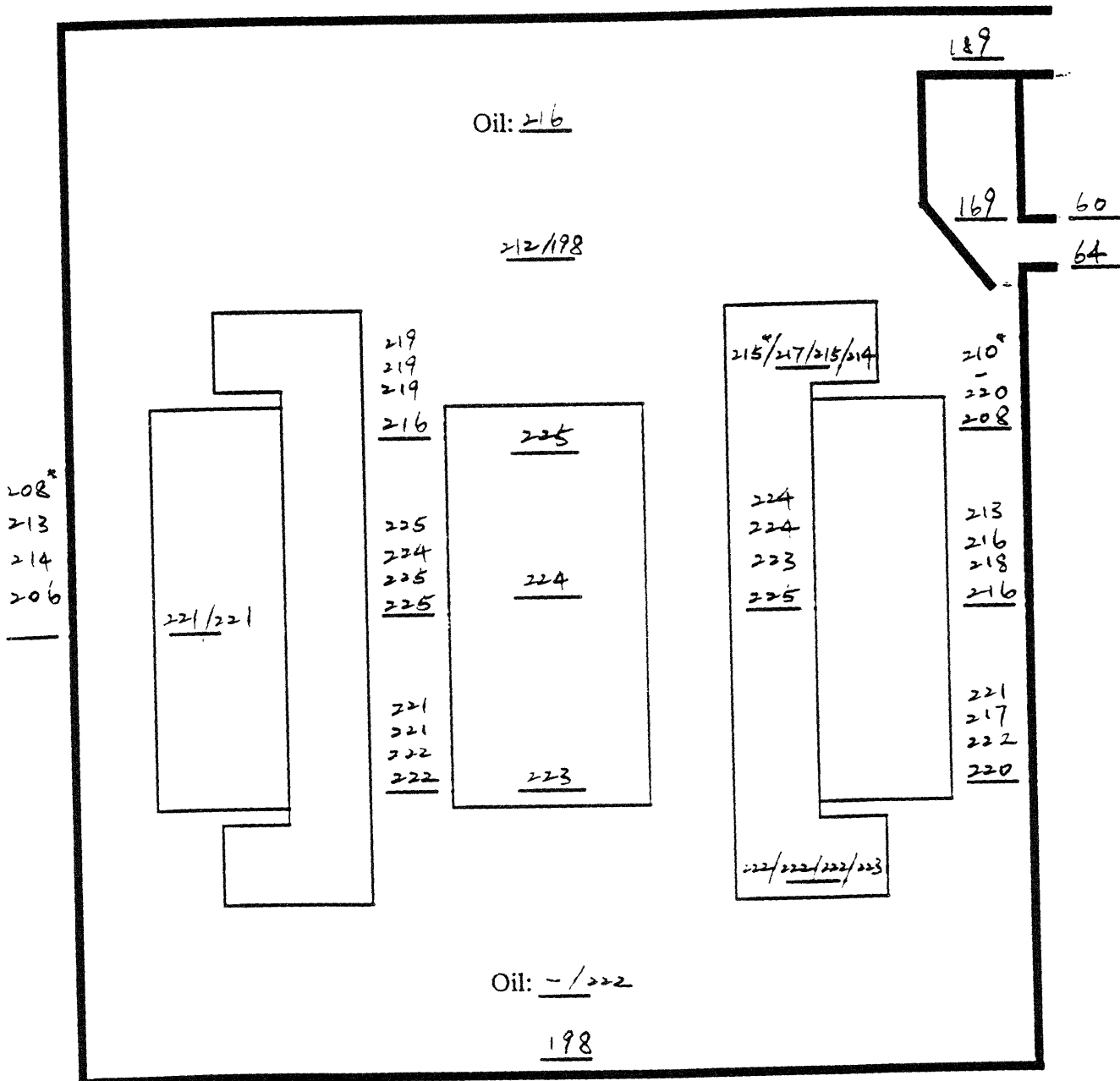
Temp Distribution Data Sheet

Date: 7/11/74 Time: 1:35 pm Test #: 7.1.94-1

Notes:

\* = below the bottom hole of the deflector plate

- = bad thermocouple



MIT - Carrier Program  
Dynamometer Test

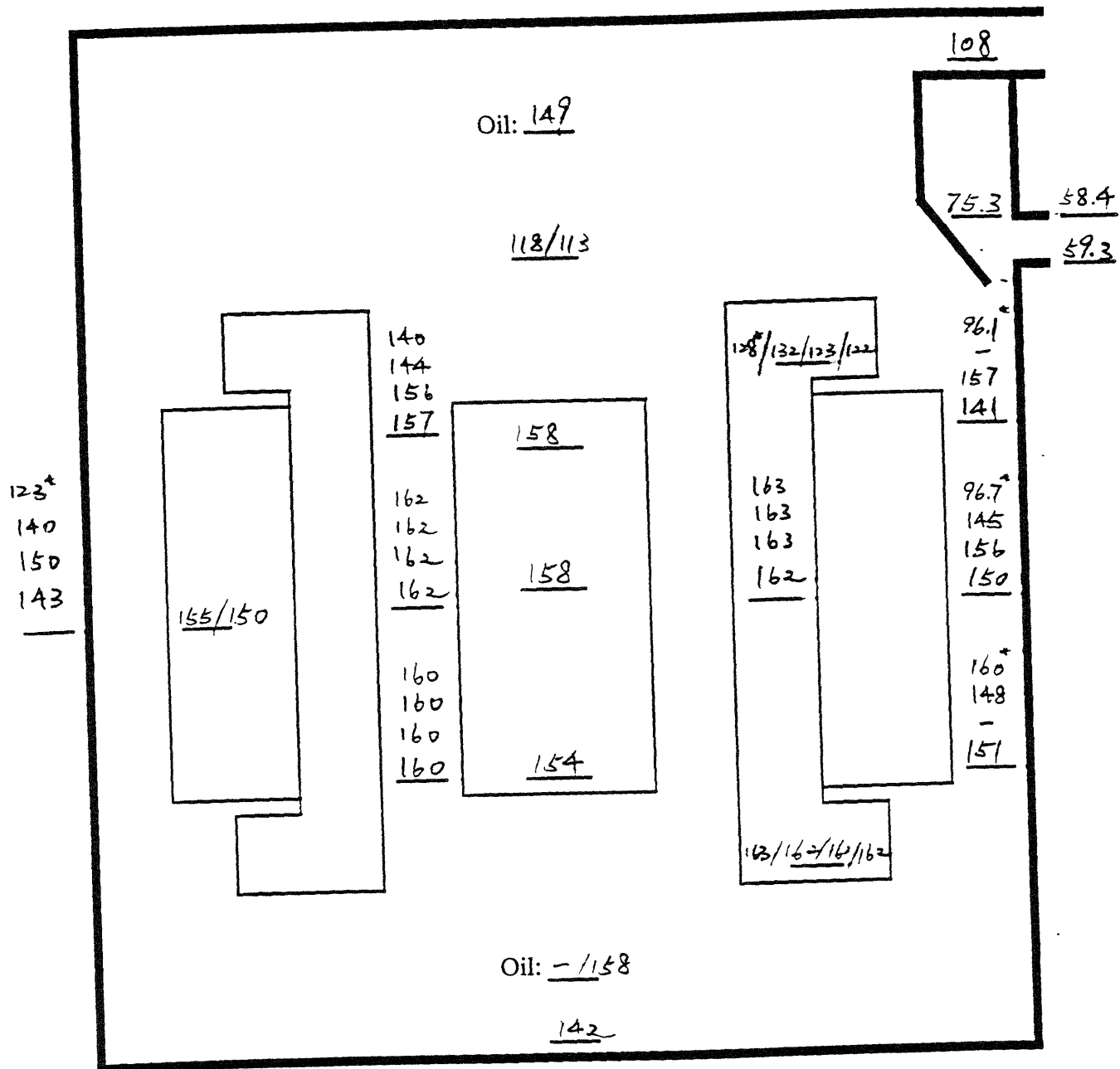
Temp Distribution Data Sheet

Date: 7/6/94 Time: 12:52 PM Test #: 76 94-1

Notes:

\* = below the bottom hole of the deflector plate

- = bad thermocouple



MIT - Carrier Program  
Dynamometer Test

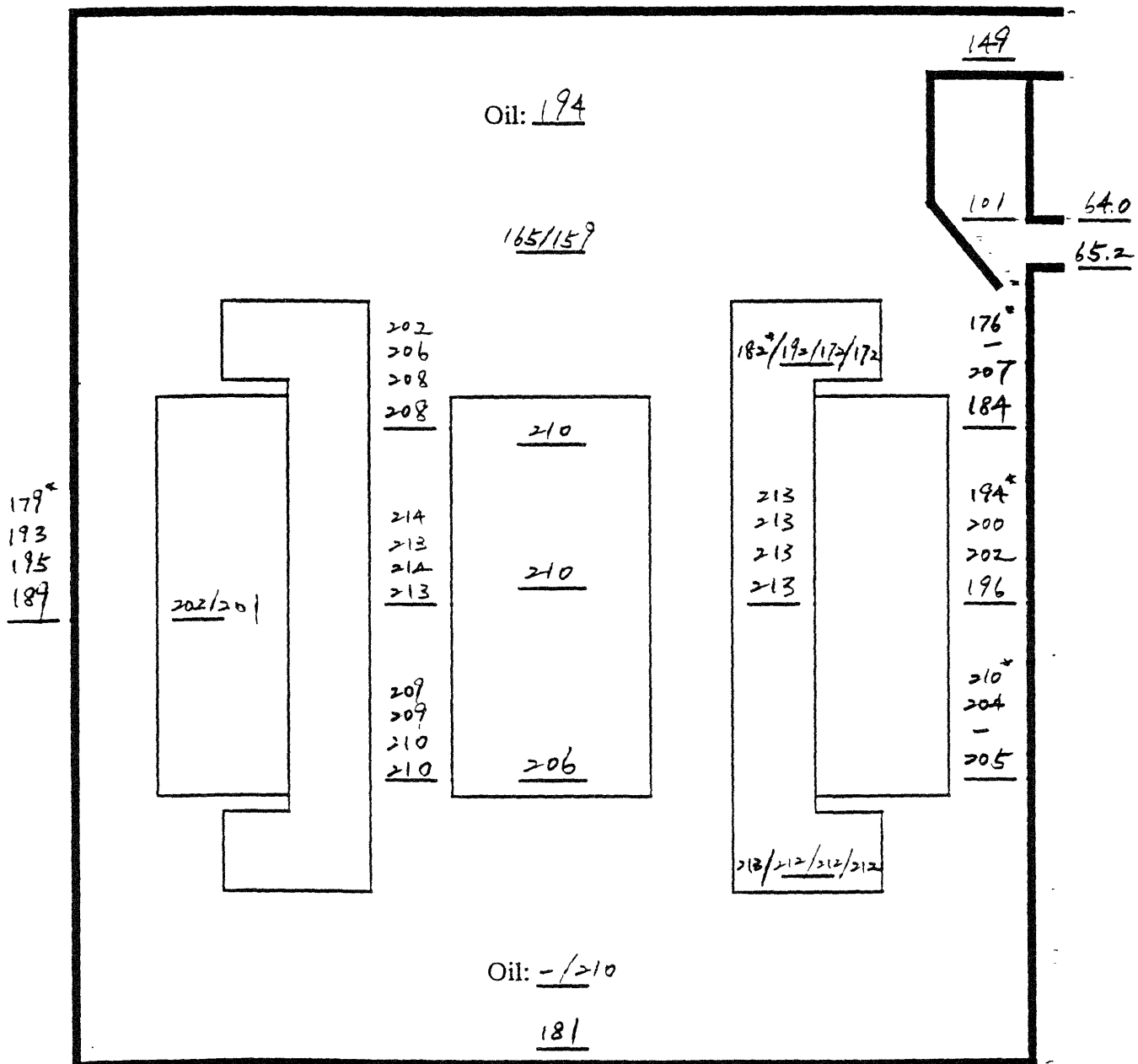
Temp Distribution Data Sheet

Date: 7/10/94 Time: 11:42 am Test #: 7.10.94 -1

Notes:

\* = below the bottom hole of the deflector plate

- = bad thermocouple





MIT - Carrier Program  
Dynamometer Test

Temp Distribution Data Sheet

Date: 7/13/94

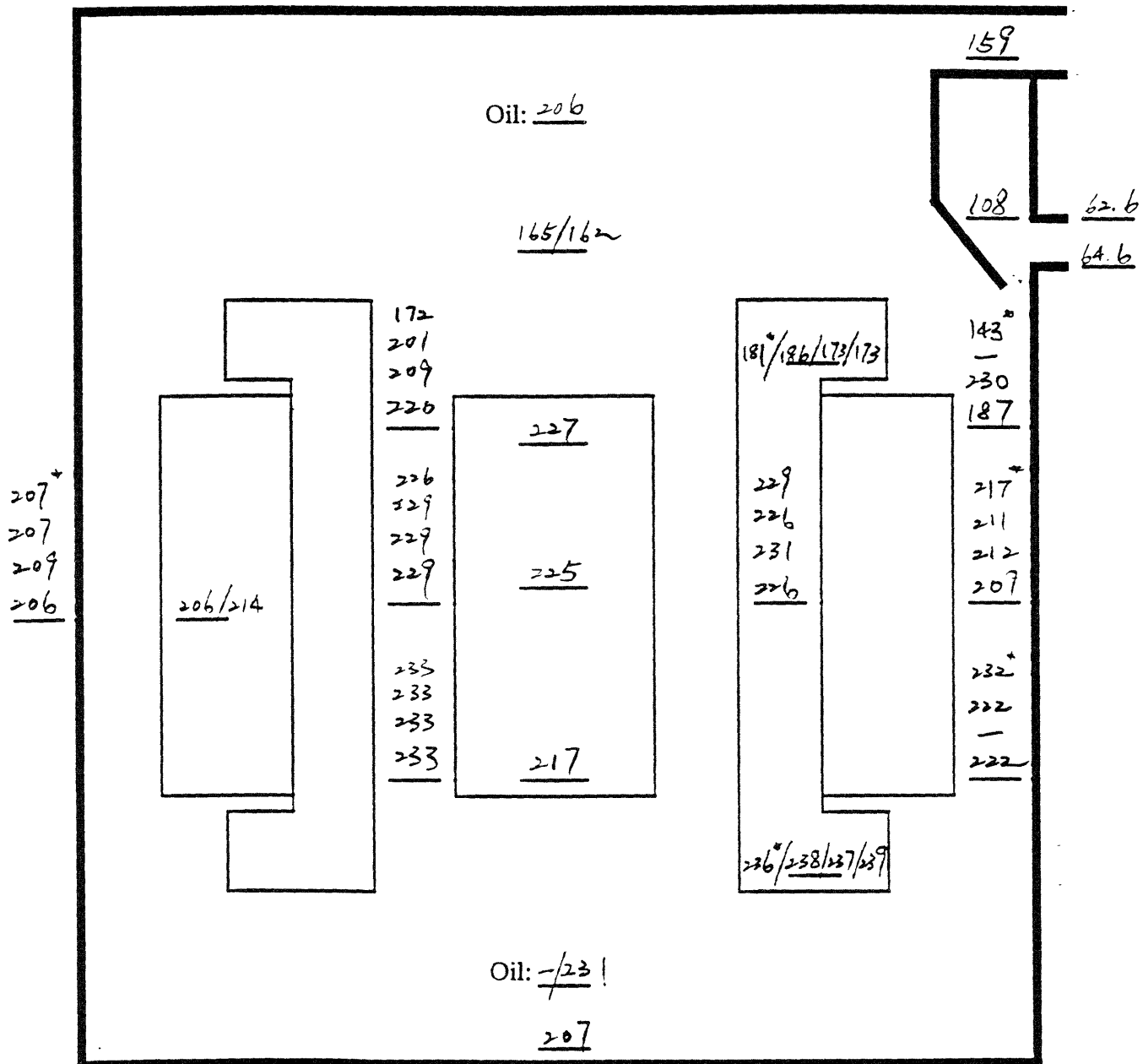
Time: 5:00 pm

Test #: 7.13.94 - 1

Notes:

\* = below the bottom hole of the deflector plate

- = bad thermocouple



MIT - Carrier Program  
Dynamometer Test

Temp Distribution Data Sheet

Date: 7/12/94 Time: 12:40 PM Test #: 7.12.94 -1

Notes:

\* = below the bottom hole of the deflector plate

- = bad thermocouple

